

Detecting and quantifying palaeoseasonality in stalagmites using geochemical and modelling approaches

Article

Accepted Version

Creative Commons: Attribution-Noncommercial-No Derivative Works 4.0

Baldini, J. U.L., Lechleitner, F. A., Breitenbach, S. F.M., van Hunen, J., Baldini, L. M., Wynn, P. M., Jamieson, R. A., Ridley, H. E., Baker, A. H. ORCID: <https://orcid.org/0000-0003-2697-1350>, Walczak, I. W. and Fohlmeister, J. (2021) Detecting and quantifying palaeoseasonality in stalagmites using geochemical and modelling approaches. *Quaternary Science Reviews*, 254. 106784. ISSN 0277-3791 doi: 10.1016/j.quascirev.2020.106784 Available at <https://centaur.reading.ac.uk/97596/>

It is advisable to refer to the publisher's version if you intend to cite from the work. See [Guidance on citing](#).

Published version at: <https://www.sciencedirect.com/science/article/pii/S0277379120307460>

To link to this article DOI: <http://dx.doi.org/10.1016/j.quascirev.2020.106784>

Publisher: Elsevier

All outputs in CentAUR are protected by Intellectual Property Rights law, including copyright law. Copyright and IPR is retained by the creators or other copyright holders. Terms and conditions for use of this material are defined in the [End User Agreement](#).

www.reading.ac.uk/centaur

CentAUR

Central Archive at the University of Reading

Reading's research outputs online

Detecting and quantifying palaeoseasonality in stalagmites using geochemical and modelling approaches

James U.L. Baldini¹, Franziska A. Lechleitner^{2, 3, 4}, Sebastian F.M. Breitenbach⁴, Jeroen van Hunen¹, Lisa M. Baldini⁵, Peter M. Wynn⁶, Robert A. Jamieson⁷, Harriet E. Ridley¹, Alexander J. Baker⁸, Izabela W. Walczak⁹, and Jens Fohlmeister^{10, 11}

¹Department of Earth Sciences, Durham University, DH1 3LE, United Kingdom.

²Department of Earth Sciences, University of Oxford, South Parks Road, Oxford OX1 3AN, United Kingdom.

³ Laboratory for the Analysis of Radiocarbon with AMS (LARA), Department of Chemistry and Biochemistry, and Oeschger Centre for Climate Change Research, University of Bern, Freiestrasse 3, 3012 Bern, Switzerland.

⁴Department of Geography and Environmental Sciences, Northumbria University, Newcastle upon Tyne, NE1 8ST, United Kingdom.

⁵School of Health & Life Sciences, Teesside University, Middlesbrough, TS1 3BX, United Kingdom

⁶Lancaster Environment Centre, Lancaster University, Lancaster, LA1 4YQ, United Kingdom.

⁷School of Earth and Environment, University of Leeds, Leeds, LS2 9JT, United Kingdom

⁸National Centre for Atmospheric Science and Department of Meteorology, University of Reading, RG6 6BB, United Kingdom.

⁹Durham Centre for Academic Development, Durham University, Durham, DH1 1TA, United Kingdom.

¹⁰Potsdam Institute for Climate Impact Research, Telegrafenberg, 14473 Potsdam, Germany.

¹¹GFZ German Research Centre for Geosciences, Section 'Climate Dynamics and Landscape Development', Telegrafenberg, 14473 Potsdam, Germany.

Abstract

Stalagmites are an extraordinarily powerful resource for the reconstruction of climatological palaeoseasonality. Here, we provide a comprehensive review of different types of seasonality preserved by stalagmites and methods for extracting this information. A new drip classification scheme is introduced, which facilitates the identification of stalagmites fed by seasonally responsive drips and which highlights the wide variability in drip types feeding stalagmites. This hydrological variability, combined with seasonality in Earth atmospheric processes, meteoric precipitation, biological processes within the soil, and cave atmosphere composition means that every stalagmite retains a different and distinct (but correct) record of environmental conditions. Replication of a record is extremely useful but should not be expected unless comparing stalagmites affected by the same processes in the same proportion. A short overview of common microanalytical techniques is presented, and suggested best practice discussed. In addition to geochemical methods, a new modelling technique for extracting meteoric precipitation and temperature palaeoseasonality from stalagmite $\delta^{18}\text{O}$ data is discussed and tested with both synthetic and real-world datasets. Finally, world maps of temperature, meteoric precipitation amount, and meteoric precipitation oxygen isotope ratio seasonality are presented and discussed, with an aim of helping to identify regions most sensitive to shifts in seasonality.

1. Introduction

Over the past few decades stalagmites have become one of the most important terrestrial archives of climate and environmental change. Their widespread distribution, amenability to

radiometric dating, and capacity for retaining seasonal to decadal-scale environmental information have made them indispensable archives for a wide variety of climate information, most commonly rainfall or temperature variability. The field has developed rapidly, and it is now clear that stalagmites generally do not record a single climate parameter (e.g., cave temperature, rainfall amount) exclusively, but instead record a combination of processes. It is increasingly acknowledged that every stalagmite contains a robust history of some aspect of environmental change. The issue is one of complexity; generally speaking, the stalagmite with the least complex signal is considered the ideal. Records generated from stalagmites with more complex stratigraphies, whose drip flow route changes through time, or that are influenced by numerous environmental processes, often prove more difficult to interpret. Some stalagmite records may miss short-lived climate excursions because they are fed by drips that do not respond to the transient climate forcing in question. Others might lose sensitivity or respond non-linearly to a climate forcing; for example, a stalagmite might record droughts faithfully, but miss exceptionally wet intervals when the epikarst (the highly fractured transition zone between soil and bedrock) is saturated with water. To exacerbate the issue further, most stalagmite records lack the requisite resolution to detect palaeoseasonality, an aspect of the climate signal that is increasingly recognised as critical to the interpretation of geochemical records from stalagmites (Baldini et al., 2019; Morellón et al., 2009; Moreno et al., 2017). In other words, the desired climate signal is often compromised by: i) inherent complexities associated with the hydrological transfer of the climate signal to the stalagmite, ii) overprinting of the desired climate-driven signal by other environmental variables, and iii) bias introduced via the necessarily selective sampling of the stalagmite for analysis. The challenge for palaeoclimatologists is to extract and correctly interpret the desired climate signal from a stalagmite, bearing these complexities in mind.

The detection of a seasonality signal within a stalagmite can greatly help interpret all datasets from a stalagmite sample, of any temporal resolution. For example, the detection of a seasonal geochemical cycle can contribute to chronological models (Baldini et al., 2002; Carlson et al., 2018; Ridley et al., 2015b), in some cases permitting the development of high-precision chronologies over extended time intervals (Ban et al., 2018; Carlson et al., 2018; Duan et al., 2015; Nagra et al., 2017; Ridley et al., 2015b; Smith et al., 2009). Unlike most other laminated records (e.g., tree rings, ice cores), high-precision radiometric dates can anchor stalagmite layer count chronologies, reducing accumulated counting errors. Proxy information from laminated stalagmites can be linked to environmental variability at seasonal resolution (Matthey et al., 2010; Orland et al., 2019; Ridley et al., 2015b), allowing much needed insights into past climatic dynamics that are difficult to obtain otherwise.

The fact that stalagmites can reveal palaeoseasonality, a notoriously difficult climate parameter to reconstruct, is critical for identifying wholesale shifts in climate belts. For example, monthly-scale geochemical data from a stalagmite has detected variability in the Intertropical Convergence Zone influence on rainfall seasonality in Central America over the last two millennia (Asmerom et al., 2020) and the shift from a maritime to a more continental climate in western Ireland in the early Holocene (Baldini et al., 2002), transitions which must otherwise be inferred using annual- to centennial-resolution data (e.g., Breitenbach et al., 2019). High spatial resolution approaches yielding palaeoseasonality can distinguish rainfall occurring at different times of the year, for example, monsoonal rainfall versus dry season rainfall (Ban et al., 2018; Ronay et al., 2019), providing a wealth of information not attainable by other means.

Seasonality is one of climate's most important aspects, and this is reflected in the basic subdivisions of the Köppen system, the most commonly used climate classification scheme (Köppen, 1918; Peel et al., 2007). Reconstructing past seasonality is not only relevant for pure palaeoclimatological studies, but also for palaeobotany and archaeology, and for establishing a benchmark by which to compare recent changes in seasonality during the Anthropocene; recent research suggests seasonality in rainfall (e.g., Feng et al., 2013) and temperature (e.g., Santer et al., 2018) are shifting under modern climate change. This is particularly concerning because changing seasonality has had broad ecological and social implications in the past. For example, human dispersal through Asia was limited more by water availability rather than temperature, and likely followed habitable corridors with favourable rainfall seasonality (Li et al., 2019; Parton et al., 2015; Taylor et al., 2018). Also, the domestication and dispersal of crops are linked to rainfall seasonality, because optimal growth conditions depend on hydrological conditions. In the Fertile Crescent, barley and wheat were sown in autumn, because in this semi-arid region the winter rains are the limiting factor for their prosperity (Spengler, 2019). Similarly, abundant evidence now exists that variability in seasonal rainfall has played a key role in the waxing and waning of major civilisations (Hsiang et al., 2013; Kennett et al., 2012).

Despite the clear importance of reconstructing palaeoseasonality, it is rarely directly observable in climate proxy records. The obfuscation of seasonality by undersampling or aliasing is often a consequence of logical and pragmatic choices designed to maximise returns from available resources. Ideally, analyses would resolve nearly the full climate signal residing within every stalagmite, but this is neither logistically (given the time and funding required) nor realistically (given that the karst system transmutes the signal) possible.

Here we review both the advantages of obtaining palaeoseasonality information and methods for its reconstruction using stalagmite geochemistry and modelling, as well as common issues in extracting this information. A short review of the history of speleothem science and techniques frames the discussion and highlights how speleothems have become the premier archives for annual- to sub-annual scale terrestrial climate reconstructions, particularly during the Quaternary. We also suggest a methodology to maximise the likelihood of successfully extracting palaeoseasonality information from a stalagmite, including evaluating the hydrological characteristics of the drip feeding a stalagmite sample prior to collection, modelling palaeoseasonality from lower resolution data, and determining the seasonality of the climate at (and in regions near) the site.

2. Background and technique development

Very early studies demonstrated the potential of stalagmites to record climate information (Allison, 1923, 1926; Broecker, 1960; Orr, 1952). However, the real growth in the application of stalagmites as climate archives occurred after the convergence of Thermal Ionisation Mass Spectrometry (TIMS) uranium-thorium dating of stalagmites in the 1990s (e.g., Edwards et al., 1987; Edwards and Gallup, 1993) (which allowed accurate dating) and high resolution sampling techniques in the 2000s (permitting the reconstruction of climate on sub-decadal timescales). The subsequent development and proliferation of multi-collector inductively coupled plasma mass spectrometry (MC-ICP-MS) permitted extraordinarily robust (precise and accurate) chronological control (e.g., Cheng et al., 2013; Hellstrom, 2003; Hoffmann et al., 2007), while the development of a variety of microanalytical techniques provided climate proxy information of an unparalleled temporal resolution. The realisation in the late 1990s

(Roberts et al., 1998) and early 2000s that stalagmite carbonate trace element compositions and isotope ratios often vary seasonally (Baldini et al., 2002; Fairchild et al., 2000; McMillan et al., 2005; Treble et al., 2003; Treble et al., 2005b) opened the door to the investigation of palaeoseasonality on an unprecedented level.

2.1. Increasing resolution of analysis

Immense technical progress has facilitated the transition from the first speleothem studies, which broadly placed periods of speleothem growth into the global climatic context (Harmon, 1979; Hendy and Wilson, 1968; Thompson et al., 1975), to increasingly detailed sub-annual resolution hydroclimate reconstructions (Fairchild et al., 2001; Johnson et al., 2006; Liu et al., 2013; Matthey et al., 2008; Maupin et al., 2014; Myers et al., 2015; Ridley et al., 2015b; Ronay et al., 2019; Treble et al., 2005a). Methodological developments, particularly after the mid-2000s and particularly with respect to trace element analysis, greatly reduced the required sample size and increased measurement precision. This included the widespread adoption of micromilling techniques (Spötl and Matthey, 2006), laser ablation (Müller et al., 2009; Treble et al., 2003), secondary ionisation mass spectrometry (Baldini et al., 2002; Fairchild et al., 2001; Finch et al., 2001; Orland et al., 2008, 2009), and the development of protocols for stable carbon and oxygen isotope measurements with reduced sample sizes (Breitenbach and Bernasconi, 2011).

Here, we apply the recently compiled Speleothem Isotope Synthesis and Analysis (SISAL) database v1b (Atsawawaranunt et al., 2018; Comas-Bru et al., 2019) to document the evolution of speleothem stable isotope record resolution. SISAL was created with the primary

objective of providing access to a comprehensive repository of published stalagmite $\delta^{18}\text{O}$ records to the palaeoclimate community and for climate model evaluation (Comas-Bru and Harrison, 2019; Comas-Bru et al., 2019). SISALv1b contains 455 speleothem records (i.e., SISAL ‘entities’) from 211 globally distributed caves published since 1992 (Comas-Bru et al., 2019). More than half the records (264) included in the database cover at least portions of the last 10,000 years.

To investigate how stable isotope record resolution has evolved over the last three decades, we extracted all records from the database and calculated their temporal resolution as the absolute difference between two consecutive samples. Hiatuses and gaps in the individual records were excluded from the analysis, as these would have erroneously suggested much lower resolution than that actually present. In a second step, we performed the same calculation, considering only Holocene records.

The analysis reveals how the number of speleothem stable isotope records steadily increased with publication year (Figure 1), highlighting the increased popularity of speleothem science over the past three decades. A trend of increasing temporal resolution with time becomes apparent after binning all records published in the same year and calculating their mean resolution (Figure 1). This trend becomes even clearer when only Holocene records are considered, with a particularly striking increase in resolution over recent years (post-2010) (records pre-2010: mean resolution = 50.1 years, STDEV = 38.9 years; records between 2010 and 2018: mean resolution = 16.5 years, STDEV = 7.4 years), and is likely related to the widespread adoption of microanalytical advances. Additionally, a record’s resolution will typically depend on the time period covered by the record; in general, resolution is higher in Holocene records compared to the full dataset, which includes older records as well. This

partly arises because of greater availability of independent data and information on climate conditions during more recent time intervals, thus requiring higher resolution records to tackle relevant research questions. It may also be partially due to typically lower growth rates during the last glaciation compared to the Holocene. However, overall only nine of the records in SISALv1b have resolution <0.5 years, allowing for investigations of paleoseasonality. This highlights the difficulties often encountered with conventional sampling techniques, as this compilation only includes stable isotope records, and does not consider other methods (e.g., laser ablation trace element analysis), which can generate higher resolution time-series. The increasing resolution possible via technological developments has largely involved the analysis of trace elements, whereas stable isotope analysis still predominantly relies on micromilling or drilling techniques.

2.2. Transition from temperature to rainfall amount to seasonality

Early speleothem palaeoclimate studies focused on using $\delta^{18}\text{O}$ to generate quantitative cave temperature records (Gascoyne et al., 1980; Hendy and Wilson, 1968; Lauritzen, 1995; Lauritzen and Lundberg, 1999), based on the insight that oxygen isotope fractionation during carbonate deposition is temperature dependent (Epstein et al., 1951; O'Neil et al., 1969), and building on similar work on marine carbonates (Emiliani, 1955). It was quickly recognised however that speleothem $\delta^{18}\text{O}$ is a complex mixed signal reflecting variations in cave temperature, changes in dripwater isotope composition, and various kinetic effects, which severely hamper the use of this proxy for quantitative temperature reconstructions (McDermott, 2004). The subsequent shift in how speleothem $\delta^{18}\text{O}$ is interpreted led to its establishment as a proxy for past hydroclimate changes, including atmospheric circulation,

210 regional temperature, moisture source dynamics, and amount of precipitation (Lachniet,
211 2009).

212 At the same time, the toolkit of geochemical proxies available to speleothem researchers
213 continued to expand. In particular, trace element concentrations in speleothem carbonate
214 emerged as tracers for numerous processes, from surface productivity to karst hydrology and
215 transport (Borsato et al., 2007; Fairchild et al., 2001; Huang and Fairchild, 2001; Treble et al.,
216 2005a). The combination of multiple proxies measured on the same speleothem provided a
217 means to disentangle complexities regarding mixed signals in individual proxies and allowed
218 a progressively deeper understanding of the archive and the associated processes in soil,
219 karst, atmosphere, and cave. In tandem with these developments regarding the climate proxy
220 development, monitoring of cave and local atmospheric conditions became increasingly
221 important, as it was recognised that understanding sometimes highly localised controls on
222 geochemical signatures is crucial for their interpretation (Genty, 2008; Matthey et al., 2008;
223 Matthey et al., 2010; Spötl et al., 2005; Verheyden et al., 2008).

224 The presence of annual petrographic cyclicity within stalagmites was recognised very early on
225 (Allison, 1926). The later identification of visible and luminescent annual banding (Baker et
226 al., 1993; Broecker, 1960; Shopov et al., 1994) underscored that the deposition, mineralogy,
227 and chemical composition of speleothems varied seasonally. However, the concept of
228 seasonal shifts in climate variables (e.g., temperature, precipitation) as contributing to the
229 net multi-annual climate signal did not gain traction until the early to mid-2000s (Wang et al.,
230 2001). Cave monitoring revealed drip rate seasonality in Pere Noel Cave, Belgium (Genty and
231 Deflandre, 1998), Crag Cave, Ireland (Baldini et al., 2006), and in Soreq Cave, Israel (Ayalon et
232 al., 1998), and seasonality was discussed within the context of a speleothem-based trace

element study at Grotta di Ernesto, Italy (Huang et al., 2001). Meteorological data were compared to seasonal trace element data for an Australian stalagmite (Treble et al., 2003), and the potential to use seasonal-scale geochemical data to reconstruct the East Asian Summer Monsoon (EASM) was investigated using a stalagmite from Heshang Cave, China (Johnson et al., 2006). Studies coupling cave environmental monitoring and ‘farmed’ carbonate precipitates were critical for clarifying the links between hydrological and cave atmosphere conditions on the chemistry of stalagmites, including at a seasonal scale (Czuppon et al., 2018; Moerman et al., 2014; Sherwin and Baldini, 2011; Tremaine et al., 2011). Drip monitoring was also key for establishing how cave hydrology attenuates seasonal and interannual rainfall variability, and was used to predict ENSO variability preservation within stalagmites (Chen and Li, 2018; Moerman et al., 2014). These studies all illustrate that a thorough understanding of annual geochemical cycles requires the development of extensive cave monitoring records, which highlight the complexities inherent in signal transfer from surface environment to the stalagmite.

2.3. Importance of monitoring for understanding the seasonal signal

Monitoring environmental conditions in and above a cave at a high temporal resolution greatly improves the accuracy of palaeoclimate interpretations derived from stalagmites. Linking proxy characteristics at a given site with current environmental conditions via monitoring is relevant for reconstructing past conditions. Although modern conditions may differ from ancient conditions, monitoring the cave environment elucidates processes operating at a site, including the timing and extent of ventilation and the general nature of a

255 hydrological signal, acknowledging that some hydrological re-routing may have occurred
256 through time for certain drip types.

257 Understanding a stalagmite geochemical proxy record is difficult without first understanding
258 how that signal is transferred and altered from the external environment to the sample.
259 Environmental changes affecting the seasonal signal fall under four main categories: **i) Earth**
260 **atmospheric, ii) Meteoric precipitation, iii) biological** (e.g., soil processes), and **iv) cave**
261 **atmospheric.**

262 **Earth atmospheric** processes affect the seasonality signal retained within stalagmites by
263 influencing meteoric precipitation isotope ratios at the cave site. Possibly the most common
264 atmospheric process is the seasonal variation in precipitation $\delta^{18}\text{O}$ induced by shifts in the
265 temperature-dependent water vapour-meteoric precipitation fractionation factor. Other
266 related changes in atmospheric processing include seasonal shifts in moisture source and
267 pathway of the moisture package to the cave site, as, for example, in monsoonal settings.

268 **Meteoric precipitation:** Meteoric precipitation variability regards the nature of the primary
269 rainfall amount-derived seasonality signal. Here we include meteoric precipitation amount
270 and seasonal distribution as separate from 'Earth atmospheric' processes (such as changes in
271 source moisture source), although clearly the latter affect the former. Meteoric precipitation
272 is a fundamental control on stalagmite seasonality that is worth considering independently of
273 other atmospheric processes. Stalagmites deposited in monsoonal climates (e.g., the East
274 Asian Summer Monsoon, Indian Summer Monsoon, South American Monsoon, and Australian
275 Summer Monsoon) with distinct wet and dry seasons are excellent examples of samples
276 whose geochemistry generally (but not always) responds to hydrologic seasonality. In
277 temperate mid-latitude settings with more evenly distributed rainfall, hydrological shifts

might record less seasonal than inter-annual (e.g., ENSO) dynamics or possess a seasonal bias (see section 3.1) derived from effective infiltration dynamics.

Biological (soil-derived) seasonality is the least clearly defined control, and predominantly affects the trace element composition and carbon isotope ratio of cave percolation waters. However, evidence also exists that increased soil bioproductivity can affect oxygen isotope ratios by preferential uptake of water during the growing season during intervals with substantial surface vegetation (Baldini et al., 2005). Trace element transport critically depends on the biological activity and water supply, both factors that are inherently variable and not necessarily in-phase. Hydrology can affect biological seasonality, as leaching of organic matter and trace elements from freshly decomposed litter depends on excess infiltration. Soils may thus produce a wet season pulse of colloidal material (organics as well as weathering products) which contributes to an annual peak in trace element concentrations in some samples; such dynamics are highly site-specific. The evidence for this pulse is derived both from synchrotron-based stalagmite studies (e.g., Borsato et al., 2007) and daily-scale automated dripwater collection schemes (Baldini et al., 2012). Treble et al. (2003) suggest phosphorous enrichment in stalagmite carbonate stemming from seasonal infiltration pulses, and monitoring at Shihua Cave (China) revealed that organic carbon was transported during the wet season (Ban et al., 2018; Tan et al., 2006). Whether this pulse is truly independent from hydrological variability is unclear, but some evidence from dripwater monitoring in temperate Irish caves suggests that the seasonal trace element pulse is not associated with increased autumnal water throughput, but rather with seasonal vegetation die-back (Baldini et al., 2012). In monsoonal north-eastern India biologically-induced litter decomposition reaches a maximum in early summer (Ramakrishnan and Subhash, 1988), which increases

element availability in the soil that can be leached during the entire wet season (Khiewtam and Ramakrishnan, 1993). The transport of trace elements may also hinge directly on the presence of natural organic matter in dripwater, which may link the dripwater directly to surface bioproductivity (Hartland et al., 2012; Hartland et al., 2011). Thus, biological seasonality is highly site-specific and likely variable through time; this and the complexities outlined above underscore the importance of dripwater monitoring campaigns.

Cave atmospheric variability can also impart a seasonal signal to a stalagmite geochemical record. Seasonal changes in cave air mixing with outside air lead to conditions within the cave that lower cave air carbon dioxide partial pressure ($p\text{CO}_2$) and potentially even contribute to dripwater evaporation, promoting calcite deposition. Cave atmosphere variability, induced by ventilation (through thermal gradients or changing wind patterns) therefore affects the calcite deposition seasonality, as well as kinetic fractionation amount. Excellent examples of caves whose stalagmites are affected by this variability include New St. Michael's (Gibraltar) (Mattey et al., 2016; Mattey et al., 2010) and numerous caves in Central Texas (Banner et al., 2007; Breecker et al., 2012; Cowan et al., 2013; Wong et al., 2011). These effects are discussed in detail below (Section 3).

3. Issues inherent to speleothem-based high-resolution climate reconstructions

Detecting any seasonal component in a stalagmite climate signal includes quantifying growth rate and input signal seasonality. It is worth noting that the input signal is sometimes unexpected, and a thorough site monitoring scheme can help identify the main contributing factors. For example, although many trace elements (and particularly Mg) are affected by recharge (often via prior carbonate precipitation (PCP) mechanisms (Fairchild and Treble, 2009)), other factors can also influence (seasonal) stalagmite geochemistry. This is the case

at ATM Cave, Belize, where various trace elements (including magnesium) increase in concentration at the beginning of the annual rainy season, and are probably linked to dry deposition during the preceding dry season followed by transport to the stalagmite with the onset of the rainy season (Jamieson et al., 2015). In other cases, the advection of atmospheric aerosols directly into the cave can affect the stalagmite trace element signal (Dredge et al., 2013). Seasonal non-deposition caused by either drying of the feeder drip or by seasonally high cave air $p\text{CO}_2$ can bias any record where every data point integrates more than a few months of deposition. From this perspective, most stalagmite records integrate palaeoseasonality information to some extent, but, without appropriate monitoring strategies in place, deconvolving the extent to which the shifting seasonal signal dominates the overall record is difficult.

3.1. Mixing within the aquifer

The degree of recharge mixing within the aquifer and epikarst is a fundamental control on the preservation of a seasonality signal within stalagmites. A long residence time and/or thorough mixing within the overlying aquifer can greatly attenuate any hydrological seasonal signal, and understanding the hydrology feeding a cave drip is therefore critical (Atkinson, 1977; Ayalon et al., 1998; Baker et al., 1997; Baker and Brunsdon, 2003; Baker et al., 2019; Kaufman et al., 2003). For conservation and logistical reasons, monitoring and classification of the drip should ideally occur prior to sampling a stalagmite.

Smart and Friedrich (1987) undertook one of the earliest efforts to comprehensively categorise cave drips. Their scheme involved measuring drip rates at G.B. Cave, in the Mendip

Hills, UK, and parameterising them by plotting maximum drip rate versus the coefficient of variation (C.V.; the standard deviation divided by the mean multiplied by 100). Baker et al. (1997) later modified the scheme, dividing drips into six categories (seepage flow, seasonal drip, percolation stream, shaft flow, vadose flow, subcutaneous flow). Other classification schemes (e.g., Arbel et al., 2010; Arbel et al., 2008) focussed on analysing drip hydrographs, and suggested terminology such as 'post-storm', 'seasonal', 'perennial', and 'overflow', which are broadly consistent with the categories introduced by Smart and Friedrich (1987). The introduction of automated drip loggers revolutionised the field (Mattey and Collister, 2008), partly by ensuring that transient hydrological events were not missed. This ensured a substantially more robust characterisation of drips than that possible via manually measuring drip rates only during on-site visits.

Understanding the hydrology feeding a stalagmite is fundamental for determining if a stalagmite retains a seasonal signal. Drip rate is controlled by surface processes (e.g., meteoric precipitation, evaporation, soil moisture capacity, and susceptibility to runoff) and aquifer characteristics including reservoir capacity and bedrock permeability (Markowska et al., 2015; Treble et al., 2013). Bedrock pathways recharging a drip are broadly divisible into matrix (or 'diffuse') and conduit (or 'fracture') flows (Ayalon et al., 1998; Baker et al., 1997; Perrin et al., 2003; Smart and Friedrich, 1987), and recent models suggest that many drips are a combination of the two. Matrix permeability typically refers to either the primary intra-granular bedrock permeability or to secondary permeability along fine fractures, and is characterised by a slow response to precipitation events and a large reservoir capacity (Atkinson, 1977; Smart and Friedrich, 1987). Fracture permeability relates to potentially solution-enlarged bedding plane partings and joints and is characterised by a rapid to intermediate response to precipitation events, and a low to moderate storage capacity.

Conduit permeability refers to often solutionally-enlarged pipe-like openings >1 cm in diameter (Atkinson, 1977; Smart and Friedrich, 1987). Such conduit flow is characterised by a rapid response to storm events followed by a rapid return to baseline flow (Baldini et al., 2006), and often carries chemically aggressive waters that do not allow secondary carbonate deposition. Large conduits or bedding planes may intersect a network of more diffuse hydrological pathways, leading to dual-component flow where the fracture is itself fed by some diffuse recharge in addition to the fracture flow. The hydrologic permeability of the fracture flow component compared to the diffuse flow component essentially defines the drip type; 100% diffuse flow would exhibit no response to storm events, whereas 100% fracture flow would usually have no drip except for immediately following storm events large enough to activate the pathway (Figure 2). Most drips would fall along the spectrum between these two endmembers; a constant base drip (the diffuse flow component) combined with a variably rapid response to storm events (the fracture flow component).

From a seasonality perspective, pure fracture-flow drips vary considerably seasonally but may experience occasional dripwater undersaturation and/or drying, and consequently the resultant stalagmite could have abundant microhiatuses (hiatuses in growth too brief to leave a clear petrographic expression, or appear in chronological models (Baker et al., 2014; Moseley et al., 2015) also referred to as ‘crypto-hiatuses’ (Stoll et al., 2015). Drips characterised by 100% diffuse flow would be stable with little hydrological or biological seasonality. The likelihood for microhiatuses or drying is low for stalagmites fed by diffuse flow, but the seasonal signal is probably muted, unless at a site where the seasonal signal is controlled by a forcing other than hydrological variability (see Section 2.4.). The optimal hydrology for imparting seasonality onto a stalagmite is a drip fed by moderately diffuse flow that is

responsive to monthly-scale shifts in rainfall, but that does not have a substantial fracture component to transmit event-scale (and possibly undersaturated) water.

3.2. Non-deposition and seasonal bias in samples

Although growth hiatuses lasting longer than a few years are often (but not always) apparent within stalagmites as horizons of detrital material followed by competitive growth of carbonate crystals (Broughton, 1983), brief growth hiatuses occurring seasonally are often undetectable (though occasionally they have a petrographic manifestation). Thus, the existence of these microhiatuses is often inferred by applying monitoring data to isolate intervals through the year where environmental conditions suggest temporary non-deposition could exist. Because drip rate is one of the fundamental controls on stalagmite growth (Genty et al., 2001), the use of drip loggers to detect seasonal drying of the stalagmite feeder drip is important for understanding whether a stalagmite record excludes a certain season's climate information.

Additionally, careful examination of sample petrography can reveal important insights into the nature of the climate signal retained by a stalagmite. Petrographic microscopy helps in identifying growth interruptions caused by lack of water, and dissolution features caused by undersaturated dripwater. An excellent example of this approach exists for Holocene stalagmites from northern Spain (Railsback et al., 2011; Railsback et al., 2017); the analysis reveals horizons of dissolution (termed Type 'E' surfaces), interpreted as reflecting occasional undersaturation of the feeder drip. Other examples of careful petrographic analysis informing seasonality studies are provided from Drotsky's Cave, Botswana, where the alternating wet

and dry seasons are manifested by alternating calcite and aragonite (respectively) couplets (Railsback et al., 1994) and from Grotta di Carburangeli, Italy, where columnar fabrics were interpreted as reflected pronounced seasonal variability in drip rates (Frisia, 2015).

Cave air carbon dioxide concentrations ($p\text{CO}_2$) have shown to be inversely linked to stalagmite growth rate (Banner et al., 2007; Sherwin and Baldini, 2011). For example, in a study of three caves across Texas, it was observed that stalagmite calcite growth rate was inversely correlated with cave air $p\text{CO}_2$ (Banner et al., 2007). Negligible calcite growth and even microhiatuses occurred during the warmest summer months, when cave air $p\text{CO}_2$ increased due to low cave ventilation rates (Banner et al., 2007). Elevated cave air $p\text{CO}_2$ discourages the dripwater's thermodynamic tendency to degas CO_2 , thereby slowing the carbonate precipitation rate. In most caves where the entrance is located above the rest of the cave, outside air with low $p\text{CO}_2$ advects into the cave when the outside air density becomes greater than the cave air density (e.g., Spötl et al., 2005). This is usually driven by temperature gradients; colder, denser air moves down into a cave during winter, lowering the cave air $p\text{CO}_2$ and encouraging stalagmite growth (James et al., 2015). However, cave air $p\text{CO}_2$ does not act in isolation, but instead the critical growth determining variable is the differential between cave air $p\text{CO}_2$ and dissolved CO_2 in dripwater (Baldini et al., 2008). Carbonate deposition thus could increase in the high cave air $p\text{CO}_2$ season if the dripwater had equilibrated with an atmosphere with even greater seasonal dissolved CO_2 increases (e.g., stemming from seasonal soil bioproductivity increases) which exceed those of the cave atmosphere. These types of drips are generally quite responsive to rain events, so determining if a seasonal growth bias exists should incorporate both hydrology and cave atmospheric chemistry. Drips with stable drip rates, that are not responsive to storm events may have more constant dissolved CO_2 and therefore

seasonal deposition rates that are affected exclusively by cave air $p\text{CO}_2$ dynamics. However, several recent publications suggest that dripwater equilibrates not only with soil air, but also with a reservoir of carbon dioxide within the unsaturated zone of aquifers (termed ‘ground air’) that may have very high $p\text{CO}_2$ values (2 to 7%), much higher than typical soils (0.1 to 2%) (Baldini et al., 2018; Bergel et al., 2017; Markowska et al., 2019; Matthey et al., 2016; Noronha et al., 2015). Thus, it is possible that drip dissolved CO_2 is often near-constant, having equilibrated with a ground air reservoir of near-constant $p\text{CO}_2$, and that carbonate precipitation is anticorrelated with cave air $p\text{CO}_2$ regardless of drip type, although this requires further research. The complexities of cave atmospheres are now reasonably well understood, but more long datasets describing the dissolved CO_2 of cave drips are essential for determining the variability of cave percolation waters.

Although a temperate-zone (Peel et al., 2007) cave’s tendency to ventilate during the winter is generally predicable from seasonality in external temperature (James et al., 2015), occasionally cave geometry provides a more dominant control. In New St. Michael’s Cave in Gibraltar, ventilation is driven by seasonal changes in wind speed and direction (Matthey et al., 2016; Matthey et al., 2009). The cave experiences the lowest cave air $p\text{CO}_2$ values in summer, and consequently growth (assuming constant drip rate) is biased towards summer (Baker et al., 2014). The cave’s position high within the Rock of Gibraltar contributes to strong winds and unusual seasonal ventilation, illustrating how cave position or geometry can dominate seasonal ventilation patterns. Other examples include Bunker Cave in Germany, where an essentially horizontal plan with little altitude difference between entrances produces very little seasonal variability in $p\text{CO}_2$ (e.g., Riechelmann et al., 2011; Riechelmann et al., 2019),

and Císařská Cave (Czech Republic) where a U-shaped cave produces nonlinearities between air temperature, density, and ventilation (Faimon and Lang, 2013).

Because seasonal microhiatuses can lack either a petrological or a geochemical manifestation, cave monitoring is critical for assessing the likelihood of seasonal non-deposition (Shen et al., 2013). Stalagmite growth rate modelling, informed by cave monitoring data, can provide invaluable information regarding how seasonal growth variability affects geochemical climate proxy records integrating more than one year's worth of growth. For example, seasonal non-deposition during summer due to either high evapotranspiration-induced drip cessation or elevated cave air $p\text{CO}_2$ might bias lower resolution records towards wintertime rainfall values (generally towards lower $\delta^{18}\text{O}$ values) (e.g., James et al., 2015) at sites where drip water is not well mixed. Stoll et al. (2012) used an inverse model to illustrate that rainfall seasonality shifts relative to the cave air $p\text{CO}_2$ can greatly affect PCP and consequently stalagmite trace element concentrations. Baldini et al. (2008) used theoretical stalagmite growth rate equations and theory developed previously (Buhmann and Dreybrodt, 1985; Dreybrodt, 1980, 1988, 1999), coupled with monitoring information, to model stalagmite $\delta^{18}\text{O}$ for various drips within Crag Cave, Ireland. The results suggest that the amount of time integrated by the analyses, the nature of the drip, and the ventilation dynamics of the cave, all strongly modulate carbonate $\delta^{18}\text{O}$ signals.

These studies all highlight how characterising the surface and depositional environment is critical for interpreting the climate signal. Either seasonal microhiatuses or reduced growth may bias annual- (or coarser-) scale geochemical records towards particular seasons. Additionally, it is also important to consider how regional climate shifts may have affected a sample in the past, because modern processes may not have applied throughout the record.

Understanding climate signal emplacement processes within stalagmite carbonate is therefore fundamental for building robust climate records.

3.3. A drip classification scheme to quantify seasonal responsiveness

Existing drip classification schemes are not designed to characterise the likelihood that a sampled stalagmite retains a hydrologically induced seasonal signal. However, such knowledge is crucial if research goals include a component of seasonal climate reconstruction. Here, we introduce a new drip categorisation scheme that not only permits the identification of stalagmites most likely to retain a hydrology-modulated seasonal climate signal, but that also helps predict the general nature of the climate signal within any sample. This is important for both the accurate interpretation of stalagmite palaeoclimate records, but also for cave conservation (i.e., to maximise the usefulness of collected samples for the purpose of the research goals) and for the appropriate usage of research-related resources. A seasonal-resolution stable isotope record of any length requires considerable resources, and we hope that this new drip classification scheme will help direct these resources to appropriate stalagmite samples.

The scheme's essence is the collection of (ideally) at least one year of hourly drip rate data for a drip feeding a stalagmite of interest. For every month, the minimum and maximum hourly drip rate values are extracted. When plotted, these data reveal the extent to which the drip is affected by seasonal activation of fracture permeability, and what proportion of the drip consists of diffuse 'baseflow' (and whether this varies through the year). Drip categorisation then involves evaluating the distribution of the datapoints, and is described with terminology broadly consistent with the Smart and Friedrich (1987) scheme. Because the

classification scheme uses multiple data points per site, a very large number of possible combinations of descriptors are possible. For example, some drip sites (e.g., drip site YOK-LD within Yok Balum Cave, Belize; (Ridley et al., 2015a) are fed by a slow diffuse flow most of the year, where the minimum and maximum monthly drip rates are almost identical (Figure 3). However, during wetter months an overflow route is activated, and the maximum drip rate increases substantially, whereas the minimum remains the same; this would be characterised as a diffuse drip with a seasonally active overflow component. If this overflow component is saturated with respect to calcite or aragonite, some seasonal signal may be preserved, but if the overflow water is undersaturated a stalagmite fed by this drip type has less potential for seasonal climate reconstructions. Similarly, drip YOK-SK is characterised by almost entirely invariant diffuse recharge and would not record seasonal changes in recharge (Figure 3). At another cave site (Leamington Cave, Bermuda, (Walczak, 2016), drip BER-drip #5 is fed by diffuse recharge during drier intervals of the year, but during wetter months more water is routed to the diffuse flow, increasing the base flow. Consequently, the drip does experience some seasonality without risk of undersaturation, and thus a stalagmite fed by it should retain hydrology-induced seasonality.

In this new drip classification plot, the drips that are expected to produce stalagmites that retain the clearest seasonal signal are those that plot with a slope approaching unity. In other words, those that are not fed by either an extremely diffuse drip or an extremely flashy drip, and that consequently respond to seasonal rainfall shifts without transient extreme rapid drip rate episodes caused by individual storm events (which may lead to dripwater undersaturation and signal loss). Consequently, the two drip sites plotted in Figure 3 that best display this type of behaviour (drips YOK-G and BER-drip #5) have both yielded stalagmites retaining exceptional seasonal signals, stalagmites YOK-G (Ridley et al., 2015b) and BER-SWI-

13 (Walczak, 2016). Other drip sites that have a slope approaching unity and have a pronounced difference between the highest and the lowest set of drip rates (Figure 3B) should also produce stalagmites with well-developed records of seasonality.

Importantly, this drip classification scheme equally helps to identify drips that are unlikely to produce good seasonality records. For example, stalagmites fed by drips that are invariant throughout the year would not record hydrologically-induced seasonality (although a seasonal signal might still be preserved based on non-hydrological factors – see Section 2.4). Stalagmites fed by drips that have one or more monthly values plotting at the origin (i.e., no drips for an entire month, Figure 3D) would contain seasonal microhiatuses and would consequently not record that interval's climate information. Drips where the diffuse flow component (i.e., the monthly minimum flow) remains constant but the fracture flow component (i.e., the monthly maximum flow) changes considerably (Figure 3C) may experience undersaturation and either non-deposition or even corrosion of the stalagmite.

This classification scheme comes with some caveats. First, as discussed in Section 2.4., it is possible that the seasonality signal is imparted onto the stalagmite independent of hydrology. If seasonal cave ventilation controls the seasonality signal, the application of the scheme would differ. For example, at a site with strong seasonal ventilation, a stalagmite deposited by a purely diffuse flow-fed drip would reflect a largely cave atmospheric seasonality signal (i.e., with no hydrological seasonality). This would reduce the complexity of the geochemical signal and obviate the need to deconvolve hydrological- and cave atmosphere-induced seasonality from any geochemical record produced. Second, some drips are so-called 'underflow' drip sites, which respond to recharge linearly up until a maximum drip rate and then become unresponsive to further drip rate increases. This is often caused by a constriction

in the flow pathway leading to the water egress point into the cave. Despite the lack of variability at high flow, the dripwater is still in dynamic equilibrium with recharge (unlike high residence time diffuse flow fed sites) and the stalagmite may reflect the dripwater isotopic variability. Similarly, some drips are affected by piston flow, whereby an increase in hydrologic head might push through a slug of older water, leading to an instantaneous response to recharge but of water with a signature more in keeping with 'old' water; careful monitoring can identify and mitigate these issues (see Section 3.4). Despite these caveats, this drip evaluation scheme will hopefully provide an efficient means for identifying actively growing stalagmite samples most likely to record a seasonal climate signal prior to collection of that sample.

3.4. Dripwater oxygen isotope seasonality

The extent that cave dripwater $\delta^{18}\text{O}$ ($\delta^{18}\text{O}_{\text{dw}}$) values reflect the $\delta^{18}\text{O}$ of meteoric precipitation ($\delta^{18}\text{O}_{\text{p}}$) is critical to climate studies and for understanding the palaeoseasonality signal in particular. Many publications have investigated the relationship between $\delta^{18}\text{O}_{\text{p}}$ and $\delta^{18}\text{O}_{\text{dw}}$ (Ayalon et al., 1998; Baker et al., 2019; Baldini et al., 2015; Bar-Matthews et al., 1996; Cruz Jr. et al., 2005; Duan et al., 2016; Feng et al., 2014; Harmon, 1979; Luo et al., 2014; Markowska et al., 2016; Mischel et al., 2015; Moquet et al., 2016; Moreno et al., 2014; Oster et al., 2012; Pu et al., 2016; Riechelmann et al., 2011; Riechelmann et al., 2017; Surić et al., 2017; Tadros et al., 2016; Tremaine et al., 2011; Verheyden et al., 2008; Wu et al., 2014; Yonge et al., 1985; Zeng et al., 2015). Depending on the drip site's hydrological characteristics (Arbel et al., 2010; Baker and Brunsdon, 2003; Smart and Friedrich, 1987), $\delta^{18}\text{O}_{\text{dw}}$ values may reflect $\delta^{18}\text{O}_{\text{p}}$ on timescales ranging from the annual weighted mean (Baker et al., 2019; Cabellero et al., 1996;

576 Chapman et al., 1992; Yonge et al., 1985) to individual (intense) recharge events (Atkinson et
577 al., 1985; Frappier et al., 2007; Harmon, 1979).

578 Factors such as depth below surface, residence time and mixing of the water within the
579 unsaturated zone, soil depth and texture, and aquifer hydraulics can vary between drip sites.
580 Important reservoirs for storage and mixing of effective rainfall are documented as the soil
581 and epikarst zones (Cabellero et al., 1996; Chapman et al., 1992; Gazis and Feng, 2004; Perrin
582 et al., 2003; Yonge et al., 1985). Rainwater infiltrating into the soil reservoir is variably lost to
583 evapotranspiration but in karst regions preferential recharge through dolines and grikes may
584 occasionally circumvent the soil and related evapotranspiration (e.g., Hess and White, 1989).
585 Secondary evaporation from infiltrating water can be detected using dripwater $\delta^{18}\text{O}$ and δD
586 values potted relative to the local meteoric water line (Ayalon et al., 1998; Breitenbach et al.,
587 2015). Bar-Matthews et al. (1996) observed a 1.5 ‰ $\delta^{18}\text{O}_{\text{dw}}$ enrichment relative to rainwater
588 and attributed this primarily to seasonal evaporation in the soil and epikarst zones above their
589 Israeli cave site. Evaporative enrichment of infiltrating rainwater is greater in arid and
590 semiarid regions than in temperate regions where conditions of water excess occur through
591 much of the year (Markowska et al., 2016; McDermott, 2004). Any excess, non-
592 evapotranspired water is then transmitted to the epikarst, karst, and finally the cave.
593 Dripwater residence times in the aquifer or epikarst are highly variable, ranging from minutes
594 to years, depending on soil thickness, hydraulic properties (Gazis and Feng, 2004), and drip
595 pathway (e.g., diffuse vs. conduit flow) (Baldini et al., 2006). Mixing of infiltrating rainwater
596 with existing epikarst water can buffer the climate signal and reduce seasonal $\delta^{18}\text{O}_{\text{dw}}$
597 variability from muted to invariant (within analytical error, and assuming no cave
598 atmosphere-induced seasonality) (Baker et al., 2019; Breitenbach et al., 2019; Onac et al.,

2008; Schwarz et al., 2009). At some cave sites, $\delta^{18}\text{O}_{\text{dw}}$ does not necessarily correlate with $\delta^{18}\text{O}_{\text{p}}$ shifts, most likely due to mixing within the aquifer (Moquet et al., 2016), underscoring that different hydrologies produce stalagmites retaining different environmental signals.

A recent global compilation of available dripwater monitoring data has further clarified the relationship between climate (e.g., mean annual temperature and annual precipitation) and $\delta^{18}\text{O}_{\text{dw}}$ (Baker et al., 2019). In cooler regions where mean annual temperature (MAT) < 10°C, $\delta^{18}\text{O}_{\text{dw}}$ most closely reflects the amount-weighted $\delta^{18}\text{O}_{\text{p}}$ (i.e., evaporation from the soil and epikarst does not exert much influence). In seasonal climates with MAT between 10°C and 16°C, $\delta^{18}\text{O}_{\text{dw}}$ values generally reflect the recharge-weighted $\delta^{18}\text{O}_{\text{p}}$ (see Fig. 1 of (Baker et al., 2019). In regions where MAT > 16°C, $\delta^{18}\text{O}_{\text{dw}}$ is generally higher relative to amount-weighted precipitation $\delta^{18}\text{O}_{\text{p}}$ because fractionation processes related to evaporative effects on stored karst water are more substantial (Baker et al., 2019). Stalagmite $\delta^{18}\text{O}$ records from regions experiencing high temperatures and/or aridity will probably not reflect rainfall $\delta^{18}\text{O}$ (Baker et al., 2019).

3.5. The uniqueness of each stalagmite record

Recent publications have made a case for the importance of replication in stalagmite geochemical records (Wong and Breecker, 2015; Zeng et al., 2015), which is a worthwhile and useful goal. Producing the same geochemical record from multiple samples ensures that no analytical issues exist and can facilitate correlating records whose growth intervals overlap in regions and for time periods with high signal-to-noise ratios. Particularly in cases where evidence for a short-lived climate anomaly exists, replication from within the same sample

and from other stalagmites is critical. However, stalagmite geochemistry is affected by a myriad of variables, and the precise combination of factors affecting any one sample are essentially unique. Thus, every stalagmite retains a different component of the environmental signal, and a lack of reproducibility does not necessarily indicate that a record is 'incorrect' or flawed. Even stalagmites that are affected by strong kinetic effects retain accurate environmental data; it is a matter of recognising this control, and basing any interpretations accordingly.

Unless two stalagmites are fed by a very similar drip type (often two samples growing near each other whose feeder drips share the same hydrological pathway), stalagmite records from the same cave may not match. This is a clear consequence of the diversity of possible drip pathways feeding individual stalagmites. For example, a stalagmite growing underneath a diffuse drip fed by an extremely low hydrologic permeability pathway that is unresponsive to large rain events would not contain the same record as a stalagmite growing underneath a drip with no diffuse component but that is instead fed by fracture flow. The former (diffuse flow-fed) stalagmite may retain long-term climate information but lack seasonal-scale information, whereas the latter (fracture flow-fed) stalagmite may retain some seasonal environmental information, but may also experience occasional undersaturation following large rain events, leading to microhiatuses and information loss. The fracture flow-fed stalagmite may have a more rapid overall growth rate, but may experience flow re-routing and stochastic drip variability due to solutional enlargement of the fracture pathway, potentially leading to a shorter overall growth interval due to the eventual diversion of water away from the stalagmite. Once cave- and site-specific ventilation factors are considered as well, it is apparent that no two stalagmites can yield precisely the same record; rather it is

imperative to understand the environmental conditions recorded by each individual sample. If the goal is to reconstruct seasonality, it is important to understand the nature of the seasonality signal for each potential sample, e.g., whether the sample is affected by hydrological seasonality or cave atmospheric seasonality. In the latter case, it is then favourable to select a stalagmite from a diffuse flow drip in order to simplify the extraction of the seasonal ventilation signal.

The considerable range of stalagmite records possible, even from the same site, is potentially advantageous. The individuality of stalagmite records may yield a powerful tool for the quantitative reconstruction of historically elusive environmental variables. For example, differences in oxygen isotope ratios between two samples from the same site could reflect in-cave temperature-induced kinetic fractionation effects, and modelling (Deininger and Scholz, 2019; Deininger et al., 2016; Dreybrodt, 1988; Dreybrodt and Deininger, 2014; Riechelmann et al., 2013) could theoretically yield the cave temperature, potentially even at a seasonal resolution. This perspective is consistent with the recent appreciation that speleothems deposited at isotopic equilibrium are extremely rare (Daëron et al., 2019; Mickler et al., 2006) and that kinetic effects are an integral part of the environmental signal retained by stalagmites (Millo et al., 2017; Sade and Halevy, 2017). The concept that kinetic effects are undesirable is a vestige of early studies attempting to extract absolute palaeotemperatures from stalagmite oxygen isotope ratios, in which case kinetic effects do indeed interfere with the extraction of the desired signal. However, because stalagmite $\delta^{18}\text{O}$ values are no longer considered pure in-cave temperature proxies, kinetic effects no longer present a serious issue, provided that they are considered within any interpretations. In fact, because kinetic effects often vary in sync with the primary rainfall signal (e.g., kinetic effects

tend to occur during drier periods accentuating the already elevated stalagmite $\delta^{18}\text{O}$ and $\delta^{13}\text{C}$ signature) they tend to help the climate signal stand out above background noise.

Stalagmite climate reconstructions are usually based around one record or an overlapping series of records; future research could use the differences between two records (considering in-cave kinetic effects) to reconstruct aspects of the environmental signal, including seasonal temperature shifts. Recent research utilising several stalagmites from along the same moisture trajectory across a wide region to reconstruct oxygen isotope systematics and temperature represent an exciting development in speleothem climate sciences (Deininger et al., 2017; Hu et al., 2008; McDermott et al., 2011; Wang et al., 2017), and similar methodologies could reveal in-cave fractionation processes that are ultimately relatable to temperature, potentially on a seasonal-scale. For example, changes in outside temperature-induced ventilation may affect samples fed by different hydrologies differently (promoting more kinetic fractionation in the slower dripping sample), and comparing the isotope ratio records may reveal the range of external seasonal temperature variability. We suggest that the comparison of multiple coeval stalagmite geochemical records from within the same cave site is a crucial research frontier that is well worth investigating further.

4. Analysis techniques

Detection of seasonal variations in stalagmite geochemical parameters requires sampling or analysis at sufficiently high spatial resolution to mitigate signal averaging (Figure 4). Sampling frequency should approach monthly resolution to detect a seasonality signal and to avoid aliasing issues during intervals with slower growth. This necessitates careful consideration

prior to analysis to ensure both sufficient resolution to detect seasonal-scale variability, and sufficient material for the analysis method. In addition to the pre-analysis considerations, we also recommend publishing complete micro-analytical data tables, in order to increase transparency. Below we discuss common microanalytical techniques capable of palaeoseasonality reconstruction and compare advantages and disadvantages of each.

4.1. Sampling for palaeoseasonality

Sub-sampling stalagmites for geochemical analysis requires careful planning and execution. We recommend a thorough reconnaissance of a sample's petrography using microscopy prior to geochemical analysis. The conversion of a sample into polished thin sections can provide critical information but is destructive. Reflected light microscopy provides a non-destructive alternative that can yield crucial information regarding crystal growth habit, the location of possible hiatuses, inclusions, and porosity.

The various methods available for the extraction of proxy data all require different sample amounts depending on analytical limits of detection and other factors (Fairchild et al., 2006). Methods are broadly categorizable as destructive and non-destructive, depending on the amount of material required. The former is further divisible into: i) macro-destructive (e.g., cuttings for fluid inclusion studies, low-concentration proxies like biomarkers or DNA) (e.g., Blyth et al., 2011; Vonhof et al., 2006; Wang et al., 2019a), ii) meso-destructive (e.g., conventional and micro-milling for U-series samples, stable isotopes, ICP-OES, ^{14}C) (e.g., Lechleitner et al., 2016a; Ridley et al., 2015b; Spötl and Matthey, 2006), and iii) micro-destructive (e.g., laser ablation or secondary ionization mass spectrometer (SIMS) analyses for traditional and non-traditional isotope systems, element concentrations or ratios) (Baldini

et al., 2002; Luetscher et al., 2015; Treble et al., 2007; Webb et al., 2014; Welte et al., 2016).

Non-destructive methods include (but are not restricted to): i) simple desktop scanning and photography, ii) μ XRF line scanning and mapping (e.g., Breitenbach et al., 2019; Scropton et al., 2018), iii) synchrotron analyses (e.g., Frisia et al., 2005; Vanghi et al., 2019; Wang et al., 2019b; Wynn et al., 2014), iv) phosphor mapping via beta-scanning (e.g., Cole et al., 2003), v) reflected light, and fluorescence, including confocal laser fluorescent microscopy (CLFM) (e.g., Orland et al., 2012) and other microscopy techniques (e.g. SEM, EMPA, RAMAN), or vi) X-ray Computed Tomography (CT) scanning (e.g., Walczak et al., 2015; Wortham et al., 2019). The choice of technique should consider suitability for answering the targeted research questions, and logistical considerations such as sample sectioning. Although the list above categorises techniques based on their destructiveness, it does not account for sample preparation; for example, SIMS analysis uses only a small amount of sample (i.e., essentially non-destructive), but requires sectioning of the stalagmite into centimetre-scale cubes, polishing and epoxy-mounting. Another major consideration is the length of the record required; it is possible (though labour-intensive) to produce seasonal-scale records extending hundreds or even thousands of years using micromilling, but this is not practical using SIMS, unless automated protocols allowing for unattended analysis can be developed (Orland et al., 2019).

Although macro-destructive sampling can inform interpretations based on higher resolution data, it cannot generally reconstruct seasonality on its own. Thus, here we discuss only selected meso-, micro-, and non-destructive techniques. The focus is first on ‘conventional drilling’ and ‘micromilling’ of powder samples, which probably are the most widely used techniques to obtain material for inorganic chemistry, followed by the highly versatile, fast, and cost-effective laser ablation sampling (LA-ICP-MS). SIMS requires substantial sample preparation, offers excellent resolution and is a good choice in situations requiring in-depth

characterisation of a short interval. Synchrotron- μ XRF (SR- μ XRF) has advanced considerably over the past decade, and it is now possible to obtain high-resolution (0.5-5 μ m) quantitative trace element data non-destructively through fast scanning of large samples (Borsato et al., 2019). Below we describe the relevance and applicability of these techniques towards the reconstruction of palaeoseasonality.

4.1.1. Conventional drilling

Conventional drilling (or ‘spot-sampling’) (Fairchild et al., 2006) is the drilling of powders from discrete spots, that are normally separated by unsampled material, and is still amongst the most widely used methods to obtain carbonate powders from speleothems. This method is comparably fast and, with a sufficiently small drill bit (typical \varnothing ca. 0.2-1 mm), can achieve a spatial resolution of up to 0.3-0.5 mm along the growth axis, although more frequently the resolution is \sim 1 mm. Conventional drilling is ideally performed with instruments that allow computer-aided control of x-y-z dimensions, such as Sherline® or Mercantek® instruments.

With typical stalagmite growth rates of 0.1 to 0.2 mm year⁻¹, this technique is usually inadequate when targeting sub-annual resolution (Figure 5). If used on samples with growth rates approaching twice the sampling interval, aliasing may occur and unfavourably affect the recovery of high-frequency variability (Fairchild et al., 2006). Furthermore, this type of spot sampling usually does not integrate all the carbonate material, i.e. the time slices at the top and bottom of the hole are under-represented in the average for the drill-hole; this undersampling could miss short-lived climate excursions. Consequently, we cannot recommend conventional drilling for recovering a seasonal signal, although the technique is effective at quickly producing a lower-resolution record and is well suited for longer records

of climate (e.g., those covering multiple glacial cycles), and for screening potential target stalagmites. Additionally, conventional drilling is possible on a large stalagmite slab, obviating the need for sectioning into multiple smaller slabs. A related technique which is preferred for sampling at seasonal scale is micromilling, discussed below.

4.1.2. Micromilling

Micromilling refers to continuous sample cutting along a trench parallel to a stalagmite's growth axis (Fairchild et al., 2006; Spötl and Matthey, 2006). Usually performed with computer-controlled milling devices (such as the ESI/New Wave micromill) this technique can achieve ~20-micron spatial resolution (e.g., Myers et al., 2015), but is critically dependent on the textural characteristics of the sample. Dense columnar, fascicular, radiaxial, or radial fibrous calcites are the most suitable material, but needle-like aragonite can also be sampled, although gaps between needle-shaped crystals may lead to loss of sample and require painstaking cleaning procedures. The sample morphology throughout the stalagmite also warrants consideration. Planar, parallel, and laterally continuous laminae across the sample are ideal, but often stalagmite laminae appear curved in a slabbed sample. These are normally convex, but in some cases are concave (particularly in the case of a 'splash' cup), and with laminae that thin towards the edges. The greater such curvature, the narrower the micromilling trough required for sub-annual (seasonal-scale) sampling (Figure 5), because a wider trench would integrate material from other laminae. Similarly, the sample should allow 2-3 mm sampling into the depth of the sample slab, and ideally the growth layers should not taper out in the third dimension. X-ray and Neutron CT scans can help visualise the 3D internal

structure of the sample (Walczak et al., 2015; Wortham et al., 2019), and the appropriate milling depth.

The determination of the x, y, and z dimensions of the sampling increment is the first step of any sampling strategy (Figure 5). For seasonal resolution, this strategy will ideally permit a very small y-axis increment (the y-axis is parallel to the stalagmite growth axis). The other dimensions must then allow the collection of enough carbonate for analysis (typically 50-120 μg for carbon and oxygen stable isotopes). Depending on sample characteristics and desired resolution, dimensions of $y = 10\text{-}100\text{ }\mu\text{m}$ and $x = 10\text{-}300 * y\text{ }\mu\text{m}$ (parallel to visible growth layers on the slab) are ideal (Figure 5). The sampling depth (z-axis) is best minimised because lamina behaviour into the sample is often unknown, unless CT scans of the sample exist. Larger sample masses are occasionally needed for non-traditional proxies.

A common issue in the speleothem sciences is the precise correlation between two datasets obtained via different means, for example a micromilled stable isotope dataset and a LA-ICPMS derived trace element dataset. Annual- to decadal-scale correlations are usually possible, but rarely are the records correlative on the seasonal- or even annual-scale. Comparisons are achievable using very careful measurements from a datum (often the stalagmite top), with or without the use of banding as 'landmarks' (e.g., (Johnson et al., 2006; Treble et al., 2005a)). A recent technological advance is the development of software, such as the open-source GIS-based QGIS software (Linzmeier et al., 2018), which integrates micro-imaging and analysis into a single spatial reference frame. This approach is particularly useful for organising different analyses derived from differently sectioned portions of samples and has been successfully applied to stalagmite data (Orland et al., 2019).

803 The problem of correlating different types of data is to some extent avoidable by sampling
804 sufficient material with the micromill for both stable isotope and trace elemental analysis via
805 ICP-MS. The sampled powder is divided into two aliquots, one for each analytical technique.
806 The resultant trace element and stable isotope data permit zero-lag cross-correlations and
807 highly robust interpretations of different environmental processes (e.g., Jamieson et al.,
808 2016).

809 For example, if planned multi-proxy analyses require 0.8 mg of carbonate powder (e.g., stable
810 isotope ratios, ^{14}C , and trace elements), and a 50 μm spatial resolution is desired using a
811 milling bit diameter of 0.8 mm, a 0.05 mm x 4.15 mm x 1 mm trench would suffice (assuming
812 calcite density of 2.7 g/cm³ and no sample loss via incomplete recovery); sample loss and a
813 particularly low-density sample would require a larger volume. An often-overlooked
814 additional consideration involves the corners that are initially unsampled when milling
815 trenches (red corner areas, Figure 5). Depending on the drill bit diameter and trench
816 dimensions, the corners at each end of the trench would lead to unwanted integration of
817 material from several sample increments and thus time slices. Use of a smaller milling bit
818 diameter minimizes this effect. Additionally, a 50% reduction of this sampling effect is
819 achieved if a trench is milled along the growth axis prior to the high-resolution milling, or if
820 the milled trench is adjacent to a longitudinal cut (Figure 5). Material from the first trench can
821 be used for reconnaissance studies. Another approach yielding similar results involves
822 collecting the desired powder, and then moving the milling bit along the horizontal sampling
823 track (i.e., parallel to the growth layer) for a distance corresponding to half the width of the
824 milling bit. This powder is then discarded (or collected as auxiliary powder), and the milling
825 bit returns to the original position, ready to produce the next aliquot of powder. Either of
826 these sampling approaches effectively reduce spatial integration of sample (Kennett et al.,

2012; Myers et al., 2015; Ridley et al., 2015b), thereby increasing the likelihood of obtaining a clear seasonal signal (Figure 6).

Other issues include growth layers that slope inward rather than geometrically perfect layers (where the layering is perpendicular to section) and the use of tapered rather than cylindrical drill bits, which would fail to sample some carbonate at depth during each run. A study comparing micromilling/IRMS and SIMS techniques on annually layered otoliths found that an offset existed between the two techniques (with SIMS yielding values $\sim 0.5\%$ lower) and that the amplitude of annual oxygen isotope signal derived via micromilling was approximately half of the SIMS signal; both of these observations are potentially explained by deviations from an ideal sample geometry, and consequently greater integration of unwanted material arising from micromilling (Helser et al., 2018). Despite these differences, both techniques were able to detect annual isotope ratio cycles (Helser et al., 2018). A thorough reconnaissance of the sample using CT scanning or other means to characterise its geometry in advance of slabbing can minimise these issues.

Other minor issues include the possible conversion of aragonite to calcite during milling, which would result in a decrease in $\delta^{18}\text{O}$ values of 0.02% for every 1% aragonite converted to calcite (Waite and Swart, 2015). This effect may have implications for modelling oxygen isotope variability or calculating deviations from equilibrium deposition. However, using a slower rotation rate of the milling bit (500-800 rpm) will minimise, or even eliminate, this effect. A final recommendation is to run micromilled samples through the IRMS non-sequentially (i.e., out of stratigraphic order). Ideally the laboratory environment is static and will not affect results, but any unaccounted for diurnal changes (e.g., lab temperature) may affect the analyses in a cyclical way. Running samples non-sequentially both helps ensures

that any cycles detected (e.g., a seasonal cycle) are not analytical artefacts and helps to identify issues, if they exist (e.g., a persistent cycle when samples are arranged in the order that they were run).

4.1.3. LA-ICPMS

Laser Ablation Inductively Coupled Plasma Mass Spectrometry (LA-ICPMS) is a beam method sampling technique. A polished speleothem slab is analysed by ablating small portions of material using a laser within a sample cell. The laser (typically an ArF excimer laser at a 193 nm wavelength) physically ablates the sample, aerosolising the material which is then carried into the ICP-MS system by a carrier gas (typically helium and/or argon, with helium yielding a greater signal intensity (Luo et al., 2018)) where trace element concentrations are measured and quantified against standards of known compositions. The specific mass spectrometer set-up depends on the research question; for example, by using a quadrupole ICP-MS for elemental measurements using a reference isotope, or a multi-collector ICP-MS for isotope ratio analyses. Additional analytical set-ups are compatible with LA-ICPMS, including reaction cells, triple-quadrupoles, and split-stream analysis using two mass spectrometers in tandem (Frick et al., 2016; Kylander-Clark et al., 2013; Woodhead et al., 2016).

The advantages of LA-ICPMS for speleothem trace element analysis are numerous and include excellent spatial resolution (down to ~3 microns (Müller and Fietzke, 2016), using a rectangular aperture with long axis oriented along laminae) whilst preserving low detection limits (Figure 6). Although historically LA-ICPMS instruments used round 'spots', some laser ablation instruments are now fitted with rectangular masks (apertures), resulting in rectangular spots optimised for speleothem analysis, where the ablation spot is oriented

perpendicular to speleothem growth axis, along the x-axis (Müller et al., 2009). This permits the ablation of a surface area equivalent to large circular spot sizes, while retaining high spatial resolution in the growth direction (similar to the micromill sampling described in 4.1.2). The speed of analysis via this method is also exceptionally high, with typical scan speed of $10 \mu\text{m s}^{-1}$ (e.g., (Jamieson et al., 2015)). Two-volume laser cells are now available, minimising sample damage incurred via sectioning and ensuring consistent aerosol flow within the cell. The coupling of a laser ablation system with a large-capacity gas exchange device even allows analysis under atmospheric air (Tabersky et al., 2013) although with somewhat elevated limits of detection. This technique is particularly suitable for large stalagmites, or archaeological samples, because it minimises physical sample destruction by requiring less sectioning.

The presence of a localised impurity can produce a trace elemental concentration peak even in the absence of a laterally contiguous geochemical horizon with that geochemistry. LA-ICPMS can produce elemental maps that can verify the spatial continuity of geochemical laminae of interest, particularly when combined with a square aperture (Evans and Müller, 2013; Rittner and Müller, 2012; Treble et al., 2005b; Woodhead et al., 2007). This permits the resolution of spatial relationships with greater confidence, and can corroborate interpretations based on stacked and parallel line scans, thereby avoiding issues related to the overinterpretation of a small number of points. Other microanalytical techniques (e.g., SIMS, synchrotron, μXRF , etc.) can also produce elemental maps, but LA-ICPMS techniques can provide greater spatial coverage more rapidly.

The most significant disadvantage to LA-ICPMS is related to difficulties with standardisation. The use of matrix matched standards (i.e., made of the same material as the sample) during

laser ablation analysis is ideal, but the limited availability, variable degrees of standard homogeneity, and accurate standardisation of carbonate materials are ongoing challenges. Orland et al. (2014) and later Müller et al. (2015) provide promising tests for a carbonate standard, albeit for a limited range of elements. Many analyses are standardised with somewhat greater uncertainty than is ideal using glasses such as NIST 620 or 622. These analyses are often regarded as semi-quantitative, with high levels of confidence regarding variability and data trends but uncertainty regarding absolute values. Another minor disadvantage is lack of precise knowledge regarding the position of individual analytical spots. The sheer number of analyses possible via this technique (often >10,000) and indistinct, continuous track means that the exact position of any one individual spot is often difficult to determine precisely, complicating the correlation with other climate proxies. This disadvantage is mitigatable by precise notetaking, syn-analytical microscopy recording, careful reflected light imaging, cross-correlation, application of QGIS or similar software, and judicious 'wobble-matching' with other proxy records, as well as creating marker laser lines at certain intervals to further help to constrain spatial uncertainties.

4.1.4. Secondary ionisation mass spectrometry

Secondary ionisation mass spectrometry (SIMS) uses a primary beam of positive (often caesium) or negative (often oxygen) ions to impact a sample surface under a vacuum, 'sputtering' secondary ions into a mass spectrometer (Wiedenbeck et al., 2012). A positively charged primary beam (commonly Cs^+) ionises negative secondary ions (e.g. C^- , O^-), and a negatively charged primary beam (commonly O^-) ionises positive secondary ions (e.g., Mg^{2+} , Sr^{2+}). The sputtered secondary ions are then accelerated into a double-focusing mass

spectrometer, and counted by ion detectors (electron multiplier or Faraday cup). This analytical technique can yield both trace element analysis and stable isotope ratio data in speleothem carbonate at the micron scale, with very little damage to the sample, and with very high sensitivity (Figure 6).

The spatial resolution typically ranges between 1 to 10 μm spot size and 1-2 μm spot depth for trace elements, with stable isotope analyses historically restricted to 20–30 μm resolution (Fairchild and Baker, 2012) but now capable of achieving 10 μm resolution (Orland et al., 2019). This represents a very high-resolution method for stable isotope analysis within speleothem carbonate, and is therefore ideal for detecting palaeoseasonality (Fairchild et al., 2006). The analysis resolution for trace elements is second only to using synchrotron radiation, but with the added advantage of full quantification of concentration data and the ability to cover much greater areas of sample. Matrix matched materials, typically calcium carbonate, are used for standardisation to ensure consistent ionisation of chemical species and ablation rates (Fairchild and Treble, 2009).

Early studies of SIMS-derived trace element trends in speleothems helped to demonstrate that many stalagmites retained a seasonal signal (Baldini et al., 2002; Finch et al., 2001; Roberts et al., 1998), representing a considerable shift in resolving power compared to the former decadal- to centennial-scale of analysis previously possible. The presence of annual trace element cycles was quickly established as the norm rather than the exception for shallow cave sites, even in the absence of visible speleothem laminations (Fairchild et al., 2001). Divalent alkaline earth metals such as magnesium and barium were suggested as palaeohydrological proxies, phosphorus as indicative of bioproductivity, and strontium as reflecting calcite growth rate and/or PCP (Fairchild et al., 2001; Fairchild et al., 2000; Treble

et al., 2003). However, need for better empirical transfer functions between speleothems and external climatic processes, and partitioning between drip waters and speleothem calcite, complicated interpretations (Fairchild et al., 2001). Subsequent process-based studies have revealed the complexity involved in interpreting trace elements at seasonal scales, highlighting the role they play in complexation with organic matter as colloids (Borsato et al., 2007), in speleothem diagenesis (Martin-Garcia et al., 2014), and the complex controls on transfer through vegetation/soil/epikarst (Hartland et al., 2009; Hartland et al., 2012), as well as controls on partitioning via internal cave microclimate and crystallographic structures (Fairchild and Treble, 2009). The use of trace element cycles obtained via SIMS as chronological markers is exemplified through the work of Smith et al. (2009), where the ability of trace element cycles to provide relative age constraints at a finer spatial resolution than traditional U-series age models is unambiguously demonstrated.

A frontier for SIMS trace element measurements lies in the potential of combining these trace element records with stable isotope measurements undertaken at sub-annual scale. Prior to the advent of SIMS techniques for stable isotope analysis, there were very few combined trace element – stable isotope studies due to the incompatibility of analytical resolution between the two parameters (Orland et al., 2014). However, the analysis of stable isotopes by SIMS now achieves a spatial resolution capable of allowing direct comparability between both isotopic and trace element indicators of seasonality (Orland et al., 2014).

SIMS stable isotope studies have investigated the $\delta^{18}\text{O}$, $\delta^{13}\text{C}$ and $\delta^{34}\text{S-SO}_4$ dynamics in stalagmite records (typical uncertainties (2σ): $\delta^{18}\text{O} = 0.2\text{‰}$ (Orland et al., 2019); $\delta^{13}\text{C} = 0.6\text{--}0.7\text{‰}$ (Oerter et al., 2016; Sliwinski et al., 2015); $\delta^{34}\text{S} = 1.6\text{‰}$ (1σ) at 70 ppm S concentrations (Wynn et al., 2010)). Whereas each of these isotope ratios reflects changing surface

environmental conditions over inter-annual timescales, only the $\delta^{18}\text{O}$ measurements by SIMS can produce records of intra-annual seasonality. Analysis of $\delta^{13}\text{C}$ in speleothem carbonate cannot be undertaken simultaneously with $\delta^{18}\text{O}$, and any available records in the literature (e.g., (Pacton et al., 2013)) are not undertaken at seasonal resolution. The apparent lack of seasonal change in cave dripwater $\delta^{34}\text{S-SO}_4$ (Borsato et al., 2015) has also so far prevented SIMS speleothem sulphur isotope measurements at the seasonal scale (Wynn et al., 2010). Treble et al. (2005a) produced the first $\delta^{18}\text{O}$ record unambiguously linking seasonal cycles in speleothem oxygen isotopes to rainfall dynamics, and corroborated these interpretations with trace element cycles and contemporary rainfall monitoring. Subsequent work at Soreq Cave, Israel, further developed the technique to detect seasonality and links with rainfall dynamics across a range of time periods (Orland et al., 2012; Orland et al., 2009; Orland et al., 2014). Coupled annual variability in fluorescence and $\delta^{18}\text{O}$ provided a seasonal marker of annual variability in rainfall from before the climate instrumental record (Orland et al., 2012; Orland et al., 2009). Careful correlation between fluorescent banding, $\delta^{18}\text{O}$ and trace element measurements, and surface environmental conditions demonstrated that the fluorescent banding represented seasonal organic colloid flux variability into the cave.

Despite the clear advantages of utilising SIMS stable isotope analyses of speleothem carbonate to reveal seasonal patterns of rainfall delivery and drivers of climatic change, the technique also comes with its analytical challenges, including the considerable impact of geometric imperfections (e.g., sample topography, porosity, inclusions, cracks, etc) (Kita et al., 2011; Pacton et al., 2013; Treble et al., 2005a). In most instances, the ability to control the precise location of SIMS analyses enable geometric imperfections to be avoided, provided good surface mapping can be used to identify optimal locations for analysis and post

processing can be used to see any geometric imperfections in each analysis pit (Orland et al., 2009). This is in contrast to micromilling, where large swathes of sample are often bulked together regardless of sample porosity or imperfections. The need to use matrix matched standard materials presents similar problems of availability and homogeneity for the accuracy of data analysis as encountered with LA-ICPMS. However, recent improvements in this area, alongside improvements in sample preparation techniques have been substantial enough to enable accurate correction for instrumental drift (Valley and Kita, 2009). The impact of trace element content on carbonate $\delta^{18}\text{O}$ and $\delta^{13}\text{C}$ analyses also requires careful consideration (Sliwinski et al., 2017), but can be corrected following careful standardisation and is generally not a problem encountered through speleothem analysis where the trace element content is typically less than 1 weight %. An emerging analytical frontier concerns the impact of water and/or organic content on SIMS carbonate $\delta^{18}\text{O}$ and $\delta^{13}\text{C}$, requiring careful pre-screening of sample material and simultaneous analysis of OH- and CH- respectively (Orland et al., 2012; Orland et al., 2015; Orland et al., 2019; Wycech et al., 2018).

Despite these issues, SIMS remains an appealing choice for palaeoseasonality reconstruction using stalagmites due to its sensitivity and resolution. SIMS has produced some of the highest resolution records of palaeoseasonality available and will continue to play an important role in linking stalagmite records to seasonal changes in environmental conditions, particularly across discrete, short-lived events. Although the technique is not suitable for building long records, the comparison of discrete timeslices permits seasonality to be contrasted for key intervals (Orland et al., 2012; Orland et al., 2015; Orland et al., 2019).

4.1.5. Synchrotron

The application of Synchrotron Radiation micro X-Ray Fluorescence (SR- μ XRF) to the study of speleothem carbonate opened up new possibilities in terms of greater resolving power for geochemical analysis (Kuczumow et al., 2003; Kuczumow et al., 2001). Based on the emission of electromagnetic radiation from charged electrons accelerated in an orbit, synchrotron radiation generates secondary radiation from speleothem carbonate based on the characteristic fluorescent properties of chemical elements. The excellent spatial resolution of analysis (0.5–5 microns), low detection limits, low background, and the ability to quantitatively map trace element variability across a given area has enabled the study of speleothem geochemical structures at the sub-annual timescale and in two dimensions (Figure 6). The use of XANES (X-Ray Absorption Near Edge structure) can define the oxidation state of the element under consideration, thereby adding further resolving power to determine environmental processes.

Applications range from using SR- μ XRF to determine long-term (100 year) secular changes in elemental signals (Frisia et al., 2005), high resolution event imaging across sub-annual to multi-annual timescales (Badertscher et al., 2014; Frisia et al., 2008; Vanghi et al., 2019; Wang et al., 2019b), and for investigating petrological controls on geochemical composition (Frisia et al., 2018; Ortega et al., 2005; Vanghi et al., 2019). However, it is at the seasonal scale of analysis where the resolving power of synchrotron radiation has really pushed the boundaries of speleothem science.

No conventional dating technique provides an absolute timeframe at the sub-annual scale of speleothem carbonate deposition. However, linking the seasonality of external environmental processes to speleothem petrology and geochemical characteristics can yield a monthly scale resolution of trace element content. SR- μ XRF was used to determine the

coincidence of trace element distributions and physical calcite characteristics within annual stalagmite laminations (Borsato et al., 2007). Based on the annually laminated stalagmite ER78 from Ernesto Cave, Italy, a suite of trace elements (P, Cu, Zn, Br, Y, and Pb) were found to form an annual peak, coincident with a characteristic thin (0.5-4 μm) brown UV-fluorescent layer in each annual couplet. The brown colouration of each UV-fluorescent layer is probably due to organic acids derived from high rates of water infiltration during each autumn (Frisia et al., 2000; Huang et al., 2001; Orland et al., 2014). The transport of trace elements is associated with colloidal organic molecules (Hartland et al., 2010; Hartland et al., 2012), and leads to the incorporation of this distinctive elemental suite on a seasonal basis associated with the autumnal rains (the 'autumnal pulse' as described in Section 2.4). SR- μXRF permits the detection of variability inherent to each individual year, which then can be contrasted against the symmetrical mean annual profile. Any differences (e.g., double peaks or shoulder peaks) provide an indication that the rainfall distribution throughout that year deviated from the mean annual profile. Strontium was observed to vary inversely to colloiddally transported elements (Borsato et al., 2007), possibly due to competition for binding to defect sites, thus limiting incorporation into the calcite lattice. SR- μXRF revealed seasonal patterns of zinc, lead, phosphorus, and strontium within speleothem Obi84 from Obir Cave, Austria, whose concentration peaks also coincided with the dark coloured visible laminae. These were similarly interpreted as hydrological event markers associated with autumnal infiltration, but could also result from dry deposition of aerosols (Dredge et al., 2013).

SR- μXRF 2D mapping within speleothem Obi84 over three annual cycles demonstrated the effects of several infiltration events each year, present as short-lived peaks in Zn concentration and which build in magnitude towards the main autumnal flush (Wynn et al., 2014) (Figure 6). Using these event peaks as markers of autumnal flushing permitted

attribution of annual sulphate cycles to summer high and winter low concentrations. At the Obir Cave site, these seasonal shifts in speleothem sulphate content were attributed to temperature-driven cave ventilation and associated cave air $p\text{CO}_2$ variability which controlled the dripwater pH and the sulphate:carbonate ratio. Wynn et al. (2018) later verified this proposed seasonal mechanism using controlled laboratory experiments, thereby permitting the extraction of seasonal temperature information based on the annual sulphate cycle's topology. SR- μXRF can thus extract geochemical expressions of seasonality, and the technique is well-suited to investigating changing rainfall and temperature seasonality dynamics back through time.

4.1.6. Data analysis

Following the geochemical analyses and data processing, the information must be interpreted. For techniques producing tens to hundreds of data points, this is not particularly challenging. On the other hand, techniques such as LA-ICPMS can produce tens of thousands of data points for multiple elements, and can greatly increase the processing time on common spreadsheet programmes. To circumvent these issues, it is possible to simplify the data using a Principal Component Analysis (PCA), a multivariate statistical analysis technique which extracts modes of variation from large multivariate timeseries datasets that best describe overall variability of those datasets. The technique is ideal for large multivariate stalagmite-derived LA-ICPMS datasets (Borsato et al., 2007; Jamieson et al., 2015; Orland et al., 2014). PCA has also been used to extract a seasonal signal from trace elemental concentrations even in the absence of visible laminae and applied towards the development of a chronology (Ban et al., 2018).

Comparing the intra-annual amplitude of a geochemical signal (Orland et al., 2012; Orland et al., 2009; Orland et al., 2014; Orland et al., 2019) from monthly-resolved datasets is ideal for extracting seasonal information from an otherwise difficult to interpret dataset. For example, Ridley et al. (2015b) used the well-developed annual carbon isotope cycles with their Belizean stalagmite to extract seasonal amplitudes, which were then interpreted in terms of the strength of the seasonal ITCZ incursion into southern Belize. Orland et al. (2015) used the topology of oxygen isotope variability within individual growth bands in a Chinese stalagmite to clarify the origin the oxygen isotope variability. Spectral analysis of well-dated samples can also reduce data complexity (Myers et al., 2015). For example, Asmerom et al. (2020) used a wavelet analysis to reconstruct the strength of the wet season in Central America over the last two millennia, and to show that modern seasonality in rainfall was only emplaced in the 15th Century. Extracting a meaningful metric from numerous more complex data using statistical techniques is one way of simplifying a complex geochemical dataset.

5. Modelling techniques

Many efforts at modelling both the hydrology feeding a stalagmite and the climate signal within exist. Proxy system models (PSMs) describe how geological or chemical archives are imprinted with climate signal (Evans et al., 2013). In terms of stalagmite-specific models, several exciting geochemical models now exist which can explore the emplacement of a geochemical signal in a stalagmite (Wong and Breecker, 2015), often based on established processes which govern stalagmite precipitation (e.g., (Buhmann and Dreybrodt, 1985)). Two recent examples (specifically of disequilibrium isotope fractionation processes proxy system

models) are the IsoCave model, which can examine disequilibrium isotope effects in speleothems and related implications for speleothem isotope thermometry (Guo and Zhou, 2019), and the ISOLUTION model which similarly helps to better understand the effect of these disequilibrium isotope fractionation processes on stalagmite proxy records (Deininger and Scholz, 2019). The I-STAL model allows the simulation of PCP and how this affects dripwater Mg, Sr, and Ba (Stoll et al., 2012). A number of models looking specifically at drip hydrology now exist (e.g., KarstHydroModel (Baker and Bradley, 2010; Treble et al., 2003)), and these are extremely useful for understanding how the rainfall input signal is transformed before reaching the stalagmite. Rather than using hydrological or geochemical modelling, a recent publication introduced a Monte Carlo approach to model rainfall and temperature seasonality in a stalagmite from La Garma Cave, northern Spain, over the Holocene (Baldini et al., 2019). Here, we build on this work and compare both synthetic and real-world input data to the results of the second-generation model.

The model requires some widely available types of input data, including: i) a stalagmite-based $\delta^{18}\text{O}$ record, ii) a record of regional mean annual temperature (MAT) of any resolution (e.g., borehole, marine sediments, stalagmite fluid inclusions) over the interval of interest, iii) monthly-scale modern instrumental records of rainfall and temperature above the site (or as close as possible to the site), and iv) cave air temperature and its relationship with above ground temperature. The relationship between meteoric precipitation $\delta^{18}\text{O}$ and temperature at the site is useful but not required information because regional or global meteoric precipitation $\delta^{18}\text{O}$ and temperature equations can provide a suitable alternative.

Essentially, the model assumes that the MAT of the cave site is similar to the MAT of the regional temperature input record (ii above), and produces a sine function around this value

of an amplitude reflecting modern temperature seasonality, but with random variability added to the absolute minimum and maximum temperatures (the amount of randomness is user-defined). A second sine function reflects the rainfall seasonality, and whereas the temperature wave's polarity is fixed (i.e., summers are always warmer than winters), the rainfall seasonality sine wave's polarity is allowed to flip randomly. The seasonal extreme values associated with either sine function are fixed to the same calendar months, linked to the timing of the modern minima and maxima.

These two sine waves produce synthetic monthly temperature and rainfall values, which are then converted to $\delta^{18}\text{O}_p$ based ideally on local temperature-rainfall $\delta^{18}\text{O}$ relationships, or in cases where this relationship is not known, to more global equations (e.g., (Schubert and Jahren, 2015)). It is assumed that the $\delta^{18}\text{O}_p$ is conveyed to the dripwater (see discussion regarding evapotranspiration, Section 4.3) and that this is converted to carbonate $\delta^{18}\text{O}$ using the Tremaine equation (Tremaine et al., 2011) at ambient cave air temperature adjusted according to observed relationships between outside and inside air. This equation was chosen as most appropriate because its empirical nature accounts for in-cave disequilibrium fractionation processes more completely than other equations. The model therefore considers seasonal changes in rainfall but is independent of total annual rainfall. The annual amount-weighted mean modelled carbonate $\delta^{18}\text{O}$ value is then compared with the actual measured carbonate $\delta^{18}\text{O}$ value, and if it is within a certain user-defined value, it is logged as a successful simulation. If the difference between the modelled and actual carbonate $\delta^{18}\text{O}$ is greater than this value (generally ~ 0.1 per mil), the simulation is logged as unsuccessful. 1,000 of these coupled temperature and rainfall simulations are conducted per time slice, all the

successful and unsuccessful simulations are logged, and the mean monthly modelled rainfall and temperature values calculated from the successful simulations.

5.1 Test Runs: Gradual shifts in rainfall polarity

The model reproduces shifts in rainfall polarity in synthetic datasets well (Figure 7). In one experiment, the input $\delta^{18}\text{O}$ dataset was created by using i) a temperature sine function that was set as invariant (i.e., it maintained its polarity and amplitude throughout the run), and ii) a rainfall sine function that shifted in polarity completely over 14 model years. The wettest month in the input rainfall record was April in Year 1, gradually changing polarity to November by Year 14. As such, model Year 7 was characterised by no seasonality (Figure 7). The model was run without *a priori* knowledge of these shifts other than the mean annually-resolved synthetic $\delta^{18}\text{O}$ record, MAT, 'modern' seasonality range, and cave temperature (i.e., the simulations were run 'modeller blind'), but the output reproduced the shifting rainfall pattern very well. The gradual shift in rainfall polarity is detected, and the lack of seasonality in the input rainfall signal during Year 7 is reproduced. The input temperature data had a 15 °C annual temperature range, and two model simulations were conducted: one derived using an annual seasonal temperature range of 10 ± 6 °C, and a second using an annual seasonal temperature range of 15 ± 6 °C. In the case of the lower annual temperature range, the model overestimates rainfall seasonality in order to compensate for the inappropriate annual temperature range, but still detects shifts in rainfall polarity (Figure 7). When the more appropriate temperature range is used, the simulation captures both the amplitude and polarity of the shifting rainfall input signal. However, this experiment highlights a limitation

of this modelling approach; $\delta^{18}\text{O}$ data is explicable both in terms of rainfall and temperature seasonality shifts, and an unknown annual temperature range introduces uncertainties.

A second experiment involved synthetic temperature and rainfall input records with both considerable inter-annual variability and noise introduced (Figure 8). Notably, one model year (Year 4) had the polarity of the rainfall signal completely reversed. Again, the model was able to extract the salient features of the input data very well. Reproduced were inter-annual variations in rainfall and temperature, and, importantly, the model detected the reversed seasonality of the rainfall signal in Year 4 (Figure 8).

5.2 Application to a stalagmite $\delta^{18}\text{O}$ dataset from a seasonally arid continental region

The first version of the model was run successfully across the Holocene using a $\delta^{18}\text{O}$ dataset derived from the maritime climate of northern Spain (Baldini et al., 2019). Here, we apply the model to a dataset from Bir-Uja Cave in the Keklik-Too mountain ridge, Kyrgyzstan, a location characterised by extremely strong seasonal fluctuations in both temperature and rainfall. The cave ($40^{\circ}29'\text{N}$, $72^{\circ}35'\text{E}$) is ~60 m long and is developed at an altitude of ~1,325 m above sea level (Fohlmeister et al., 2017). The input data consisted of the $\delta^{18}\text{O}$ dataset from stalagmite Keklik1 reported on in Fohlmeister et al. (2017), a 500-year long, centennial-resolution borehole temperature record from the Tian Shan mountains (~461 km to the north of the cave site) (Huang et al., 2000), instrumental precipitation and temperature records since 1880 C.E. from Tashkent, Uzbekistan (~300 km to the east) (Menne et al., 2012), and cave temperature (Fohlmeister et al., 2017). The $\delta^{18}\text{O}$ input data were decadal-resolved, and the stalagmite was dated using a recently developed radiocarbon technique (Fohlmeister and

1193 Lechleitner, 2019; Fohlmeister et al., 2017; Lechleitner et al., 2016b). The Keklik1 record
1194 extends from 2011 C.E. back to 1150 C.E., but the borehole record only extends back to 1500
1195 C.E., so the interval modelled only extends to 1500 C.E. On average, the site receives ~450
1196 mm of precipitation per year (based on Global Network of Isotopes in Precipitation data from
1197 Tashkent), with ~80% falling from November to April. Summers are very dry, with August (the
1198 driest month) receiving ~5 mm of rainfall. Monthly temperatures range from -1.4 °C in January
1199 to 25.0 °C in July, with a MAT of 12.1 °C. Stalagmite Keklik1 was located ~40 meters from the
1200 cave entrance and was collected in October 2011. Cave temperature varies seasonally, from
1201 12 °C from the end of November until April, to a maximum of 16.5 °C in May. The site is
1202 characterised by near 100% relative humidity in the cold season which drops considerably to
1203 ~60% during the warmer months (Fohlmeister et al., 2017).

1204 Unlike the Spanish GAR-01 record which extended back to ~13,500 years BP and was
1205 modelled using 100-year timeslices (Baldini et al., 2019), the Keklik1 $\delta^{18}\text{O}$ record was
1206 modelled using annual timeslices. The timings of the minimum and maximum values of the
1207 modelled temperature sine function were fixed at January and July, respectively. These
1208 months were also designated as the minimum/maximum of the modelled rainfall sine wave,
1209 which fits present day observations, but the sine function's polarity was not prescribed in
1210 advance.

1211 Baldini et al. (2019) noted that the modelled temperature curve for northern Iberia closely
1212 resembled a previously published temperature reconstruction for the region (Martin-Chivelet
1213 et al., 2011) with a temporal resolution that exceeded the information provided by the low-
1214 resolution input dataset. Although no annual-scale MAT record exists in the Kyrgyzstan region
1215 for the last 500 years, summer temperatures are well constrained by tree ring records. A

comparison of the modelled July temperature derived from the Keklik1 $\delta^{18}\text{O}$ record reveals a very good match with the NTREND AG2 temperature anomalies (~300 km to the north of the cave site) (Anchukaitis et al., 2017; Cook et al., 2013) (Figure 9). The model's ability to reconstruct palaeotemperature may reflect the fact that the probability of a successful model run is maximised when modelled temperature approximates the actual temperature shift. Successful model runs with a different (and incorrect) temperature pattern are possible with certain modelled rainfall simulations, but the mean monthly temperature values (reflecting the mean of all successful runs) will be biased towards model simulations with the correct temperature shift. The apparently robust reconstruction of warm-season palaeotemperature is an unexpected and exciting model outcome, but one that requires further evaluation.

The rainfall reconstruction reproduces many of the same features highlighted by Fohlmeister et al. (2017). In particular, decreases in the winter rainfall contributions in the late 1500s, the mid-1700s, and the early 1800s are apparent in both records. Although to a certain extent this is expected because the $\delta^{18}\text{O}$ record is integral to both reconstructions, it is interesting that the two reconstructions use two fundamentally different techniques (numerical versus geochemical modelling) to estimate the importance of winter rainfall to the overall annual water budget at the site, and arrive at broadly similar results. For example, a winter rainfall peak occurs in 1797 CE in both records and transitions to drier winters by 1815 CE, with ~22% and ~50% reductions in winter rainfall implied by the model and $\delta^{18}\text{O}$ data, respectively. The model underestimating the reduction in rainfall probably arises because of the model's utilisation of smooth sine waves rather than more step-like functions; in other words, although it is possible for one month per year to have zero rainfall in the model, the adjacent two months must necessarily have some rainfall, whereas in reality, several dry months per

summer could occur. The use of step functions would permit the incorporation of several dry months annually and would amplify apparent shifts in seasonal rainfall amounts. Modelled DJFM rainfall compares reasonably well with GHCN rainfall from Tashkent (Figure 9), particularly considering that the Tashkent meteorological station is ~300 km away from and ~1,000 m lower in altitude than the cave site.

5.3 Limitations to the modelling technique and future work

Several limitations to the presented modelling technique exist. First, the timing of the rainfall minima and maxima versus temperature signal could affect the model's efficacy; for example, if the rainiest month occurs three months after (or before) the warmest month, the use of the sine function means that all outcomes are possible. This is because the maxima/minima in one parameter's sine function occur at the nodes of the other sine wave, effectively making both sine waves independent of each other. At many sites, temperature and rainfall are intrinsically linked and their seasonal cycle broadly synchronous, but the above may be an issue at some locations. Additionally, the model would require a differently shaped rainfall-function to model rainfall at locations with two distinct rainy intervals every year, such as low latitude sites affected by the ITCZ twice each year.

The current version of the model does not incorporate evapotranspiration, and this is an obvious oversimplification. This may have repercussions for sites like Kyrgyzstan that experience a pronounced hot and dry season with negative effective infiltration. Similarly, variable kinetic fractionation almost certainly occurred within the cave (Fohlmeister et al., 2017) but is not considered within the model. Future versions of the model will incorporate

1261 both evapotranspiration and kinetic effects, but the model currently likely overcomes this
1262 limitation simply by reducing rainfall amount for months with high evapotranspiration rates.
1263 Potentially, coupling the new model discussed here with a dripwater isotope evolution model
1264 (e.g., ISOLUTION (Deininger and Scholz, 2019)) could produce very robust results. The model
1265 also cannot identify intervals characterized by changes in moisture pathway or fractionation
1266 amount; rather, it highlights intervals that are not explicable in terms of changes in
1267 temperature or rainfall amount seasonality (intervals where the model cannot converge on
1268 any solutions), and thus points to the involvement of other processes.

1269 The model is allowed to randomly vary MAT above or below the low-resolution temperature
1270 input record, but only within user-defined bounds. Too great a range of permissible MAT
1271 values would allow essentially any outcome. For example, if there were no limits to minimum
1272 winter temperature, a low $\delta^{18}\text{O}$ value could be modelled as either a very cold winter with a
1273 subdued rainfall seasonality or as a mild winter but with substantial winter rain. Limiting the
1274 temperature seasonality to reasonable bounds (for example, based modern interannual MAT
1275 variability) permits assessing whether any given month is warmer or colder than the low-
1276 resolution temperature input, but may underestimate the total amount of cooling and
1277 warming. In extreme cases, this may manifest itself as a failure to converge upon any
1278 successful model, thus highlighting timeslices that require closer inspection and potentially
1279 an alternative explanation.

1280 As discussed in Section 5.2, the utilisation of step functions to describe rainfall seasonality
1281 may facilitate the modelling of climate for sites where several months receive similar amounts
1282 of rainfall. Future studies should investigate the ramifications of function choice on output.
1283 Additionally, theoretically arriving at a mathematical solution utilising the relevant equations

and input data is possible, obviating the need for MC simulations, and future research will investigate this possibility. Finally, future models could incorporate options for geochemical modelling of drip and carbonate chemistry.

6. Regional seasonality

In this section we analyse global meteoric precipitation and temperature data to highlight regions experiencing pronounced seasonal variability in temperature, precipitation amount, and precipitation $\delta^{18}\text{O}$ (Figures 10 and 11), helping to facilitate the identification of cave sites sensitive to seasonality. This also highlights locations that are at the margins of such regions, where seasonality may have affected the record in the past, despite the lack of a modern influence.

6.1. Identification of seasonally sensitive regions

WorldClim Version 2 data were obtained at a 2.5 minute (~ 4.5 km at the equator) spatial resolution (Fick and Hijmans, 2017). Inland continental regions within the mid- to high-latitudes of the Northern Hemisphere (e.g., central and northern Canada, eastern Russia, northeast China, and Mongolia) are characterised by the greatest mean annual temperature range (Figure 10a). A greater annual temperature range is characteristic of continental climates due to the reduced oceanic influence, with ocean water's high heat capacity and moderating influence on air temperature. The lowest mean annual temperature ranges occur in the low latitudes (where insolation remains high year-round) and maritime regions of the

world (where oceans moderate temperature variability) (Figure 10a). The pattern of global temperature seasonality (herein calculated as the maximum temperature of the warmest month minus the minimum temperature of the coldest month averaged over the period 1970 – 2000 based on WorldClim Version 2 data) is consistent with the geographic pattern of cave air ventilation reported in (James et al., 2015), a study concerning the role of outside temperature seasonality in the seasonal ventilation of caves.

Seasonality in precipitation amount (Figure 10b) is greatest in the low latitudes due to the annual migration of the Intertropical Convergence Zone (ITCZ) and monsoonal systems that cause distinct wet and dry seasons, along the western coast of North America, southern South America, and Europe where seasonal westerlies preferentially bring enhanced winter precipitation, and bordering the Mediterranean where a ‘Mediterranean climate’ characterised by wet-winters and dry-summer dominates (Figure 10b). The lowest precipitation amount seasonality occurs in arid and semi-arid regions of the world and the non-coastal mid- to high-latitudes of the northern and southern hemispheres.

Global seasonality in amount-weighted $\delta^{18}\text{O}_p$ (Figure 11) approximates the pattern of temperature seasonality (Figure 10a), with the greatest annual range in $\delta^{18}\text{O}_p$ observed at Northern Hemisphere continental interior and high latitude sites (e.g., northeast Asia, central Canada, northern Greenland). In addition, high altitude sites (e.g., the Andes in western South America, the Caucasus Mountains at the intersection of Europe and Asia) also exhibit higher annual WM $\delta^{18}\text{O}_p$ ranges due to the altitude effect. The lowest $\delta^{18}\text{O}_p$ seasonality occurs within maritime (e.g., NW Europe, SW and SE Australia) and arid/semi-arid regions (e.g., East Africa, eastern Brazil, South Africa). Many stalagmite records are from temperate regions where modern MAT ranges from 10 to 16 °C (Baldini et al., 2019; Baldini et al., 2015; Ban et al., 2018;

Huang et al., 2001; Johnson et al., 2006; Orland et al., 2014). Global cave dripwater $\delta^{18}\text{O}$ data reveal that caves from regions with this MAT range have dripwater chemistry that reflects recharge-weighted $\delta^{18}\text{O}_p$ (Baker et al., 2019). The seasonal distribution of $\delta^{18}\text{O}_p$ is therefore a critical control in the case of many different stalagmite samples.

In other cases, very pronounced seasonality inherent in stalagmite geochemical records are not due to seasonality in $\delta^{18}\text{O}_p$, but instead to seasonality in rainfall amount (Ridley et al., 2015b) and associated shifts in bioproductivity (Baldini et al., 2005) or PCP (Fairchild and Hartland, 2010; Fairchild et al., 2006). Seasonality in temperature can also induce cave ventilation in temperate zone caves during the winter (providing the cave geometry is appropriate), promoting carbonate deposition within the cave and biasing annual- to decadal-scale records towards the winter season rainfall (James et al., 2015). The maps provided herein can help identify regions containing speleothems retaining the desired seasonal signal, and determine what the most likely control is on any seasonal signal found within a stalagmite. Furthermore, the maps help highlight cave sites that are located on the peripheries of climatologically seasonal zones at present, where past seasonality shifts could have influenced a record. Examples include the Sahel and southern Belize (Figure 12), both currently at the very northern extent of the ITCZ, where a small ITCZ shift to the south would produce both severe drying and a substantial decrease in rainfall seasonality. This perspective was underscored by recent results from Central America that used monthly-scale rainfall proxy data over the last two millennia to suggest that the region has only been affected by the ITCZ since ~1400 C.E., and that the ITCZ influence may wane in the near future (Asmerom et al., 2020) (Figure 12).

6.2. Complexities despite strong seasonality: northeast India as an example

The seasonality maps presented here highlight regions most likely to contain stalagmites which retain seasonal signals in temperature, rainfall amount, or $\delta^{18}\text{O}_p$. However, they also illustrate that not all seasonal variations in $\delta^{18}\text{O}_p$ are explicable in regional temperature or rainfall amount terms. In many cases, complex moisture source variability overprints temperature-induced seasonality, hampering the use of models such as the one presented in Section 5. Here, we discuss the Indian Summer Monsoon (ISM) as an example of such a situation, and focus specifically on Mawmluh Cave in Meghalaya, northeast India, one of the most seasonal locations on Earth in terms of rainfall amount (Fig. 10). In Meghalaya, hydroclimate is characterised by extreme seasonality, as the plateau constitutes the first topographic barrier for moisture-laden air masses travelling inland from the Bay of Bengal (Murata et al., 2007; Prokop and Walanus, 2003). At present, the ISM brings ~80% of the annual rainfall to the cave site, inducing extreme amounts of rainfall (up to 12 meters per year (Breitenbach et al., 2015). The seasonal precipitation cycle is reflected in rainfall $\delta^{18}\text{O}$ composition (Berkelhammer et al., 2012; Breitenbach et al., 2010). Rainfall $\delta^{18}\text{O}$ becomes progressively lighter during the ISM, but this effect is only partially driven by increasing precipitation intensity and the amount effect because the period of maximum precipitation (June-August) precedes maximum ^{18}O depletion (August-October) (Breitenbach et al., 2010)). Instead, the ^{18}O -depletion results predominantly from the moisture source shifting from a proximal location (the Bay of Bengal) in the early and late ISM to a more distal location (the open Indian Ocean) during the peak ISM (longer transport times resulting in more Rayleigh distillation). Rainfall and dripwater $\delta^{18}\text{O}$ at Mawmluh Cave are thus highly seasonal, but the relationship between temperature, rainfall amount, and rainfall $\delta^{18}\text{O}$ is not straightforward

(Breitenbach et al., 2010; Breitenbach et al., 2015). Additional complexity arises from the filtering and buffering capacity of the karst aquifer through which rainwater percolates *en route* to a stalagmite. Although a clear seasonal dripwater $\delta^{18}\text{O}$ cycle exists, with its lowest value approximating ISM rainfall $\delta^{18}\text{O}$, its annual amplitude is compressed, reflecting buffering in the karst (Breitenbach et al., 2015). This further complicates the interpretation of $\delta^{18}\text{O}$ records from these stalagmites, and information from independent proxies that are sensitive to processes dominating during the winter season is required to disentangle such processes. Combining summer-sensitive $\delta^{18}\text{O}$ with winter-sensitive Mg/Ca (reflecting PCP) permitted disentangling ISM strength and the degree of dry season dryness in a stalagmite from Mawmluh Cave (Myers et al., 2015; Ronay et al., 2019). Such a multi-proxy approach, supported by local monitoring and karst process modelling, allows robust interpretations of seasonal-scale climate from stalagmites, even when the proxy seasonality is driven by more complex processes than temperature or rainfall amount alone.

8. Future directions and recommendations

In this review, we introduce and discuss several concepts that we hope will facilitate the development and interpretation of robust seasonal-resolution climate records from stalagmites, will improve the extraction and interpretation of seasonal information from stalagmites, and promote future discussion, including: **A)** that replication of records should not always be an expectation without *a priori* knowledge that the drip type and environmental conditions responsible for the deposition of the stalagmites are comparable (e.g., some stalagmites retain seasonal information, whereas others do not), **B)** that every stalagmite-based geochemical record is different and records a unique component of the

1397 environmental signal of varying complexity (i.e., each stalagmite retains an accurate history
1398 of its environment; the question is whether or not this history can be deconvolved), and **(C)**
1399 that the application of at least one year's worth of hourly-resolved drip rate monitoring
1400 combined with a new drip classification scheme presented here may help identify stalagmites
1401 retaining a seasonal signal. Furthermore, we have **(D)** developed global seasonality maps of
1402 temperature (as was done previously by (James et al., 2015)), meteoric precipitation amount,
1403 and meteoric precipitation $\delta^{18}\text{O}$ ratios which allow the identification of regions sensitive to
1404 different types of seasonality recordable by stalagmites. The maps facilitate predicting what
1405 type of seasonality potentially affects modern stalagmite samples from that region. They also
1406 assist in palaeoclimate interpretations by identifying locations proximal to regions with
1407 pronounced seasonality, where past migration of key atmospheric circulation systems could
1408 have altered the geochemical record retained by a stalagmite. On a similar note, we **(E)**
1409 present a model that interprets annual- to centennial-scale stalagmite $\delta^{18}\text{O}$ records in terms
1410 of seasonal temperature and meteoric precipitation seasonality shifts. Although we stress
1411 that this model only highlights one possible interpretation (that the data were modulated
1412 primarily by regional long-term mean annual temperature variability combined with
1413 seasonality shifts in rainfall and temperature), often this interpretation is the most
1414 parsimonious. The modelling technique also helps identify time intervals when altered
1415 seasonality cannot account for the observed isotope shifts, suggesting that another variable
1416 needs consideration. We **(F)** discuss four major controls on the seasonality signal within
1417 stalagmites: i) Earth atmospheric, ii) Meteoric precipitation, iii) biological (e.g., soil processes),
1418 and iv) cave atmospheric, and **(G)** discuss a case study from India that serves as an example
1419 of a stalagmite whose seasonal signal is not derived from rainfall amount or regional

1420 temperature, but instead results from seasonal shifts in air mass trajectories (i.e., affected by
1421 seasonal shifts in Earth atmospheric processes).

1422 Stalagmites are remarkable archives of information regarding climate (on both seasonal and
1423 longer timescales), surface and cave environmental conditions, dry deposition, moisture
1424 source pathway, marine aerosols contributions, and hydrological routing. Replication of proxy
1425 records present strong support for palaeoclimatic interpretations, and should remain a goal
1426 of any stalagmite science research programme, but unless the climate signal-to-noise ratio of
1427 a region is unusually high, replication is only possible when comparing stalagmites deposited
1428 under similar conditions. A thorough understanding of the environmental processes affecting
1429 both entire caves (e.g., ventilation) as well as individual stalagmites (e.g., drip rate) facilitates
1430 replication efforts. The geochemical record from even adjacent stalagmites will reflect
1431 numerous processes, some of which are common to the two samples but many which are
1432 not, and only through a thorough understanding of the processes affecting each sample are
1433 robust (and replicable) climate interpretations achievable. However, unless analytical issues
1434 exist, non-replication does not imply that one record is incorrect; rather it generally implies
1435 that the two records simply record different environmental parameters.

1436 Cave monitoring prior to the collection of a stalagmite will increase the likelihood of obtaining
1437 a record of the desired sensitivity to seasonal climate shifts, or other desired forcing. We
1438 recommend monitoring the drip feeding the stalagmite for at least one year using an
1439 automated drip logger and plotting the results in a diagram similar to Figure 3 to evaluate a
1440 stalagmite's likelihood of retaining hydrological seasonality. We recommend monitoring
1441 multiple sites within the cave and selecting the most appropriate stalagmite for collection
1442 based on the monitoring results. It is worth bearing in mind that unless the seasonality signal

1443 in a stalagmite is conveyed via seasonal cave ventilation, stalagmites fed by diffuse flow drips
1444 with long residence times may not retain seasonal information. Other drips that are
1445 seasonally either dry or undersaturated with respect to carbonate will lead to the formation
1446 of microhiatuses in the stalagmites and signal loss for that particular season. Monitoring a
1447 stalagmite's drip rate and drip chemistry for as long as possible represents one of the simplest
1448 but most effective means of understanding the potential climate signal contained within a
1449 sample prior to collection. This also has implications for cave conservation and protection
1450 efforts, because clearly formulated research goals and drip monitoring prior to stalagmite
1451 sample collection can greatly reduce the number of samples removed from a cave for
1452 research purposes.

1453 If sample growth rate permits, we suggest that the extraction of the palaeoseasonality signal
1454 over long timescales is best achieved via micromilling, leaving no gap between adjacent
1455 samples, or LA-ICPMS. The major disadvantages of micromilling is that it is resource intensive,
1456 and that many samples may not have growth rates high enough to permit the required
1457 resolution; the major disadvantage of LA-ICPMS is that the trace element signature of a
1458 stalagmite is often dominated by site-specific factors such as temperature, sea spray, volcanic
1459 aerosols, fire, variable throughput of colloidal material, or rainfall, and consequently aligning
1460 the data with other records is sometimes complex. Micromilled carbonate powders that are
1461 divided into two or more aliquots that are subsequently analysed for stable isotope ratios,
1462 trace elements, and other geochemical proxies can provide very robust interpretations (e.g.,
1463 Jamieson et al., 2016). This eliminates issues of cross-correlation and enables a powerful
1464 multiproxy approach, where each stable isotope ratio value is linked directly and
1465 unambiguously to numerous elemental concentration values. The technique can yield

important information regarding palaeoseasonality but is considerably more resource intensive than running multiple LA-ICPMS tracks parallel to each other and the micromilled stable isotope track. An alternative is to produce a long decadal-scale isotope ratio traverse complemented by higher resolution transects or maps across key intervals of interest using LA-ICPMS, SIMS, synchrotron, or μ XRF to corroborate interpretations based on the longer transects. In the future, proxy mapping at micron-scale resolution using these techniques will help reduce uncertainties related to geometric ambiguities such as those associated with crystal boundaries and improve the robustness of interpretations.

9. Conclusions

The reconstruction of palaeoseasonality using stalagmites is an exciting research direction that has yet to mature into its full potential. Numerous records of palaeoseasonality exist, but few direct reconstructions extend before the last two millennia. Ideally, future studies concluding that a decadal- to annual-scale isotope ratio record is affected by seasonality changes should support this by either using short windows of sub-annual data or by modelling.

Any climate proxy record is affected by inherent complexities in climate signal transfer to the stalagmite and by selective sampling of the stalagmite for analysis. A high-resolution (sub-annual to annual-scale) sampling strategy coupled with appropriate site monitoring maximises the likelihood of extracting a signal approximating the climate input signal. For long records annual- to decadal-scale resolution is ideal, and shorter records could benefit from an even higher resolution if resources permit. Large shifts in isotope ratios could reflect

changes in seasonality, potentially associated with the migration of key atmospheric circulation systems over the cave site. New models incorporating seasonality can provide information regarding whether observed geochemical shifts are interpretable in terms of altered seasonality, and these represent an exciting and inexpensive new research tool. A seasonal-scale sampling strategy over short intervals of interest can verify these model interpretations, and LA-ICPMS or line-scan μ XRF represent potentially the most efficient methods to achieve this; other alternatives include monthly-scale micromilling, synchrotron analysis (SR- μ XRF), and SIMS.

The robust interpretation of stalagmite geochemical records in terms of seasonality represents a key challenge for the next decade. Achieving this is complicated by multiple in-cave and exogenic environmental forcings with dynamic seasonality, including: rainfall, temperature, humidity, bioproductivity, cave air $p\text{CO}_2$, drip rate, source moisture region and $\delta^{18}\text{O}$, and moisture mass trajectory from the source region. Even apparently straightforward $\delta^{18}\text{O}$ records from regions with high signal-to-noise ratios typically interpretable as either varying total annual rainfall or summer rainfall may instead reflect another parameter instead (e.g., a change in moisture source or rainfall seasonality), as is the case with the Indian Summer Monsoon. Most records would benefit from a rigorous multi-proxy approach utilising not only multiple geochemical proxy datasets, but also site monitoring and new modelling approaches. Similarly, focussing research efforts at the same well-understood cave sites both maximises the quality of interpretations and contributes to the conservation of caves and stalagmite samples. The application of multiple stalagmites from the same site but with different drip rates and affected by different amounts of disequilibrium fractionation may provide the key to reconstructing formerly elusive climate variables, such as temperature.

1511 Instead of representing an irresolvable issue, we suggest that disequilibrium fractionation
1512 may present opportunities to quantify temperature, potentially even at seasonal resolutions.
1513 Similarly, multi-proxy data could yield seasonal information even in the absence of seasonal
1514 sampling resolution; if two or more independent proxies reflect different seasonal data,
1515 combining the proxies could yield palaeoseasonality.

1516 Over the past few decades stalagmites have provided some of the most iconic records in
1517 palaeoclimatology. In the future, stalagmites will continue to not only provide long records of
1518 exceptional quality, but they will also provide rare glimpses into palaeoseasonality at
1519 unprecedented temporal resolution. Recent microanalytical advances have facilitated the
1520 construction of exquisitely resolved stalagmite-based climate records; we are now at a stage
1521 where the interpretation of these records is catching up with their remarkable technical
1522 aspects. Extracting quantitative and accurate seasonal climate information from these
1523 geochemical records is a key challenge over the next decade, and, if this is achieved,
1524 stalagmites will truly be considered in a class of their own as climate archives.

1526 **Acknowledgements**

1527 We thank SISAL and PAGES for access to the SISAL database v1b. Portions of this research
1528 were funded by European Research Council Grant #240167. Tim Horscroft is thanked for his
1529 support in facilitating the preparation of the manuscript. Ian Orland and an anonymous
1530 reviewer are thanked for detailed constructive reviews that greatly improved the manuscript.
1531 Alex Iveson is thanked for useful comments regarding LA-ICPMS.

1533 **References:**

- 1534 Allison, V.C., 1923. The growth of stalagmites and stalactites. *Journal of Geology* 31, 106-125.
- 1535 Allison, V.C., 1926. The antiquity of the deposit in Jacob's cavern. *American Museum of Natural*
- 1536 *History, Anthropological Papers* 19, 204-225.
- 1537 Anchukaitis, K.J., Wilson, R., Briffa, K.R., Buntgen, U., Cook, E.R., D'Arrigo, R., Davi, N., Esper, J.,
- 1538 Frank, D., Gunnarson, B.E., Hegerl, G., Helama, S., Klesse, S., Krusic, P.J., Linderholm, H.W., Myglan,
- 1539 V., Osborn, T.J., Zhang, P., Rydval, M., Schneider, L., Schurer, A., Wiles, G., Zorita, E., 2017. Last
- 1540 millennium Northern Hemisphere summer temperatures from tree rings: Part II, spatially resolved
- 1541 reconstructions. *Quaternary Sci. Rev.* 163, 1-22.
- 1542 Arbel, Y., Greenbaum, N., Lange, J., Inbar, M., 2010. Infiltration processes and flow rates in
- 1543 developed karst vadose zone using tracers in cave drips. *Earth Surface Processes and Landforms* 35,
- 1544 1682-1693.
- 1545 Arbel, Y., Greenbaum, N., Lange, J., Shtober-Zisu, N., Grodek, T., Wittenberg, L., Inbar, M., 2008.
- 1546 Hydrologic classification of cave drips in a Mediterranean climate, based on hydrograph separation
- 1547 and flow mechanisms. *Israel Journal of Earth Sciences* 57, 291-310.
- 1548 Asmerom, Y., Baldini, J.U.L., Prufer, K.M., Polyak, V.J., Ridley, H.E., Aquino, V.V., Baldini, L.M.,
- 1549 Breitenbach, S.F.M., Macpherson, C.G., Kennett, D.J., 2020. Intertropical convergence zone
- 1550 variability in the Neotropics during the Common Era. *Science Advances* 6, eaax3644.
- 1551 Atkinson, T.C., 1977. Diffuse flow and conduit flow in limestone terrain in the Mendip Hills, Somerset
- 1552 (Great Britain). *Journal of Hydrology* 35, 93-110.
- 1553 Atkinson, T.C., Hess, J.W., Harmon, R.S., 1985. Stable isotope variations in recharge to a karstic
- 1554 aquifer, Yorkshire dales, England. *Annales de la Société Géologique de Belgique* 108, 225.

1555 Atsawawaranunt, K., Comas-Bru, L., Mozhdehi, S.A., Deininger, M., Harrison, S.P., Baker, A., Boyd,
 1556 M., Kaushal, N., Ahmad, S.M., Brahim, Y.A., Arienzo, M., Bajo, P., Braun, K., Burstyn, Y., Chawchai, S.,
 1557 Duan, W.H., Hatvani, I.G., Hu, J., Kern, Z., Labuhn, I., Lachniet, M., Lechleitner, F.A., Lorrey, A., Perez-
 1558 Mejias, C., Pickering, R., Scropton, N., Members, S.W.G., 2018. The SISAL database: a global resource
 1559 to document oxygen and carbon isotope records from speleothems. *Earth System Science Data* 10,
 1560 1687-1713.

1561 Ayalon, A., Bar-Matthews, M., Sass, E., 1998. Rainfall-recharge relationships within a karstic terrain
 1562 in the Eastern Mediterranean semi-arid region, Israel: $\delta^{18}\text{O}$ and δD characteristics *Journal of*
 1563 *Hydrology* 207, 18-31.

1564 Badertscher, S., Borsato, A., Frisia, S., Cheng, H., Edwards, R.L., Tuysuz, O., Fleitmann, D., 2014.
 1565 Speleothems as sensitive recorders of volcanic eruptions - the Bronze Age Minoan eruption recorded
 1566 in a stalagmite from Turkey. *Earth Planet. Sci. Lett.* 392, 58-66.

1567 Baker, A., Barnes, W.L., Smart, P.L., 1997. Variations in the discharge and organic matter content of
 1568 stalagmite drip waters in Lower Cave, Bristol. *Hydrol Process* 11, 1541-1555.

1569 Baker, A., Bradley, C., 2010. Modern stalagmite $\delta^{18}\text{O}$: Instrumental calibration and forward
 1570 modelling. *Global and Planetary Change* 71, 201-206.

1571 Baker, A., Brunsdon, C., 2003. Non-linearities in drip water hydrology: an example from Stump Cross
 1572 Caverns, Yorkshire. *J Hydrol* 277, 151-163.

1573 Baker, A., Hartmann, A., Duan, W., Hankin, S., Comas-Bru, L., Cuthbert, M.O., Treble, P.C., Banner, J.,
 1574 Genty, D., Baldini, L.M., Bartolomé, M., Moreno, A., Pérez-Mejías, C., Werner, M., 2019. Global
 1575 analysis reveals climatic controls on the oxygen isotope composition of cave drip water. *Nature*
 1576 *Communications* 10, 2984.

1577 Baker, A., Smart, P.L., Edwards, R.L., Richards, D.A., 1993. Annual growth banding in a cave
1578 stalagmite. *Nature* 364, 518-520.

1579 Baker, A.J., Matthey, D.P., Baldini, J.U.L., 2014. Reconstructing modern stalagmite growth from cave
1580 monitoring, local meteorology, and experimental measurements of dripwater films. *Earth and*
1581 *Planetary Science Letters* 392, 239-249.

1582 Baldini, J.U.L., Bertram, R.A., Ridley, H.E., 2018. Ground air: A first approximation of the Earth's
1583 second largest reservoir of carbon dioxide gas. *Sci. Total Environ.* 616-617, 1007-1013.

1584 Baldini, J.U.L., McDermott, F., Baker, A., Baldini, L.M., Matthey, D.P., Railsback, L.B., 2005. Biomass
1585 effects on stalagmite growth and isotope ratios: A 20th century analogue from Wiltshire, England.
1586 *Earth Planet. Sci. Lett.* 240, 486-494.

1587 Baldini, J.U.L., McDermott, F., Baldini, L.M., Ottley, C.J., Linge, K.L., Clipson, N., Jarvis, K.E., 2012.
1588 Identifying short-term and seasonal trends in cave drip water trace element concentrations based on
1589 a daily-scale automatically collected drip water dataset. *Chem. Geol.* 330, 1-16.

1590 Baldini, J.U.L., McDermott, F., Fairchild, I.J., 2002. Structure of the 8200-year cold event revealed by
1591 a speleothem trace element record. *Science* 296, 2203-2206.

1592 Baldini, J.U.L., McDermott, F., Fairchild, I.J., 2006. Spatial variability in cave drip water
1593 hydrochemistry: Implications for stalagmite paleoclimate records. *Chem. Geol.* 235, 390-404.

1594 Baldini, J.U.L., McDermott, F., Hoffmann, D.L., Richards, D.A., Clipson, N., 2008. Very high-frequency
1595 and seasonal cave atmosphere P_{CO_2} variability: Implications for stalagmite growth and oxygen
1596 isotope-based paleoclimate records. *Earth Planet. Sci. Lett.* 272, 118-129.

1597 Baldini, L.M., Baldini, J.U.L., McDermott, F., Arias, P., Cueto, M., Fairchild, I.J., Hoffmann, D.L.,
1598 Matthey, D.P., Müller, W., Nita, D.C., Ontañón, R., García-Moncó, C., Richards, D.A., 2019. North

1599 Iberian temperature and rainfall seasonality over the Younger Dryas and Holocene. Quaternary
1600 Science Reviews 226, 105998.

1601 Baldini, L.M., McDermott, F., Baldini, J.U.L., Arias, P., Cueto, M., Fairchild, I.J., Hoffmann, D.L.,
1602 Matthey, D.P., Müller, W., Nita, D.C., Ontañón, R., García-Moncó, C., Richards, D.A., 2015. Regional
1603 temperature, atmospheric circulation, and sea-ice variability within the Younger Dryas Event
1604 constrained using a speleothem from northern Iberia. Earth Planet. Sci. Lett. 419, 101-110.

1605 Ban, F.M., Baker, A., Marjo, C.E., Duan, W.H., Li, X.L., Han, J.X., Coleborn, K., Akter, R., Tan, M.,
1606 Nagra, G., 2018. An optimized chronology for a stalagmite using seasonal trace element cycles from
1607 Shihua Cave, Beijing, North China. Scientific Reports 8, 4551.

1608 Banner, J.L., Guilfoyle, A., James, E.W., Stern, L.A., Musgrove, M., 2007. Seasonal variations in
1609 modern speleothem calcite growth in Central Texas, USA. J Sediment Res 77, 615-622.

1610 Bar-Matthews, M., Ayalon, A., Matthews, A., Sass, E., Halicz, L., 1996. Carbon and oxygen isotope
1611 study of the active water-carbonate system in a karstic Mediterranean cave: Implications for
1612 paleoclimate research in semiarid regions. Geochim. Cosmochim. Acta 60, 337-347.

1613 Bergel, S.J., Carlson, P.E., Larson, T.E., Wood, C.T., Johnson, K.R., Banner, J., Breecker, D.O., 2017.
1614 Constraining the subsoil carbon source to cave-air CO₂ and speleothem calcite in central Texas. 217,
1615 112-127.

1616 Berkelhammer, M., Sinha, A., Stott, L., Cheng, H., Pausata, F.S.R., Yoshimura, K., 2012. An abrupt
1617 shift in the Indian Monsoon 4000 years ago. Geophysical Monograph Series 198, 75-87.

1618 Blyth, A.J., Baker, A., Thomas, L.E., Van Calsteren, P., 2011. A 2000-year lipid biomarker record
1619 preserved in a stalagmite from north-west Scotland. J. of Quaternary Sci. 26, 326-334.

1620 Borsato, A., Frisia, S., Fairchild, I.J., Somogyi, A., Susini, J., 2007. Trace element distribution in annual
 1621 stalagmite laminae mapped by micrometer-resolution X-ray fluorescence: implications for
 1622 incorporation of environmentally significant species. *Geochim. Cosmochim. Acta* 71, 1494-1512.

1623 Borsato, A., Frisia, S., Hellstrom, J., Treble, P., Johnson, K., Howard, D., Greig, A., 2019. Fast high-
 1624 resolution synchrotron micro-XRF mapping of annually laminated stalagmites, European Geoscience
 1625 Union General Assembly. EGU, Vienna.

1626 Borsato, A., Frisia, S., Wynn, P.M., Fairchild, I.J., Miorandi, R., 2015. Sulphate concentration in cave
 1627 dripwater and speleothems: long-term trends and overview of its significance as proxy for
 1628 environmental processes and climate changes. *Quaternary Sci. Rev.* 127, 48-60.

1629 Breecker, D.O., Payne, A.E., Quade, J., Banner, J.L., Ball, C.E., Meyer, K.W., Cowan, B.D., 2012. The
 1630 sources and sinks of CO₂ in caves under mixed woodland and grassland vegetation. *Geochim.*
 1631 *Cosmochim. Acta* 96, 230-246.

1632 Breitenbach, S.F.M., Adkins, J.F., Meyer, H., Marwan, N., Kumar, K.K., Haug, G.H., 2010. Strong
 1633 influence of water vapor source dynamics on stable isotopes in precipitation observed in Southern
 1634 Meghalaya, NE India. *Earth and Planetary Science Letters* 292, 212-220.

1635 Breitenbach, S.F.M., Bernasconi, S.M., 2011. Carbon and oxygen isotope analysis of small carbonate
 1636 samples (20 to 100 μ g) with a GasBench II preparation device. *Rapid Commun. Mass Spectrom.*
 1637 25, 1910-1914.

1638 Breitenbach, S.F.M., Lechleitner, F.A., Meyer, H., Diengdoh, G., Matthey, D., Marwan, N., 2015. Cave
 1639 ventilation and rainfall signals in dripwater in a monsoonal setting – a monitoring study from NE
 1640 India. *Chemical Geology* 402, 111-124.

1641 Breitenbach, S.F.M., Plessen, B., Waltgenbach, S., Tjallingii, R., Leonhardt, J., Jochum, K.P., Meyer, H.,
 1642 Goswami, B., Marwan, N., Scholz, D., 2019. Holocene interaction of maritime and continental climate

1643 in Central Europe: New speleothem evidence from Central Germany. *Global and Planet. Change* 176,
 1644 144-161.

1645 Broecker, W.S., 1960. Radiocarbon measurements and annual rings in cave formations. *Nature* 185,
 1646 93-94.

1647 Broughton, P.L., 1983. Environmental Implications of competitive growth fabrics in stalactitic
 1648 carbonate. *International Journal of Speleology*. 13, 31-41.

1649 Buhmann, D., Dreybrodt, W., 1985. The kinetics of calcite dissolution and precipitation in
 1650 geologically relevant situations of karst areas. 2. closed system. *Chemical Geology* 53, 109-124.

1651 Cabellero, E., Jimenez de Cisneros, C., Reyes, E., 1996. A stable isotope study of cave seepage waters.
 1652 *Applied Geochemistry* 11, 583-587.

1653 Carlson, P.E., Miller, N.R., Banner, J.L., Breecker, D.O., Casteel, R.C., 2018. The potential of near-
 1654 entrance stalagmites as high-resolution terrestrial paleoclimate proxies: Application of isotope and
 1655 trace-element geochemistry to seasonally-resolved chronology. *Geochimica et Cosmochimica Acta*
 1656 235, 55-75.

1657 Chapman, J.B., Ingraham, N.L., Hess, J.W., 1992. Isotopic investigation of infiltration and unsaturated
 1658 zone flow processes at Carlsbad Caverns. *Journal of Hydrology* 133, 343-363.

1659 Chen, C.-J., Li, T.-Y., 2018. Geochemical characteristics of cave drip water respond to ENSO based on
 1660 a 6-year monitoring work in Yangkou Cave, Southwest China. *Journal of Hydrology* 561, 896-907.

1661 Cheng, H., Lawrence Edwards, R., Shen, C.-C., Polyak, V.J., Asmerom, Y., Woodhead, J., Hellstrom, J.,
 1662 Wang, Y., Kong, X., Spötl, C., Wang, X., Calvin Alexander, E., 2013. Improvements in ^{230}Th dating,
 1663 ^{230}Th and ^{234}U half-life values, and U–Th isotopic measurements by multi-collector inductively
 1664 coupled plasma mass spectrometry. *Earth and Planetary Science Letters* 371-372, 82-91.

1665 Cole, J.M., Nienstedt, J., Spataro, G., Rasbury, E.T., Lanzirrotti, A., Celestian, A.J., Nilsson, M., Hanson,
 1666 G.N., 2003. Phosphor imaging as a tool for in situ mapping of ppm levels of uranium and thorium in
 1667 rocks and minerals. *Chem. Geol.* 193, 127-136.

1668 Comas-Bru, L., Harrison, S.P., 2019. SISAL: Bringing Added Value to Speleothem Research.
 1669 *Quaternary* 2, 7.

1670 Comas-Bru, L., Harrison, S.P., Werner, M., Rehfeld, K., Scroxton, N., Veiga-Pires, C., Ahmad, S.M.,
 1671 Brahim, Y.A., Mozhdghi, S.A., Arienzo, M., Atsawawaranunt, K., Baker, A., Braun, K., Breitenbach, S.,
 1672 Burstyn, Y., Chawchai, S., Columbu, A., Deininger, M., Demeny, A., Dixon, B., Hatvani, I.G., Hu, J.,
 1673 Kaushal, N., Kern, Z., Labuhn, I., Lachniet, M.S., Lechleitner, F.A., Lorrey, A., Markowska, M., Nehme,
 1674 C., Novello, V.F., Oster, J., Perez-Mejias, C., Pickering, R., Sekhon, N., Wang, X.F., Warken, S.,
 1675 Atkinson, T., Ayalon, A., Baldini, J., Bar-Matthews, M., Bernal, J.P., Boch, R., Borsato, A., Boyd, M.,
 1676 Brierley, C., Cai, Y.J., Carolin, S., Cheng, H., Constantin, S., Couchoud, I., Cruz, F., Denniston, R.,
 1677 Dragusin, V., Duan, W.H., Ersek, V., Finne, M., Fleitmann, D., Fohlmeister, J., Frappier, A., Genty, D.,
 1678 Holzkamper, S., Hopley, P., Johnston, V., Kathayat, G., Keenan-Jones, D., Koltai, G., Li, T.Y., Lone,
 1679 M.A., Luetscher, M., Matthey, D., Moreno, A., Moseley, G., Psomiadis, D., Ruan, J.Y., Scholz, D., Sha,
 1680 L.J., Smith, A.C., Strikis, N., Treble, P., Unal-Imer, E., Vaks, A., Vansteenberge, S., Voarintsoa, N.R.G.,
 1681 Wong, C., Wortham, B., Wurtzel, J., Zhang, H., Grp, S.W., 2019. Evaluating model outputs using
 1682 integrated global speleothem records of climate change since the last glacial. *Clim Past* 15, 1557-
 1683 1579.

1684 Cook, E.R., Krusic, P.J., Anchukaitis, K.J., Buckley, B.M., Nakatsuka, T., Sano, M., Asia2K, P., 2013.
 1685 Tree-ring reconstructed summer temperature anomalies for temperate East Asia since 800 CE. *Clim.*
 1686 *Dynam.* 41, 2957-2972.

1687 Cowan, B.D., Osborne, M.C., Banner, J.L., 2013. Temporal variability of cave air PCO₂ in Central
 1688 Texas. *J Cave Karst Stud* 75, 38-50.

1689 Cruz Jr., F.W., Karmann, I., Vianna, J., O., Burns, S.J., Ferrari, J.A., Vuille, M., Sial, A.N., Moreira, M.Z.,
1690 2005. Stable isotope study of cave percolation waters in subtropical Brazil: Implications for
1691 paleoclimate inferences from speleothems. *Chemical Geology* 220, 245-262.

1692 Czuppon, G., Demény, A., Leél-Össy, S., Óvari, M., Stieber, J., Kiss, K., Kármán, K., Surányi, G.,
1693 Haszpra, L., 2018. Cave monitoring in the Béke and Baradla caves (Northeastern Hungary):
1694 implications for the conditions for the formation cave carbonates. *International Journal of*
1695 *Speleology*, 13-28.

1696 Daëron, M., Drysdale, R.N., Peral, M., Huyghe, D., Blamart, D., Coplen, T.B., Lartaud, F., Zanchetta,
1697 G., 2019. Most Earth-surface calcites precipitate out of isotopic equilibrium. *Nat Commun* 10.

1698 Deininger, M., McDermott, F., Mudelsee, M., Werner, M., Frank, N., Mangini, A., 2017. Coherency of
1699 late Holocene European speleothem delta O-18 records linked to North Atlantic Ocean circulation.
1700 *Clim. Dynam.* 49, 595-618.

1701 Deininger, M., Scholz, D., 2019. ISOLUTION 1.0: an ISOtope evoLUTION model describing the stable
1702 oxygen (delta O-18) and carbon (delta C-13) isotope values of speleothems. *International Journal of*
1703 *Speleology* 48, 21-32.

1704 Deininger, M., Werner, M., McDermott, F., 2016. North Atlantic Oscillation controls on oxygen and
1705 hydrogen isotope gradients in winter precipitation across Europe; implications for palaeoclimate
1706 studies. *Clim Past* 12, 2127-2143.

1707 Dredge, J., Fairchild, I.J., Harrison, R.M., Fernandez-Cortes, A., Sanchez-Moral, S., Jurado, V., Gunn, J.,
1708 Smith, A., Spotl, C., Matthey, D., Wynn, P.M., Grassineau, N., 2013. Cave aerosols: distribution and
1709 contribution to speleothem geochemistry. *Quaternary Sci. Rev.* 63, 23-41.

1710 Dreybrodt, W., 1980. Deposition of calcite from thin films of natural calcareous solutions and the
1711 growth of speleothems. *Chem. Geol.* 29, 89-105.

1712 Dreybrodt, W., 1988. Processes in karst systems - physics, chemistry and geology. Springer, Berlin,
1713 New York.

1714 Dreybrodt, W., 1999. Chemical kinetics, speleothem growth and climate. *Boreas* 28, 347-356.

1715 Dreybrodt, W., Deininger, M., 2014. The impact of evaporation to the isotope composition of DIC in
1716 calcite precipitating water films in equilibrium and kinetic fractionation models. *Geochim.*
1717 *Cosmochim. Acta* 125, 433-439.

1718 Duan, F.C., Wu, J.Y., Wang, Y.J., Edwards, R.L., Cheng, H., Kong, X.G., Zhang, W.H., 2015. A 3000-yr
1719 annually laminated stalagmite record of the Last Glacial Maximum from Hulu Cave, China.
1720 *Quaternary Res.* 83, 360-369.

1721 Duan, W., Ruan, J., Luo, W., Li, T., Tian, L., Zeng, G., Zhang, D., Bai, Y., Li, J., Tao, T., Zhang, P., Baker,
1722 A., Tan, M., 2016. The transfer of seasonal isotopic variability between precipitation and drip water
1723 at eight caves in the monsoon regions of China. *Geochim. Cosmochim. Acta* 183, 250-266.

1724 Edwards, L.R., Chen, J.H., Wasserburg, G.J., 1987. ^{238}U - ^{234}U - ^{230}Th - ^{232}Th systematics and the
1725 precise measurement of time over the past 500,000 years. *Earth Planet. Sci. Lett.* 81, 175-192.

1726 Edwards, R.L., Gallup, C.D., 1993. Dating of the Devils Hole Calcite Vein. *Science* 259, 1626-1627.

1727 Emiliani, C., 1955. Pleistocene temperatures. *Journal of Geology* 63, 538-578.

1728 Epstein, S., Buchsbaum, R., Lowenstam, H.A., Urey, H.C., 1951. Carbonate-water isotopic
1729 temperature scale. *Bulletin of the Geological Society of America* 62, 417-427.

1730 Evans, D., Müller, W., 2013. LA-ICPMS elemental imaging of complex discontinuous carbonates: An
1731 example using large benthic foraminifera. *J. Anal. At. Spectrom.* 28, 1039-1044.

1732 Evans, M.N., Tolwinski-Ward, S.E., Thompson, D.M., Achukaitis, K.J., 2013. Applications of proxy
1733 system modeling in high resolution paleoclimatology. *Quaternary Science Reviews* 76, 16-28.

1734 Faimon, J., Lang, M., 2013. Variances in airflows during different ventilation modes in a dynamic U-
 1735 shaped cave. *Int J Speleol* 42, 115-122.

1736 Fairchild, I.J., Baker, A., 2012. *Speleothem Science: From Processes to Past Environments*. Wiley-
 1737 Blackwell, Chichester, UK.

1738 Fairchild, I.J., Baker, A., Borsato, A., Frisia, S., Hinton, R.W., McDermott, F., Tooth, A.F., 2001. Annual
 1739 to sub-annual resolution of multiple trace-element trends in speleothems. *J. Geol. Soc. London* 158,
 1740 831-841.

1741 Fairchild, I.J., Borsato, A., Tooth, A.F., Frisia, S., Hawkesworth, C.J., Huang, Y., McDermott, F., Spiro,
 1742 B., 2000. Controls on trace element (Sr-Mg) compositions of carbonate cave waters: implications for
 1743 speleothem climatic records. *Chem. Geol.* 166, 255-269.

1744 Fairchild, I.J., Hartland, A., 2010. Trace element variations in stalagmites: controls by climate and by
 1745 karst system processes. *EMU Notes in Mineralogy* 10, 259-287.

1746 Fairchild, I.J., Smith, C.L., Baker, A., Fuller, L., Spotl, C., Matthey, D., McDermott, F., Eimp, 2006.
 1747 Modification and preservation of environmental signals in speleothems. *Earth Sci. Rev.* 75, 105-153.

1748 Fairchild, I.J., Treble, P.C., 2009. Trace elements in speleothems as recorders of environmental
 1749 change. *Quaternary Sci. Rev.* 28, 449-468.

1750 Feng, W., Casteel, R.C., Banner, J.L., Heinze-Fry, A., 2014. Oxygen isotope variations in rainfall, drip-
 1751 water and speleothem calcite from a well-ventilated cave in Texas, USA: Assessing a new
 1752 speleothem temperature proxy. *Geochim. Cosmochim. Acta* 127, 233-250.

1753 Feng, X., Porporato, A., Rodriguez-Iturbe, I., 2013. Changes in rainfall seasonality in the tropics.
 1754 *Nature Climate Change* 3, 811-815.

1755 Fick, S.E., Hijmans, R.J., 2017. WorldClim 2: new 1-km spatial resolution climate surfaces for global
1756 land areas. *Int J Climatol* 37, 4302-4315.

1757 Finch, A.A., Shaw, P.A., Weedon, G.P., Holmgren, K., 2001. Trace element variation in speleothem
1758 aragonite: potential for palaeoenvironmental reconstruction. *Earth and Planetary Science Letters*
1759 186, 255-267.

1760 Fohlmeister, J., Lechleitner, F.A., 2019. STAlagmite dating by radiocarbon (star): A software tool for
1761 reliable and fast age depth modelling. *Quat Geochronol* 51, 120-129.

1762 Fohlmeister, J., Plessen, B., Dudashvili, A.S., Tjallingii, R., Wolff, C., Gafurov, A., Cheng, H., 2017.
1763 Winter precipitation changes during the Medieval Climate Anomaly and the Little Ice Age in arid
1764 Central Asia. *Quaternary Sci. Rev.* 178, 24-36.

1765 Frappier, A.B., Sahagian, D., Carpenter, S.J., González, L.A., Frappier, B.R., 2007. Stalagmite stable
1766 isotope record of recent tropical cyclone events. *Geology* 35.

1767 Frick, D.A., Schuessler, J.A., von Blanckenburg, F., 2016. Development of routines for simultaneous in
1768 situ chemical composition and stable Si isotope ratio analysis by femtosecond laser ablation
1769 inductively coupled plasma mass spectrometry. *Analytica Chimica Acta* 938, 33-43.

1770 Frisia, S., 2015. Microstratigraphic logging of calcite fabrics in speleothems as tool for palaeoclimate
1771 studies. *Int J Speleol* 44, 1-16.

1772 Frisia, S., Borsato, A., Fairchild, I.J., McDermott, F., 2000. Calcite fabrics, growth mechanisms, and
1773 environments of formation in speleothems from the Italian Alps and southwestern Ireland. *J*
1774 *Sediment Res* 70, 1183-1196.

1775 Frisia, S., Borsato, A., Fairchild, I.J., Susini, J., 2005. Variations in atmospheric sulphate recorded in
1776 stalagmites by synchrotron micro-XU and XANES analyses. *Earth Planet. Sci. Lett.* 235, 729-740.

1777 Frisia, S., Borsato, A., Hellstrom, J., 2018. High spatial resolution investigation of nucleation, growth
 1778 and early diagenesis in speleothems as exemplar for sedimentary carbonates. *Earth Sci. Rev.* 178, 68-
 1779 91.

1780 Frisia, S., Borsato, A., Susini, J., 2008. Synchrotron radiation applications to past volcanism archived
 1781 in speleothems: An overview. *J. Volcanol. Geotherm. Res.* 177, 96-100.

1782 Gascoyne, M., Schwarcz, H.P., Ford, D.C., 1980. A palaeotemperature record for the mid-Wisconsin
 1783 in Vancouver Island. *Nature* 285, 474-476.

1784 Gazis, C., Feng, X.H., 2004. A stable isotope study of soil water: evidence for mixing and preferential
 1785 flow paths. *Geoderma* 119, 97-111.

1786 Genty, D., 2008. Palaeoclimate research in Villars Cave (Dordogne, SW France). *Int J Speleol* 37, 173-
 1787 191.

1788 Genty, D., Baker, A., Vokal, B., 2001. Intra- and inter-annual growth rate of modern stalagmites.
 1789 *Chemical Geology* 176, 191-212.

1790 Genty, D., Deflandre, G., 1998. Drip flow variations under a stalactite of the Père Noël cave
 1791 (Belgium). Evidence of seasonal variations and air pressure constraints. *J Hydrol* 211, 208-232.

1792 Guo, W., Zhou, C., 2019. Patterns and controls of disequilibrium isotope effects in speleothems:
 1793 Insights from an isotope-enabled diffusion-reaction model and implications for quantitative
 1794 thermometry. *Geochimica et Cosmochimica Acta* 267, 196-226.

1795 Harmon, R.S., 1979. An isotopic study of groundwater seepage in the Central Kentucky karst. *Water*
 1796 *Resources Research* 15, 476.

1797 Hartland, A., Fairchild, I.J., Lead, J.R., 2009. Colloids in karstic percolation waters: Implications for the
 1798 interpretation of trace element variations in speleothems. *Geochim. Cosmochim. Acta* 73, A498-
 1799 A498.

1800 Hartland, A., Fairchild, I.J., Lead, J.R., Baker, A., 2010. Fluorescent properties of organic carbon in
 1801 cave dripwaters: Effects of filtration, temperature and pH. *Sci. Total Environ.* 408, 5940-5950.

1802 Hartland, A., Fairchild, I.J., Lead, J.R., Borsato, A., Baker, A., Frisia, S., Baalousha, M., 2012. From soil
 1803 to cave: Transport of trace metals by natural organic matter in karst dripwaters. *Chem. Geol.* 304,
 1804 68-82.

1805 Hartland, A., Fairchild, I.J., Lead, J.R., Zhang, H., Baalousha, M., 2011. Size, speciation and lability of
 1806 NOM-metal complexes in hyperalkaline cave dripwater. *Geochim. Cosmochim. Acta* 75, 7533-7551.

1807 Hellstrom, J., 2003. Rapid and accurate U/Th dating using parallel ion-counting multi-collector ICP-
 1808 MS. *J. Anal. At. Spectrom.* 18, 1346-1351.

1809 Helser, T.E., Kastelle, C.R., McKay, J.L., Orland, I.J., Kodzon, R., Valley, J.W., 2018. Evaluation of
 1810 micromilling/conventional isotope ratio mass spectrometry and secondary ion mass spectrometry of
 1811 $\delta^{18}\text{O}$ values in fish otoliths for sclerochronology. *Rapid Commun Mass Spectrom* 32, 1781-1790.

1812 Hendy, C.H., Wilson, A.T., 1968. Paleoclimatic data from speleothems. *Nature* 216, 48-51.

1813 Hess, J.W., White, W.B., 1989. Water Budget and Physical Hydrology, in: B., W.W., White, E.L. (Eds.),
 1814 *Karst Hydrology: Concepts from the Mammoth Cave Area*. Springer-Verlag, Boston, pp. 105-126.

1815 Hoffmann, D.L., Prytulak, J., Richards, D.A., Elliott, T.R., Coath, C.D., Smart, P.L., Scholz, D., 2007.
 1816 Procedures for accurate U and Th isotope measurements by high precision MC-ICPMS. *Int. J. Mass*
 1817 *Spectrom. Ion Processes* 264, 97-109.

1818 Hsiang, S.M., Burke, M., Miguel, E., 2013. Quantifying the Influence of Climate on Human Conflict.
1819 Science 341, 1235367.

1820 Hu, C., Henderson, G.M., Huang, J., Xie, S., Sun, Y., Johnson, K.R., 2008. Quantification of Holocene
1821 Asian monsoon rainfall from spatially separated cave records. Earth Planet. Sci. Lett. 266, 221-232.

1822 Huang, S.P., Pollack, H.N., Shen, P.Y., 2000. Temperature trends over the past five centuries
1823 reconstructed from borehole temperatures. Nature 403, 756-758.

1824 Huang, Y., Fairchild, I.J., 2001. Partitioning of Sr^{2+} and Mg^{2+} into calcite under karst-analogue
1825 experimental conditions. Geochim. Cosmochim. Acta 65, 47-62.

1826 Huang, Y., Fairchild, I.J., Borsato, A., Frisia, S., Cassidy, N.J., McDermott, F., Hawkesworth, C.J., 2001.
1827 Seasonal variations in Sr, Mg and P in modern speleothems (Grotta di Ernesto, Italy). Chem. Geol.
1828 175, 429-448.

1829 IAEA, 2001. GNIP Maps and Animations. , Vienna.

1830 IAEA/WMO, 2001. Global Network of Isotopes in Precipitation. The GNIP Database.

1831 James, E., Banner, J., Hardt, B., 2015. A global model for cave ventilation and seasonal bias in
1832 speleothem paleoclimate records.

1833 Jamieson, R.A., Baldini, J.U.L., Brett, M.J., Taylor, J., Ridley, H.E., Ottley, C.J., Prufer, K.M.,
1834 Wassenburg, J.A., Scholz, D., Breitenbach, S.F.M., 2016. Intra- and inter-annual uranium
1835 concentration variability in a Belizean stalagmite controlled by prior aragonite precipitation: A new
1836 tool for reconstructing hydro-climate using aragonitic speleothems. Geochim. Cosmochim. Acta 190,
1837 332-346.

1838 Jamieson, R.A., Baldini, J.U.L., Frappier, A.B., Müller, W., 2015. Volcanic ash fall events identified
 1839 using principle component analysis of a high-resolution speleothem trace element dataset. *Earth*
 1840 *and Planetary Science Letters* 426, 36-45.

1841 Johnson, K.R., Hu, C., Belshaw, N.S., Henderson, G.M., 2006. Seasonal trace-element and stable-
 1842 isotope variations in a Chinese speleothem: The potential for high-resolution paleomonsoon
 1843 reconstruction. *Earth and Planetary Science Letters* 244, 394-407.

1844 Kaufman, A., Bar-Matthews, M., Ayalon, A., Carmi, I., 2003. The vadose flow above Soreq Cave,
 1845 Israel: a tritium study of the cave waters. *Journal of Hydrology* 273, 155-163.

1846 Kennett, D.J., Breitenbach, S.F.M., Aquino, V.V., Asmerom, Y., Awe, J., Baldini, J.U.L., Bartlein, P.,
 1847 Culleton, B.J., Ebert, C., Jazwa, C., Macri, M.J., Marwan, N., Polyak, V., Prufer, K.M., Ridley, H.E.,
 1848 Sodemann, H., Winterhalder, B., Haug, G.H., 2012. Development and Disintegration of Maya Political
 1849 Systems in Response to Climate Change. *Science* 338, 788-791.

1850 Khiewtam, R.S., Ramakrishnan, P.S., 1993. Litter and fine root dynamics of a relict sacred grove
 1851 forest at Cherrapunji in north-eastern India. *Forest Ecology and Management* 60, 327-344.

1852 Kita, N.T., Huberty, J.M., Kozdon, R., Beard, B.L., Valley, J.W., 2011. High-precision SIMS oxygen,
 1853 sulfur and iron stable isotope analyses of geological materials: accuracy, surface topography and
 1854 crystal orientation. *Surf. Interface Anal.* 43, 427-431.

1855 Köppen, W., 1918. Classification of climates according to temperature, precipitation and course of
 1856 the year. *Petermanns Mitt* 64, 193-203.

1857 Kuczumow, A., Genty, D., Chevallier, P., Nowak, J., Ro, C.U., 2003. Annual resolution analysis of a
 1858 SW-France stalagmite by X-ray synchrotron microprobe analysis. *Spectrochim Acta B* 58, 851-865.

1859 Kuczumow, A., Vekemans, B., Schalm, O., Gysels, K., Ro, C.U., Van Grieken, R., 2001. Analysis of
 1860 speleothems by electron and X-ray microprobes. *J. Anal. At. Spectrom.* 16, 90-95.

1861 Kylander-Clark, A.R.C., Hacker, B.R., Cottle, J.M., 2013. Laser-ablation split-stream ICP
 1862 petrochronology. *Chemical Geology* 345, 99-112.

1863 Lachniet, M.S., 2009. Climatic and environmental controls on speleothem oxygen-isotope values.
 1864 *Quaternary Science Reviews* 28, 412-432.

1865 Lauritzen, S., 1995. High Resolution Paleotemperature Proxy Record for the Last Interglaciation
 1866 Based on Norwegian Speleothems. *Quaternary Res.* 43, 133-146.

1867 Lauritzen, S., Lundberg, J., 1999. Calibration of the speleothem delta function: an absolute
 1868 temperature record for the Holocene in northern Norway. *Holocene* 9, 659-669.

1869 Lechleitner, F.A., Baldini, J.U.L., Breitenbach, S.F.M., Fohlmeister, J., McIntyre, C., Goswami, B.,
 1870 Jamieson, R.A., van der Voort, T.S., Prufer, K., Marwan, N., Culleton, B.J., Kennett, D.J., Asmerom, Y.,
 1871 Polyak, V., Eglinton, T.I., 2016a. Hydrological and climatological controls on radiocarbon
 1872 concentrations in a tropical stalagmite. *Geochim. Cosmochim. Acta* 194, 233-252.

1873 Lechleitner, F.A., Fohlmeister, J., McIntyre, C., Baldini, L.M., Jamieson, R.A., Hercman, H.,
 1874 Gąsiorowski, M., Pawlak, J., Stefaniak, K., Socha, P., Eglinton, T.I., Baldini, J.U.L., 2016b. A novel
 1875 approach for construction of radiocarbon-based chronologies for speleothems. *Quat Geochronol* 35,
 1876 54-66.

1877 Li, F., Vanwezer, N., Boivin, N., Gao, X., Ott, F., Petraglia, M., Roberts, P., 2019. Heading north: Late
 1878 Pleistocene environments and human dispersals in central and eastern Asia. *Plos One* 14, e0216433.

1879 Linzmeier, B.J., Kitajima, K., Denny, A.C., Cammack, J.N., 2018. Making maps on a micrometer scale.
 1880 *Eos* 99.

1881 Liu, Y.H., Henderson, G.M., Hu, C.Y., Mason, A.J., Charnley, N., Johnson, K.R., Xie, S.C., 2013. Links
 1882 between the East Asian monsoon and North Atlantic climate during the 8,200 year event. *Nat.*
 1883 *Geosci.* 6, 117-120.

1884 Luetscher, M., Boch, R., Sodemann, H., Spotl, C., Cheng, H., Edwards, R.L., Frisia, S., Hof, F., Müller,
 1885 W., 2015. North Atlantic storm track changes during the Last Glacial Maximum recorded by Alpine
 1886 speleothems. *Nat Commun* 6, 6344.

1887 Luo, T., Hu, Z., Zhang, W., Günther, D., Liu, Y., Zong, K., Hu, S., 2018. Reassessment of the influence
 1888 of carrier gases He and Ar on signal intensities in 193 nm excimer LA-ICP-MS analysis. *Journal of*
 1889 *Analytical Atomic Spectrometry* 33, 1655-1663.

1890 Luo, W., Wang, S., Zeng, G., Zhu, X., Liu, W., 2014. Daily response of drip water isotopes to
 1891 precipitation in Liangfeng Cave, Guizhou Province, SW China. *Quaternary International* 349, 153-158.

1892 Markowska, M., Baker, A., Andersen, M.S., Jex, C.N., Cuthbert, M.O., Rau, G.C., Graham, P.W.,
 1893 Rutledge, H., Mariethoz, G., Marjo, C.E., Treble, P.C., Edwards, N., 2016. Semi-arid zone caves:
 1894 Evaporation and hydrological controls on delta O-18 drip water composition and implications for
 1895 speleothem paleoclimate reconstructions. *Quaternary Sci. Rev.* 131, 285-301.

1896 Markowska, M., Baker, A., Treble, P.C., Andersen, M.S., Hankin, S., Jex, C.N., Tadros, C.V., Roach, R.,
 1897 2015. Unsaturated zone hydrology and cave drip discharge water response: Implications for
 1898 speleothem paleoclimate record variability. *J Hydrol* 529, 662-675.

1899 Markowska, M., Fohlmeister, J., Treble, P.C., Baker, A., Andersen, M.S., Hua, Q., 2019. Modelling the
 1900 ¹⁴C bomb-pulse in young speleothems using a soil carbon continuum model. *Geochim. Cosmochim.*
 1901 *Acta* 261, 342-367.

- 1902 Martin-Chivelet, J., Munoz-Garcia, M.B., Edwards, R.L., Turrero, M.J., Ortega, A.I., 2011. Land surface
1903 temperature changes in Northern Iberia since 4000 yr BP, based on delta C-13 of speleothems.
1904 *Global and Planet. Change* 77, 1-12.
- 1905 Martin-Garcia, R., Alonso-Zarza, A.M., Martin-Perez, A., Schroder-Ritzrau, A., Ludwig, T., 2014.
1906 Relationships between colour and diagenesis in the aragonite-calcite speleothems in Basajaun Etxea
1907 cave, Spain. *Sediment Geol* 312, 63-75.
- 1908 Matthey, D., Collister, C., 2008. Controls on water drop volume at speleothem drip sites: An
1909 experimental study. *J Hydrol* 358, 259-267.
- 1910 Matthey, D., Lowry, D., Duffet, J., Fisher, R., Hodge, E., Frisia, S., 2008. A 53 year seasonally resolved
1911 oxygen and carbon isotope record from a modern Gibraltar speleothem: Reconstructed drip water
1912 and relationship to local precipitation. *Earth Planet. Sci. Lett.* 269, 80-95.
- 1913 Matthey, D.P., Atkinson, T.C., Barker, J.A., Fisher, R., Latin, J.P., Durell, R., Ainsworth, M., 2016. Carbon
1914 dioxide, ground air and carbon cycling in Gibraltar karst. *Geochim. Cosmochim. Acta* 184, 88-113.
- 1915 Matthey, D.P., Fairchild, I.J., Atkinson, T.C., 2009. Seasonal microclimate control on calcite fabrics,
1916 stable isotopes and trace elements in modern speleothem from St. Michaels Cave, Gibraltar.
1917 *Geochim. Cosmochim. Acta* 73, A849-A849.
- 1918 Matthey, D.P., Fairchild, I.J., Atkinson, T.C., Latin, J.-P., Ainsworth, M., Durell, R., 2010. Seasonal
1919 microclimate control of calcite fabrics, stable isotopes and trace elements in modern speleothem
1920 from St Michaels cave, Gibraltar in: Pedley, H.M., Rogerson, M. (Eds.), *Tufas and Speleothems:*
1921 *Unravelling the Microbial and Physical Controls.* Geological Society of London Special Publication,
1922 London, pp. 323-344.

- 1923 Maupin, C.R., Partin, J.W., Shen, C.C., Quinn, T.M., Lin, K., Taylor, F.W., Banner, J.L., Thirumalai, K.,
 1924 Sinclair, D.J., 2014. Persistent decadal-scale rainfall variability in the tropical South Pacific
 1925 Convergence Zone through the past six centuries. *Clim Past* 10, 1319-1332.
- 1926 McDermott, F., 2004. Palaeo-climate reconstruction from stable isotope variations in speleothems: a
 1927 review. *Quaternary Sci. Rev.* 23, 901-918.
- 1928 McDermott, F., Atkinson, T.C., Fairchild, I.J., Baldini, L.M., Matthey, D.P., 2011. A first evaluation of the
 1929 spatial gradients in delta O-18 recorded by European Holocene speleothems. *Global and Planet.*
 1930 *Change* 79, 275-287.
- 1931 McMillan, E.A., Fairchild, I.J., Frisia, S., Borsato, A., McDermott, F., 2005. Annual trace element cycles
 1932 in calcite-aragonite speleothems: evidence of drought in the western Mediterranean 1200-1100 yr
 1933 BP. *J. of Quaternary Sci.* 20, 423-433.
- 1934 Menne, M.J., Durre, I., Vose, R.S., Gleason, B.E., Houston, T.G., 2012. An Overview of the Global
 1935 Historical Climatology Network-Daily Database. *J Atmos Ocean Tech* 29, 897-910.
- 1936 Mickler, P.J., Stern, L.A., Banner, J.L., 2006. Large kinetic isotope effects in modern speleothems.
 1937 *Geol. Soc. Am. Bull.* 118, 65-81.
- 1938 Millo, C., Strikis, N.M., Vonhof, H.B., Deininger, M., da Cruz, F.W., Wang, X.F., Cheng, H., Edwards,
 1939 R.L., 2017. Last glacial and Holocene stable isotope record of fossil dripwater from subtropical Brazil
 1940 based on analysis of fluid inclusions in stalagmites. *Chem. Geol.* 468, 84-96.
- 1941 Mischel, S.A., Scholz, D., Spötl, C., 2015. $\delta^{18}\text{O}$ values of cave drip water: a promising proxy for the
 1942 reconstruction of the North Atlantic Oscillation? *Climate Dynamics* 45, 3035-3050.

- 1943 Moerman, J.W., Cobb, K.M., Partin, J.W., Meckler, A.N., Carolin, S.A., Adkins, J.F., Lejau, S., Malang,
1944 J., Clark, B., Tuen, A.A., 2014. Transformation of ENSO-related rainwater to dripwater $\delta^{18}\text{O}$
1945 variability by vadose water mixing. *Geophys Res Lett* 41, 7907-7915.
- 1946 Moquet, J.S., Cruz, F.W., Novello, V.F., Strikis, N.M., Deininger, M., Karmann, I., Santos, R.V., Millo,
1947 C., Apaestegui, J., Guyot, J.L., Siffedine, A., Vuille, M., Cheng, H., Edwards, R.L., Santini, W., 2016.
1948 Calibration of speleothem delta O-18 records against hydroclimate instrumental records in Central
1949 Brazil. *Global and Planet. Change* 139, 151-164.
- 1950 Morellón, M., Valero-Garcés, B., Vegas-Villarrúbia, T., González-Sampériz, P., Romero, O., Delgado-
1951 Huertas, A., Mata, P., Moreno, A., Rico, M., Corella, J.P., 2009. Lateglacial and Holocene
1952 palaeohydrology in the western Mediterranean region: the Lake Estanya record (NE Spain).
1953 *Quaternary Science Reviews* 28, 2582-2599.
- 1954 Moreno, A., Pérez-Mejías, C., Bartolomé, M., Sancho, C., Cacho, I., Stoll, H., Delgado-Huertas, A.,
1955 Hellstrom, J., Edwards, R.L., Cheng, H., 2017. New speleothem data from Molinos and Ejulve caves
1956 reveal Holocene hydrological variability in northeast Iberia. *Quaternary Research* 88, 223-233.
- 1957 Moreno, A., Sancho, C., Bartolomé, M., Oliva-Urcia, B., Delgado-Huertas, A., Estrela, M.J., Corell, D.,
1958 López-Moreno, J.I., Cacho, I., 2014. Climate controls on rainfall isotopes and their effects on cave
1959 drip water and speleothem growth: the case of Molinos cave (Teruel, NE Spain). *Climate Dynamics*
1960 43, 221-241.
- 1961 Moseley, G.E., Spötl, C., Cheng, H., Boch, R., Min, A., Edwards, R.L., 2015. Termination-II
1962 interstadial/stadial climate change recorded in two stalagmites from the north European Alps.
1963 *Quaternary Science Reviews* 127, 229-239.
- 1964 Müller, W., Fietzke, J., 2016. The role of LA-ICP-MS in palaeoclimate research. *Elements* 12, 329-334.

1965 Müller, W., Shelley, M., Miller, P., Broude, S., 2009. Initial performance metrics of a new custom-
 1966 designed ArF excimer LA-ICPMS system coupled to a two-volume laser-ablation cell. *J. Anal. At.*
 1967 *Spectrom.* 24, 209-214.

1968 Müller, W., Valley, J.W., Warter, V., Kodzon, R., Evans, D., Orland, I.J., 2015. Natural high-
 1969 temperature metamorphic calcite as compositionally homogenous microanalytical standard?,
 1970 *Goldschmidt 2015*, Prague.

1971 Murata, F., Terao, T., Hayashi, T., Asada, H., Matsumoto, J., 2007. Relationship between atmospheric
 1972 conditions at Dhaka, Bangladesh, and rainfall at Cherrapunjee, India. *Natural Hazards* 44, 399-410.

1973 Myers, C.G., Oster, J.L., Sharp, W.D., Bennartz, R., Kelley, N.P., Covey, A.K., Breitenbach, S.F.M.,
 1974 2015. Northeast Indian stalagmite records Pacific decadal climate change: Implications for moisture
 1975 transport and drought in India. *Geophysical Research Letters* 42, 4124-4132.

1976 Nagra, G., Treble, P.C., Andersen, M.S., Bajo, P., Hellstrom, J., Baker, A., 2017. Dating stalagmites in
 1977 mediterranean climates using annual trace element cycles. *Sci. Rep.* 7, 621.

1978 Noronha, A.L., Johnson, K.R., Southon, J.R., Hu, C., Ruan, J., McCabe-Glynn, S., 2015. Radiocarbon
 1979 evidence for decomposition of aged organic matter in the vadose zone as the main source of
 1980 speleothem carbon. *Quaternary Sci. Rev.* 127, 37-47.

1981 O'Neil, J.R., Clayton, R.M., Mayeda, T., 1969. Oxygen isotope fractionation in divalent metal
 1982 carbonates. *J. Chem. Phys.* 30, 5547-5558.

1983 Oerter, E.J., Sharp, W.D., Oster, J.L., Ebeling, A., Valley, J.W., Kodzon, R., Orland, I.J., Hellstrom, J.,
 1984 Woodhead, J.D., Hergt, J.M., Chadwick, O.A., Amundson, R., 2016. Pedothem carbonates reveal
 1985 anomalous North American atmospheric circulation 70,000–55,000 years ago. *Proc Natl Acad Sci U S*
 1986 *A* 113, 919-924.

- 1987 Onac, B.P., Pace-Graczyk, K., Atudirei, V., 2008. Stable isotope study of precipitation and cave drip
1988 water in Florida (USA): implications for speleothem-based paleoclimate studies. *Isot. Environ. Health*
1989 *Stud.* 44, 149-161.
- 1990 Orland, I.J., Bar-Matthews, M., Ayalon, A., Matthews, A., Kozdon, R., Ushikubo, T., Valley, J.W., 2012.
1991 Seasonal resolution of Eastern Mediterranean climate change since 34 ka from a Soreq Cave
1992 speleothem. *Geochimica Et Cosmochimica Acta* 89, 240-255.
- 1993 Orland, I.J., Bar-Matthews, M., Kita, N.T., Ayalon, A., Matthews, A., Valley, J.W., 2008. Seasonal
1994 climate change as revealed by ion microprobe analysis of delta O-18 in Soreq Cave (Israel)
1995 speleothems. *Geochimica Et Cosmochimica Acta* 72, A709-A709.
- 1996 Orland, I.J., Bar-Matthews, M., Kita, N.T., Ayalon, A., Matthews, A., Valley, J.W., 2009. Climate
1997 deterioration in the Eastern Mediterranean as revealed by ion microprobe analysis of a speleothem
1998 that grew from 2.2 to 0.9 ka in Soreq Cave, Israel. *Quaternary Res.* 71, 27-35.
- 1999 Orland, I.J., Burstyn, Y., Bar-Matthews, M., Kozdon, R., Ayalon, A., Matthews, A., Valley, J.W., 2014.
2000 Seasonal climate signals (1990-2008) in a modern Soreq Cave stalagmite as revealed by high-
2001 resolution geochemical analysis. *Chem. Geol.* 363, 322-333.
- 2002 Orland, I.J., Edwards, R.L., Cheng, H., Kozdon, R., Cross, M., Valley, J.W., 2015. Direct measurements
2003 of deglacial monsoon strength in a Chinese stalagmite. *Geology* 43, 555-558.
- 2004 Orland, I.J., He, F., Bar-Matthews, M., Chen, G., Ayalon, A., Kutzbach, J.E., 2019. Resolving seasonal
2005 rainfall changes in the Middle East during the last interglacial period. *Proc Natl Acad Sci U S A* 116,
2006 24985-24990.
- 2007 Orr, P.C., 1952. Excavations in Moaning Cave. *Santa Barbara Museum of Natural History Bulletin* 1, 1-
2008 19.

- 2009 Ortega, R., Maire, R., Deves, G., Quinif, Y., 2005. High-resolution mapping of uranium and other trace
2010 elements in recrystallized aragonite-calcite speleothems from caves in the Pyrenees (France):
2011 Implications for U-series dating. *Earth Planet. Sci. Lett.* 237, 911-023.
- 2012 Oster, J.L., Montañez, I.P., Kelley, N.P., 2012. Response of a modern cave system to large seasonal
2013 precipitation variability. *Geochim. Cosmochim. Acta* 91, 92-108.
- 2014 Pacton, M., Breitenbach, S.F.M., Lechleitner, F.A., Vaks, A., Rollion-Bard, C., Gutareva, O.S., Osintcev,
2015 A.V., Vasconcelos, C., 2013. The role of microorganisms in the formation of a stalactite in Botovskaya
2016 Cave, Siberia – paleoenvironmental implications. *Biogeosciences* 10, 6115-6130.
- 2017 Parton, A., Farrant, A.R., Leng, M.J., Telfer, M.W., Groucutt, H.S., Petraglia, M.D., Parker, A.G., 2015.
2018 Alluvial fan records from southeast Arabia reveal multiple windows for human dispersal. *Geol.* 43,
2019 295-298.
- 2020 Peel, M.C., Finlayson, B.L., McMahon, T.A., 2007. Updated world map of the Köppen-Geiger climate
2021 classification. *Hydrology and Earth System Sciences* 11, 1633-1644.
- 2022 Perrin, J., Jeannin, P.-Y., Zwahlen, F., 2003. Epikarst storage in a karst aquifer: a conceptual model
2023 based on isotopic data, Milandre test site, Switzerland. *Journal of Hydrology* 279, 106-124.
- 2024 Prokop, P., Walanus, A., 2003. Trends and periodicity in the longest instrumental rainfall series for
2025 the area of most extreme rainfall in the world, northeast India. *Geographia Polonica* 76, 25-35.
- 2026 Pu, J., Wang, A., Shen, L., Yin, J., Yuan, D., Zhao, H., 2016. Factors controlling the growth rate, carbon
2027 and oxygen isotope variation in modern calcite precipitation in a subtropical cave, Southwest China.
2028 *Journal of Asian Earth Sciences* 119, 167-178.

2029 Railsback, L.B., Brook, G.A., Chen, J., Kalin, R., Fleisher, C., 1994. Environmental controls on the
 2030 petrology of a late Holocene speleothem from Botswana with annual layers of aragonite and calcite.
 2031 J Sediment Res A64, 147-155.

2032 Railsback, L.B., Liang, F.Y., Romani, J.R.V., Grandal-d'Anglade, A., Rodriguez, M.V., Fidalgo, L.S.,
 2033 Mosquera, D.F., Cheng, H., Edwards, R.L., 2011. Petrographic and isotopic evidence for Holocene
 2034 long-term climate change and shorter-term environmental shifts from a stalagmite from the Serra
 2035 do Courel of northwestern Spain, and implications for climatic history across Europe and the
 2036 Mediterranean. *Palaeogeography Palaeoclimatol.* 305, 172-184.

2037 Railsback, L.B., Liang, F.Y., Vidal-Romani, J.R., Garrett, K.B., Sellers, R.C., Vaquero-Rodriguez, M.,
 2038 Grandal-d'Anglade, A., Cheng, H., Edwards, R.L., 2017. Radiometric, isotopic, and petrographic
 2039 evidence of changing interglacials over the past 550,000 years from six stalagmites from the Serra do
 2040 Courel in the Cordillera Cantabrica of northwestern Spain. *Palaeogeography Palaeoclimatol.* 466, 137-152.

2041 Ramakrishnan, P.S., Subhash, C.R., 1988. Vegetation, biomass and productivity of seral grasslands of
 2042 Cherrapunji in north-east India. *Vegetatio* 74, 47-53.

2043 Ridley, H., Baldini, J., Prufer, K., Walczak, I., Breitenbach, S., 2015a. High-resolution monitoring of Yok
 2044 Balum Cave, Belize: An investigation of seasonal ventilation regimes and the atmospheric and drip-
 2045 flow response to a local earthquake. *Journal of Cave and Karst Studies* 77, 183-199.

2046 Ridley, H.E., Asmerom, Y., Baldini, J.U.L., Breitenbach, S.F.M., Aquino, V.V., Prufer, K.M., Culleton,
 2047 B.J., Polyak, V., Lechleitner, F.A., Kennett, D.J., Zhang, M., Marwan, N., Macpherson, C.G., Baldini,
 2048 L.M., Xiao, T., Peterkin, J.L., Awe, J., Haug, G.H., 2015b. Aerosol forcing of the position of the
 2049 intertropical convergence zone since AD1550. *Nat. Geosci.* 8, 195–200.

2050 Riechelmann, D.F.C., Deininger, M., Scholz, D., Riechelmann, S., Schroder-Ritzrau, A., Spotl, C.,
 2051 Richter, D.K., Mangini, A., Immenhauser, A., 2013. Disequilibrium carbon and oxygen isotope

2052 fractionation in recent cave calcite: Comparison of cave precipitates and model data. *Geochim.*
2053 *Cosmochim. Acta* 103, 232-244.

2054 Riechelmann, D.F.C., Schroder-Ritzrau, A., Scholz, D., Fohlmeister, J., Spotl, C., Richter, D.K., Mangini,
2055 A., 2011. Monitoring Bunker Cave (NW Germany): A prerequisite to interpret geochemical proxy
2056 data of speleothems from this site. *J Hydrol* 409, 682-695.

2057 Riechelmann, S., Breitenbach, S.F.M., Schroder-Ritzrau, A., Mangini, A., Immenhauser, A., 2019.
2058 Ventilation and Cave Air PCO₂ in the Bunker-Emst Cave System (NW Germany): Implications for
2059 Speleothem Proxy Data. *J Cave Karst Stud* 81, 98-112.

2060 Riechelmann, S., Schröder-Ritzrau, A., Spötl, C., Riechelmann, D.F.C., Richter, D.K., Mangini, A.,
2061 Frank, N., Breitenbach, S.F.M., Immenhauser, A., 2017. Sensitivity of Bunker Cave to climatic forcings
2062 highlighted through multi-annual monitoring of rain-, soil-, and dripwaters. *Chemical Geology* 449,
2063 194-205.

2064 Rittner, M., Müller, W., 2012. 2D mapping of LA-ICPMS trace element distributions using R.
2065 *Computers & Geosciences* 42, 152-161.

2066 Roberts, M.S., Smart, P.L., Baker, A., 1998. Annual trace element variations in a Holocene
2067 speleothem. *Earth Planet. Sci. Lett.* 154, 237-246.

2068 Ronay, E.R., Breitenbach, S.F.M., Oster, J.L., 2019. Sensitivity of speleothem records in the Indian
2069 Summer Monsoon region to dry season infiltration. *Sci Rep* 9, 5091.

2070 Sade, Z., Halevy, I., 2017. New constraints on kinetic isotope effects during CO₂(aq) hydration and
2071 hydroxylation: Revisiting theoretical and experimental data. *Geochim. Cosmochim. Acta* 214, 246-
2072 265.

2073 Santer, B.D., Po-Chedley, S., Zelinka, M.D., Cvijanovic, I., Bonfils, C., Durack, P.J., Fu, Q., Kiehl, J.,
 2074 Mears, C., Painter, J., Pallotta, G., Solomon, S., Wentz, F.J., Zou, C.-Z., 2018. Human influence on the
 2075 seasonal cycle of tropospheric temperature. *Science* 361, eaas8806.

2076 Schubert, B.A., Jahren, A.H., 2015. Seasonal temperature and precipitation recorded in the intra-
 2077 annual oxygen isotope pattern of meteoric water and tree-ring cellulose. *Quaternary Science*
 2078 *Reviews* 125, 1-14.

2079 Schwarz, K., Barth, J.A.C., Postigo-Rebollo, C., Grathwohl, P., 2009. Mixing and transport of water in a
 2080 karst catchment: a case study from precipitation via seepage to the spring. *Hydrology and Earth*
 2081 *System Sciences* 13, 285-292.

2082 Scroxton, N., Burns, S.J., Dawson, P., Rhodes, J.M., Brent, K., McGee, D., Heijnis, H., Gadd, P.,
 2083 Hantoro, W., Gagan, M., 2018. Rapid measurement of strontium in speleothems using core-scanning
 2084 micro X-ray fluorescence. *Chemical Geology* 487, 12-22.

2085 Shen, C.C., Lin, K., Duan, W., Jiang, X., Partin, J.W., Edwards, R.L., Cheng, H., Tan, M., 2013. Testing
 2086 the annual nature of speleothem banding. *Sci Rep* 3, 2633.

2087 Sherwin, C.M., Baldini, J.U.L., 2011. Cave air and hydrological controls on prior calcite precipitation
 2088 and stalagmite growth rates: Implications for palaeoclimate reconstructions using speleothems.
 2089 *Geochim. Cosmochim. Acta* 75, 3915-3929.

2090 Shopov, Y.Y., Ford, D.C., Schwarcz, H.P., 1994. Luminescent microbanding in speleothems - high-
 2091 resolution chronology and paleoclimate. *Geol.* 22, 407-410.

2092 Sliwinski, M.G., Kitajima, K., Kodzon, R., Spicuzza, M., Denny, A., Valley, J.W., 2017. In situ $\delta^{13}\text{C}$ and
 2093 $\delta^{18}\text{O}$ microanalysis by SIMS: A method for characterizing the carbonate components of natural and
 2094 engineered CO_2 -reservoirs. *International Journal of Greenhouse Gas Control* 57, 116-133.

2095 Sliwinski, M.G., Kodzon, R., Kitajima, K., Denny, A., Spicuzza, M., Valley, J.W., 2015. In-Situ, Micron-
 2096 Scale $\delta^{13}\text{C}$ & $\delta^{18}\text{O}$ Analyses (by SIMS) of Chemo-Isotopically Zoned Carbonate Cements of
 2097 Diagenetic Origin—A Case Study on the Implications for the Thermal and Burial History of the Eau
 2098 Claire Fm., Illinois Basin (USA). AAPG Annual Convention and Exhibition.

2099 Smart, P.L., Friedrich, H., 1987. Water movement and storage in the unsaturated zone of a maturely
 2100 karstified aquifer, Mendip Hills, England, The conference on environmental problems in karst
 2101 terrains and their solution. National Water Well Association, Bowling Green, Kentucky, pp. 57-87.

2102 Smith, C.L., Fairchild, I.J., Spotl, C., Frisia, S., Borsato, A., Moreton, S.G., Wynn, P.M., 2009.
 2103 Chronology building using objective identification of annual signals in trace element profiles of
 2104 stalagmites. *Quat Geochronol* 4, 11-21.

2105 Spengler, R.N., 2019. *Fruit from the Sands: The Silk Road Origins of the Foods We Eat*, 1 ed.
 2106 University of California Press, Oakland, California.

2107 Spötl, C., Fairchild, I.J., Tooth, A.F., 2005. Cave air control on dripwater geochemistry, Obir Caves
 2108 (Austria): implications for speleothem deposition in dynamically ventilated caves. *Geochim.*
 2109 *Cosmochim. Acta* 69, 2451-2468.

2110 Spötl, C., Matthey, D., 2006. Stable isotope microsampling of speleothems for palaeoenvironmental
 2111 studies: A comparison of microdrill, micromill and laser ablation techniques. *Chem. Geol.* 235, 48-58.

2112 Stoll, H., Mendez-Vicente, A., Gonzalez-Lemos, S., Moreno, A., Cacho, I., Cheng, H., Edwards, R.L.,
 2113 2015. Interpretation of orbital scale variability in mid-latitude speleothem $\delta^{18}\text{O}$: Significance of
 2114 growth rate controlled kinetic fractionation effects. *Quaternary Science Reviews* 127, 215-228.

2115 Stoll, H.M., Müller, W., Prieto, M., 2012. I-STAL, a model for interpretation of Mg/Ca, Sr/Ca and
 2116 Ba/Ca variations in speleothems and its forward and inverse application on seasonal to millennial
 2117 scales. *Geochemistry Geophysics Geosystems* 13, 09004.

2118 Surić, M., Lončarić, R., Lončar, N., Buzjak, N., Bajo, P., Drysdale, R.N., 2017. Isotopic characterization
 2119 of cave environments at varying altitudes on the eastern Adriatic coast (Croatia) – Implications for
 2120 future speleothem-based studies. *Journal of Hydrology* 545, 367-380.

2121 Tabersky, D., Nishiguchi, K., Utani, K., Ohata, M., Dietiker, R., Fricker, M.B., de Maddalena, I.M.,
 2122 Koch, J., Gunther, D., 2013. Aerosol entrainment and a large-capacity gas exchange device (Q-GED)
 2123 for laser ablation inductively coupled plasma mass spectrometry in atmospheric pressure air. *J. Anal.*
 2124 *At. Spectrom.* 28, 831-842.

2125 Tadros, C.V., Treble, P.C., Baker, A., Fairchild, I., Hankin, S., Roach, R., Markowska, M., McDonald, J.,
 2126 2016. ENSO-cave drip water hydrochemical relationship: a 7-year dataset from south-eastern
 2127 Australia. *Hydrology and Earth System Sciences* 20, 4625-4640.

2128 Tan, M., Baker, A., Genty, D., Smith, C., Esper, J., Cai, B.G., 2006. Applications of stalagmite laminae
 2129 to paleoclimate reconstructions: Comparison with dendrochronology/climatology. *Quaternary Sci.*
 2130 *Rev.* 25, 2103-2117.

2131 Taylor, W., Shnaider, S., Abdykanova, A., Fages, A., Welker, F., Irmer, F., Seguin-Orlando, A., Khan, N.,
 2132 Douka, K., Kolobova, K., Orlando, L., Krivoshapkin, A., Boivin, N., 2018. Early pastoral economies
 2133 along the Ancient Silk Road: Biomolecular evidence from the Alay Valley, Kyrgyzstan. *Plos One* 13,
 2134 e0205646.

2135 Thompson, G.M., Lumsden, D.N., Walker, R.L., Carter, J.A., 1975. Uranium series dating of
 2136 stalagmites from Blanchard Springs Caverns, U.S.A. *Geochim. Cosmochim. Acta* 39, 1211-1218.

2137 Treble, P., Shelley, J.M.G., Chappell, J., 2003. Comparison of high resolution sub-annual records of
 2138 trace elements in a modern (1911-1992) speleothem with instrumental climate data from southwest
 2139 Australia. *Earth Planet. Sci. Lett.* 216, 141-153.

2140 Treble, P.C., Bradley, C., Wood, A., Baker, A., Jex, C.N., Fairchild, I.J., Gagan, M.K., Cowley, J., Azcurra,
 2141 C., 2013. An isotopic and modelling study of flow paths and storage in Quaternary calcarenite, SW
 2142 Australia; implications for speleothem paleoclimate records. *Quaternary Sci. Rev.* 64, 90-103.

2143 Treble, P.C., Chappell, J., Gagan, M.K., McKeegan, K.D., Harrison, T.M., 2005a. In situ measurement
 2144 of seasonal $\delta^{18}\text{O}$ variations and analysis of isotopic trends in a modern speleothem from southwest
 2145 Australia. *Earth Planet. Sci. Lett.* 233, 17-32.

2146 Treble, P.C., Chappell, J., Shelley, J.M.G., 2005b. Complex speleothem growth processes revealed by
 2147 trace element mapping and scanning electron microscopy of annual layers. *Geochim. Cosmochim.*
 2148 *Acta* 69, 4855-4863.

2149 Treble, P.C., Schmitt, A.K., Edwards, R.L., McKeegan, K.D., Harrison, T.M., Grove, M., Cheng, H.,
 2150 Wang, Y.J., 2007. High resolution Secondary Ionisation Mass Spectrometry (SIMS) $\delta\text{O-18}$
 2151 analyses of Hulu Cave speleothem at the time of Heinrich Event 1. *Chem. Geol.* 238, 197-212.

2152 Tremaine, D.M., Froelich, P.N., Wang, Y., 2011. Speleothem calcite formed in situ: Modern
 2153 calibration of $\delta^{18}\text{O}$ and $\delta^{13}\text{C}$ paleoclimate proxies in a continuously-monitored natural cave system.
 2154 *Geochim. Cosmochim. Acta* 75, 4929-4950.

2155 Valley, J.W., Kita, N.T., 2009. In situ oxygen isotope geochemistry by ion microprobe, MAC short
 2156 course: secondary ion mass spectrometry in the earth sciences, pp. 19-63.

2157 Vanghi, V., Borsato, A., Frisia, S., Howard, D., Gloy, G., Hellstrom, J., Bajo, P., 2019. High-resolution
 2158 synchrotron X-ray fluorescence investigation of calcite coralloid speleothems: Elemental
 2159 incorporation and their potential as environmental archives. *Sedimentology* 66, 2661–2685.

2160 Verheyden, S., Genty, D., Deflandre, G., Quinif, Y., Keppens, E., 2008. Monitoring climatological,
 2161 hydrological and geochemical parameters in the Pere Noel cave (Belgium): implication for the
 2162 interpretation of speleothem isotopic and geochemical time-series. *Int J Speleol* 37, 221-234.

2163 Vonhof, H.B., van Breukelen, M.R., Postma, O., Rowe, P.J., Atkinson, T.C., Kroon, D., 2006. A
 2164 continuous-flow crushing device for on-line delta H-2 analysis of fluid inclusion water in
 2165 speleothems. *Rapid Commun. Mass Spectrom.* 20, 2553-2558.

2166 Waite, A.J., Swart, P.K., 2015. The inversion of aragonite to calcite during the sampling of skeletal
 2167 archives: Implications for proxy interpretation. *Rapid Commun Mass Spectrom* 29, 955-964.

2168 Walczak, I.W., 2016. Holocene climate variability revealed using geochemistry and Computed
 2169 Tomography scanning of stalagmites from the North Atlantic Basin, *Earth Sciences*. Durham
 2170 University, Durham, p. 199.

2171 Walczak, I.W., Baldini, J.U.L., Baldini, L.M., McDermott, F., Marsden, S., Standish, C.D., Richards, D.A.,
 2172 Andreo, B., Slater, J., 2015. Reconstructing high-resolution climate using CT scanning of unsectioned
 2173 stalagmites: A case study identifying the mid-Holocene onset of the Mediterranean climate in
 2174 southern Iberia. *Quaternary Sci. Rev.* 127, 117-128.

2175 Wang, C., Bendle, J.A., Greene, S.E., Griffiths, M.L., Huang, J., Moossen, H., Zhang, H., Ashley, K., Xie,
 2176 S., 2019a. Speleothem biomarker evidence for a negative terrestrial feedback on climate during
 2177 Holocene warm periods. *Earth Planet. Sci. Lett.* 525, 115754.

2178 Wang, J.K., Johnson, K.R., Borsato, A., Amaya, D.J., Griffiths, M.L., Henderson, G.M., Frisia, S., Mason,
 2179 A., 2019b. Hydroclimatic variability in Southeast Asia over the past two millennia. *Earth Planet. Sci.*
 2180 *Lett.* 525, 115737.

2181 Wang, X.F., Edwards, R.L., Auler, A.S., Cheng, H., Kong, X.G., Wang, Y.J., Cruz, F.W., Dorale, J.A.,
 2182 Chiang, H.W., 2017. Hydroclimate changes across the Amazon lowlands over the past 45,000 years.
 2183 *Nature* 541, 204–207.

2184 Wang, Y.J., Cheng, H., Edwards, R.L., An, Z.S., Wu, J.Y., Shen, C.-C., Dorale, J.A., 2001. A high-
 2185 resolution absolute-dated late Pleistocene monsoon record from Hulu Cave, China. *Science* 294,
 2186 2345-2348.

2187 Webb, M., Dredge, J., Barker, P.A., Müller, W., Jex, C., Desmarchelier, J., Hellstrom, J., Wynn, P.M.,
 2188 2014. Quaternary climatic instability in south-east Australia from a multi-proxy speleothem record. *J.*
 2189 *of Quaternary Sci.* 29, 589-596.

2190 Welte, C., Wacker, L., Hattendorf, B., Christl, M., Fohlmeister, J., Breitenbach, S.F.M., Robinson, L.F.,
 2191 Andrews, A.H., Freiwald, A., Farmer, J.R., Yeman, C., Synal, H.A., Gunther, D., 2016. Laser Ablation -
 2192 Accelerator Mass Spectrometry: An Approach for Rapid Radiocarbon Analyses of Carbonate Archives
 2193 at High Spatial Resolution. *Anal. Chem.* 88, 8570-8576.

2194 Wiedenbeck, M., Bugoi, R., Duke, M.J.M., Dunai, T., Enzweiler, J., Horan, M., Jochum, K.P., Linge, K.,
 2195 Kosler, J., Merchel, S., Morales, L.F.G., Nasdala, L., Stalder, R., Sylvester, P., Weis, U., Zoubir, A., 2012.
 2196 GGR Biennial Critical Review: Analytical Developments Since 2010. *Geostandards and Geoanalytical*
 2197 *Research* 36, 337-398.

2198 Wong, C.I., Banner, J.L., Musgrove, M., 2011. Seasonal dripwater Mg/Ca and Sr/Ca variations driven
 2199 by cave ventilation: Implications for and modeling of speleothem paleoclimate records. *Geochimica*
 2200 *et Cosmochimica Acta* 75, 3514-3529.

2201 Wong, C.I., Breecker, D.O., 2015. Advancements in the use of speleothems as climate archives.
 2202 *Quaternary Science Reviews* 127, 1-18.

2203 Woodhead, J.D., Hellstrom, J., Hergt, J.M., Greig, A., Maas, R., 2007. Isotopic and elemental imaging
 2204 of geological materials by laser ablation inductively coupled plasma-mass spectrometry.
 2205 *Geostandards and Geoanalytical Research* 31, 331-343.

- 2206 Woodhead, J.D., Horstwood, M.S.A., Cottle, J.M., 2016. Advances in isotope ratio determination by
2207 LA-ICP-MS. *Elements* 12, 317-322.
- 2208 Wortham, B.E., Montanez, I.P., Rowland, D.J., Lerche, M., Browning, A., 2019. Mapping Fluid-Filled
2209 Inclusions in Stalagmites Using Coupled X-Ray and Neutron Computed Tomography: Potential as a
2210 Water Excess Proxy. *Geochemistry Geophysics Geosystems* 20, 2647-2656.
- 2211 Wu, X., Zhu, X., Pan, M., Zhang, M., 2014. Seasonal variability of oxygen and hydrogen stable
2212 isotopes in precipitation and cave drip water at Guilin, southwest China. *Environmental Earth*
2213 *Sciences* 72, 3183-3191.
- 2214 Wycech, J.B., Kelly, D.C., Kozdon, R., Orland, I.J., Spero, H.J., Valley, J.W., 2018. Comparison of $\delta^{18}\text{O}$
2215 analyses on individual planktic foraminifer (*Orbulina universa*) shells by SIMS and gas-source mass
2216 spectrometry. *Chemical Geology* 483, 119-130.
- 2217 Wynn, P.M., Fairchild, I.J., Borsato, A., Spotl, C., Hartland, A., Baker, A., Frisia, S., Baldini, J.U.L., 2018.
2218 Sulphate partitioning into calcite: Experimental verification of pH control and application to
2219 seasonality in speleothems. *Geochim. Cosmochim. Acta* 226, 69-83.
- 2220 Wynn, P.M., Fairchild, I.J., Frisia, S., Spotl, C., Baker, A., Borsato, A., EIMF, 2010. High-resolution
2221 sulphur isotope analysis of speleothem carbonate by secondary ionisation mass spectrometry.
2222 *Chem. Geol.* 271, 101-107.
- 2223 Wynn, P.M., Fairchild, I.J., Spotl, C., Hartland, A., Matthey, D., Fayard, B., Cotte, M., 2014. Synchrotron
2224 X-ray distinction of seasonal hydrological and temperature patterns in speleothem carbonate.
2225 *Environ Chem* 11, 28-36.
- 2226 Yonge, C.J., Ford, D.C., Gray, J., Schwarcz, H.P., 1985. Stable isotope studies of cave seepage water.
2227 *Chemical Geology* 58, 97-105.

2228 Zeng, G., Luo, W., Wang, S., Du, X., 2015. Hydrogeochemical and climatic interpretations of isotopic
2229 signals from precipitation to drip waters in Liangfeng Cave, Guizhou Province, China. Environmental
2230 Earth Sciences 74, 1509-1519.

2231

2232 **Figure Captions:**

2233 Figure 1: Top Panel: Resolution of speleothem isotope records over time, compiled from the
2234 SISALv1b database. Individual record resolution (small black circles) and mean resolution of
2235 all available (black bars) and Holocene (blue bars) records published in a given year. Bottom
2236 panel: Total number of stalagmite records identified (grey bars), total number of stalagmite
2237 records in SISALv1b (black bars), and total number of Holocene records in SISALv1b (blue
2238 bars).

2239 Figure 2: Illustration of different drip responses from Yok Balum Cave, Belize, over
2240 approximately two months as captured by a series of automated drip loggers. Two clear rain
2241 events and the subsequent drip responses are indicated by the vertical dashed red lines.
2242 Rainfall amount is recorded directly over the cave site using a tipping bucket rain gauge.
2243 Techniques are discussed in more detail in (Ridley et al., 2015a).

2244 Figure 3: A new drip categorisation scheme designed to emphasise cave drip seasonality.
2245 The scheme does not use classification boundaries as such, but instead uses the data
2246 distribution to understand the hydrology. The scheme uses descriptors that map onto
2247 established drip terminology (see Panels B-D and main text for examples). A) Minimum and
2248 maximum hourly drip rates extracted for every month of record for numerous cave drips
2249 globally. The dashed line represents the 1:1 line, and all data points must necessarily plot

2250 over this (i.e., the minimum drip rate cannot exceed the maximum drip rate for any given
2251 month). The closer a point plots to the dashed line, the lower the difference between
2252 monthly maximum and minimum values for that point; if a point sits on the line the
2253 minimum and maximum values for that month are identical. Panels B-D illustrate some
2254 common drip types (using synthetic data) and their pattern when plotted on this diagram.
2255 Panels B-D are schematic and are not based on actual collected datasets; the symbols used
2256 are arbitrary and are not linked to the symbols used in Panel A.

2257 Figure 4: The simulated effects of sampling resolution on the climate signal extracted from a
2258 stalagmite. The stalagmite data are from stalagmite YOK-G (Yok Balum Cave, Belize), which
2259 was originally sampled with a micromill at a 100 micron (0.1 mm) step size (Ridley et al.,
2260 2015b). The chronology for the stalagmite is precise at the seasonal scale. The rainfall data
2261 (bottom panel) are from the Punta Gorda meteorological station (~30 km to the southeast
2262 of the cave site).

2263 Figure 5: Schematic of a sampling scheme for achieving ~50 micron spatial resolution. Plan
2264 view of a stalagmite surface with 1 mm conventional holes on the right and trenches cut for
2265 low and high resolution. The red trench was milled with a 0.8 mm diameter drill and the (blue-
2266 shaded) higher resolution trench was cut laterally, with each sample integrating 50 μm . The
2267 red corners highlight the area that is incorporated into subsequent steps, which in this case
2268 includes material from the current and the previous sample. In this example each high-
2269 resolution sample (e.g., yellow shaded area) integrates a minimal amount of powder of an
2270 older sample (because the milling direction is upward).

2271 Figure 6: Several examples of output generated by different geochemical-based techniques
2272 for extracting seasonal climate. A) Variability in sulphate in speleothem calcite (Obi84, Obir

2273 cave, Austria) as determined by SR- μ XRF (Wynn et al., 2014). The clear annual sulphur maxima
2274 are evident as brighter green colours. B) Ion microprobe-resolved strontium and phosphorous
2275 cycles apparent in stalagmite CC3 from Crag Cave, southwestern Ireland (Baldini et al., 2002).
2276 The well-developed cycles illustrate stronger seasonality at the time of deposition (~ 8.336 ka
2277 BP) than currently present. C) Annual UV-luminescent banding in a stalagmite from Shihua
2278 Cave, Beijing, China (adapted from Tan et al. (2006)). D) well-develop carbon isotope ratio
2279 cycles in stalagmite YOK-G from Yok Balum Cave, Belize, constructed using data obtained via
2280 micromilling at a 100-micron spatial resolution and analyses of powders on an IRMS (Ridley
2281 et al., 2015b) (see also Figure 4). E) Mg cycles apparent in stalagmite BER-SWI-13 from
2282 Leamington Cave, Bermuda, resolved using LA-ICPMS-derived Mg data (Walczak, 2016). All
2283 panels show three to four cycles, interpreted as annual.

2284 Figure 7: A synthetic rainfall input signal (orange circles) with an annual temperature range of
2285 15°C compared with two mean model outputs, one derived using an annual temperature
2286 range of $10 \pm 6^{\circ}\text{C}$ (grey line), and another derived using an annual temperature range of $15 \pm$
2287 6°C (blue line). At the beginning of the simulated rainfall input signal record (year = 0), April
2288 is the wettest month and November the driest month, but this shifts in polarity slowly through
2289 the record, moving through a brief phase with no seasonality in rainfall (year = 7), and then
2290 transitioning into a phase where April is the driest month (from year = 8). The vertical gridlines
2291 highlight the month of April during every model year. The simulated rainfall input signal
2292 amplitude and polarity is reproduced by the model very satisfactorily, provided that the
2293 model temperature range is realistic, as it is in Model 2. Note that the polarity of the simulated
2294 rainfall input signal is still reproduced by Model 1, but modelled rainfall seasonal amplitude
2295 is too large in order to compensate for the low amplitude of the modelled temperature range.

2296 Figure 8: Temperature (top panel) and rainfall (bottom panel) modelling results (black
2297 dashed lines) against 'noisy' synthetic input datasets (solid coloured lines) for seven model
2298 years. The grey rectangle highlights one model year (Year 4) where the input rainfall signal
2299 polarity was reversed; the model detects this shift. The modelling results presented are the
2300 mean values of all successful model runs for each timeslice.

2301 Figure 9: Mean modelled monthly temperature and rainfall data against Global Historical
2302 Climate Network (GHCN) and tree ring data. A) Stalagmite Keklik1 oxygen isotope ratio data
2303 from Bir-Uja Cave, Kyrgyzstan (input data) (Fohlmeister et al., 2017). B) Centennial-scale
2304 borehole temperature data from the Tian Shan region (Huang et al., 2000) from 1500 to
2305 2000 C.E. (input data, shifted upwards for clarity) (blue diamonds), modelled July
2306 temperature (black curve) (output), and NTREND summer temperature reconstruction for
2307 Asia Grid 2 (AG2) (red curve) (Cook et al., 2013). C) Modelled January rainfall (black curve)
2308 (output) and GHCN January rainfall for Tashkent (orange curve), both in % of total annual
2309 rainfall. The grey rectangles highlight the years 1797 and 1815 C.E. discussed in the text.

2310 Figure 10: Global seasonality in annual temperature (°C) and annual precipitation (mm). A)
2311 The annual temperature range was calculated as the maximum temperature of the warmest
2312 month minus the minimum temperature of the coldest month averaged over the period
2313 1970-2000. B) Precipitation seasonality was calculated as the precipitation amount of the
2314 wettest month minus the precipitation amount of the driest month averaged over the
2315 period 1970-2000. WorldClim Version 2 data (<https://www.worldclim.org/>) were obtained
2316 at a 2.5 minute (~4.5 km at the equator) spatial resolution (Fick and Hijmans, 2017). The
2317 data span the period 1970-2000 and thus may reflect anthropogenically-influenced
2318 temperature seasonality as discussed in Santer et al. (2018). Therefore, although the general

spatial pattern of temperature (and potentially precipitation) seasonality may persist into the past, the magnitude of seasonality shifts may deviate from that presented here, particularly when extending records into the preindustrial era.

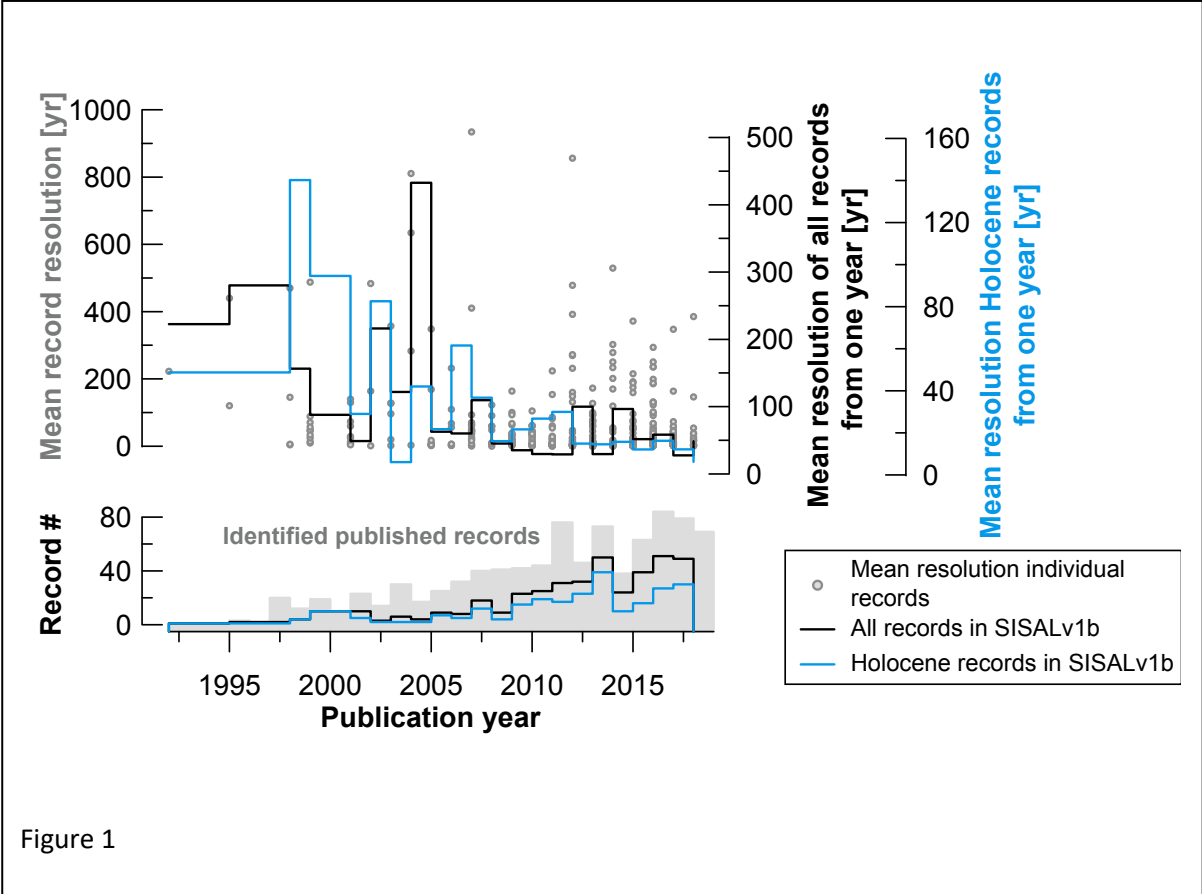
Figure 11: Global seasonality in amount-weighted precipitation $\delta^{18}\text{O}$ (‰ VWMOW). The amount-weighted mean (WM) monthly precipitation $\delta^{18}\text{O}$ data (IAEA/WMO, 2001) were used to determine the annual range in precipitation isotopes globally (calculated as the maximum monthly WM $\delta^{18}\text{O}$ minus minimum monthly WM $\delta^{18}\text{O}$ at 267 stations (yellow symbols) with a complete 12-month dataset over the period 1961-1999. GNIP station data were interpolated onto a $2.5^\circ \times 2.5^\circ$ global grid ($\sim 278 \text{ km} \times 278 \text{ km}$) (IAEA, 2001).

Figure 12: A Hovmöller plot of the annual cycle of total-column precipitable water vapour for Central America, based on daily ERA5 re-analysis data across the region from -110° to -80°W and 0° to 35°N for the period 1979-2018. Also indicated are the latitudes of three key cave sites that have yielded stalagmites which have produced oxygen isotope records of rainfall.

2334 Figures:

2335

2336



2337

2338

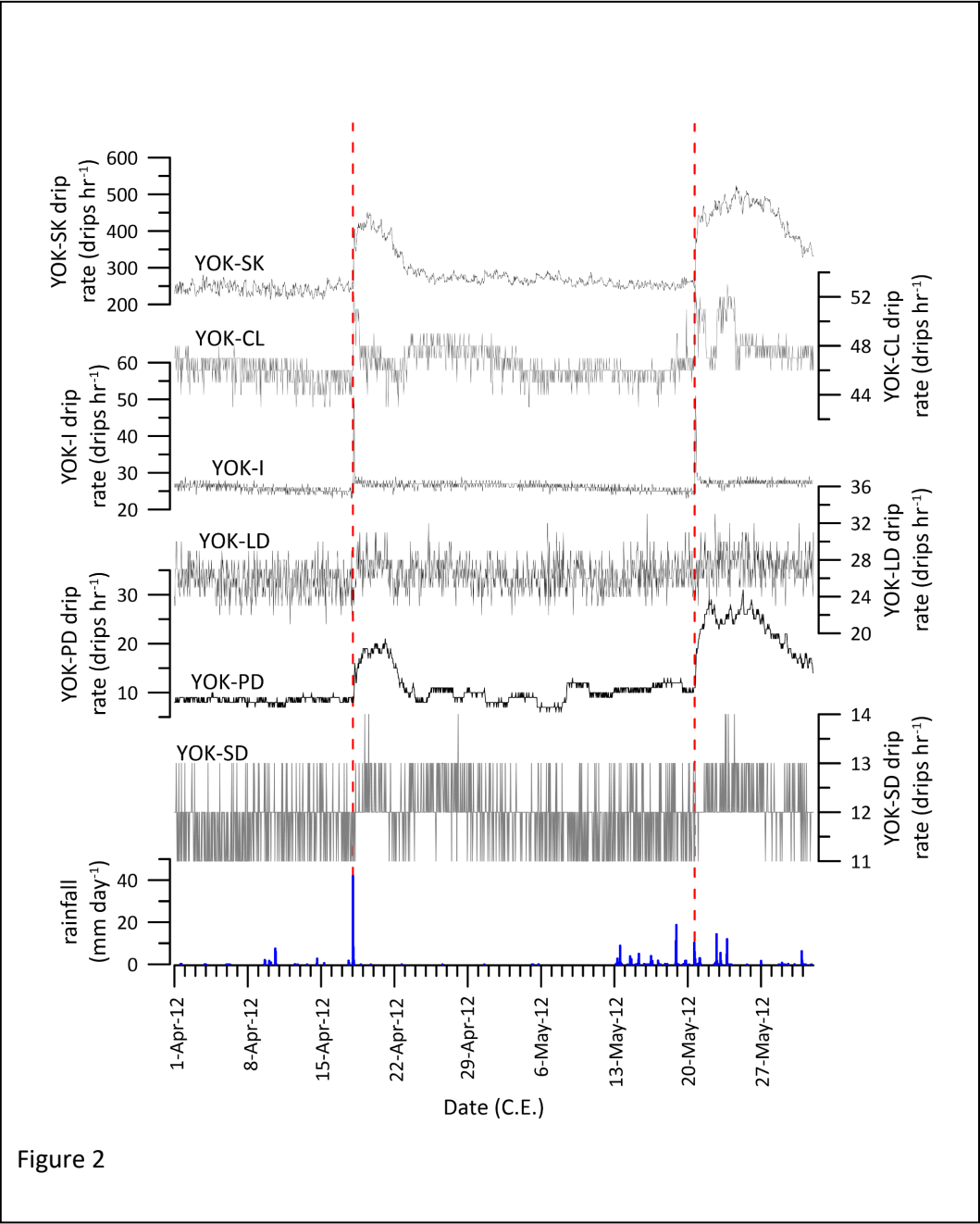


Figure 2

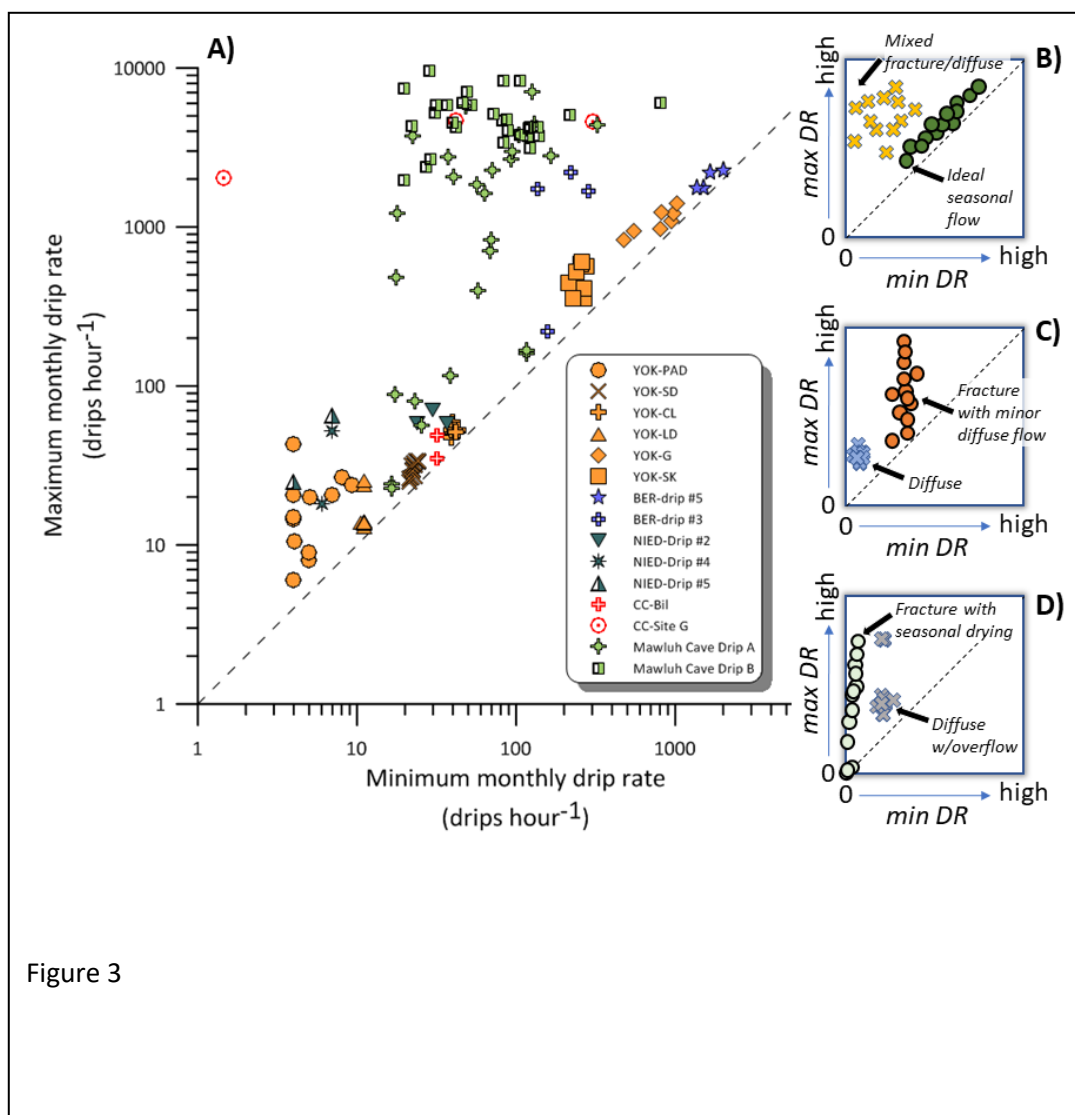


Figure 3

2344

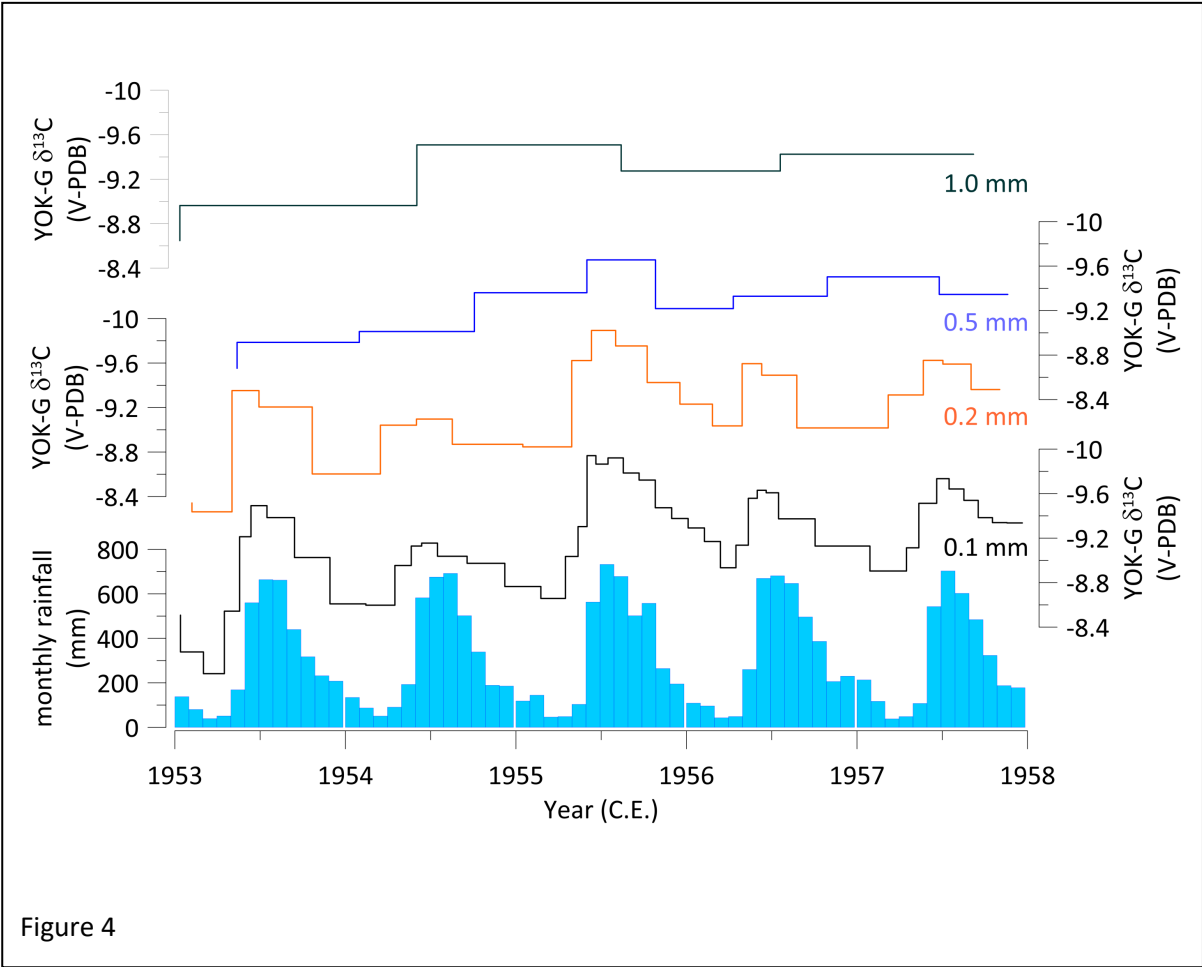


Figure 4

2345

2346

2347

2348

2349

2350

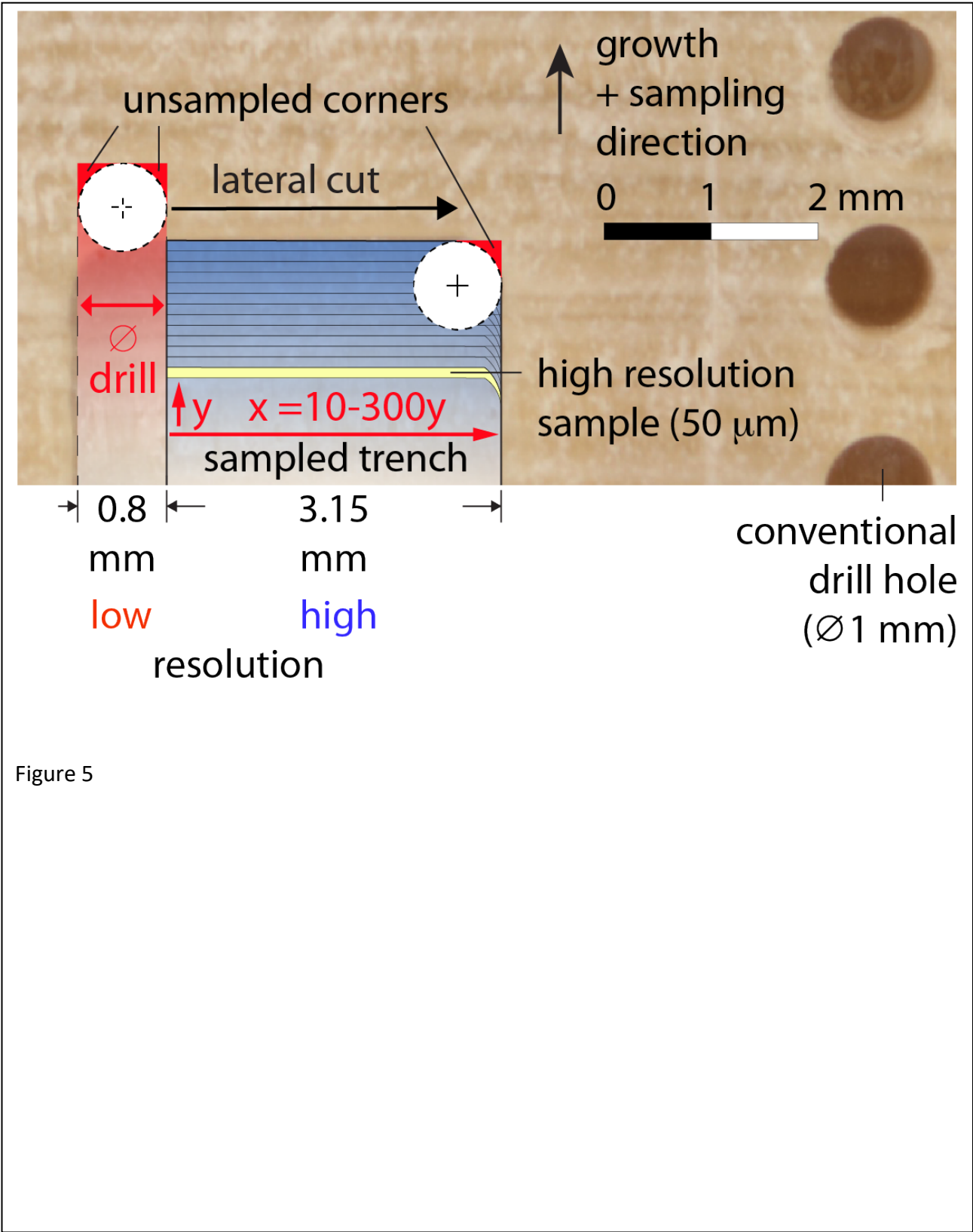
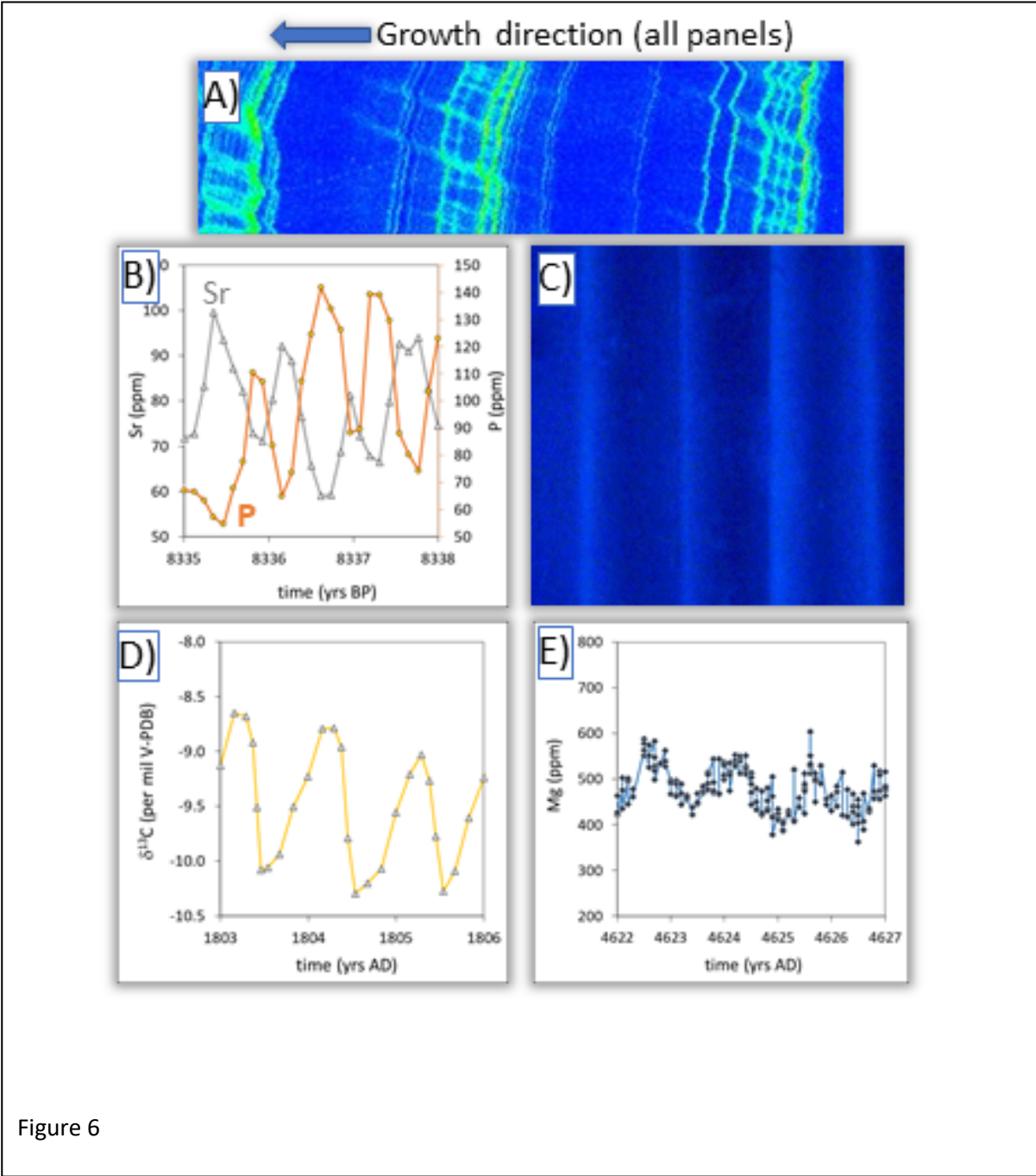


Figure 5

2353

2354

2355



2356

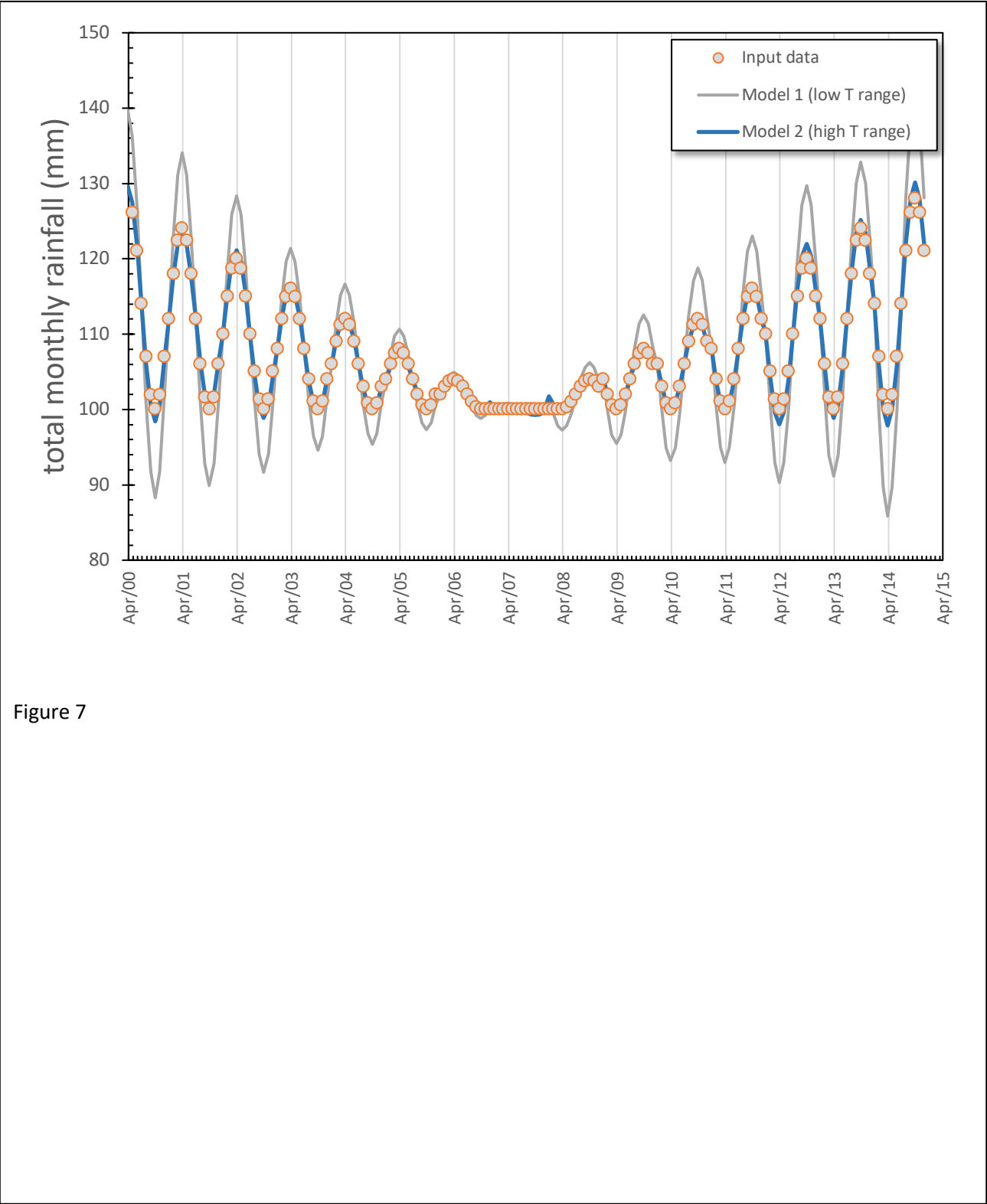


Figure 7

2358

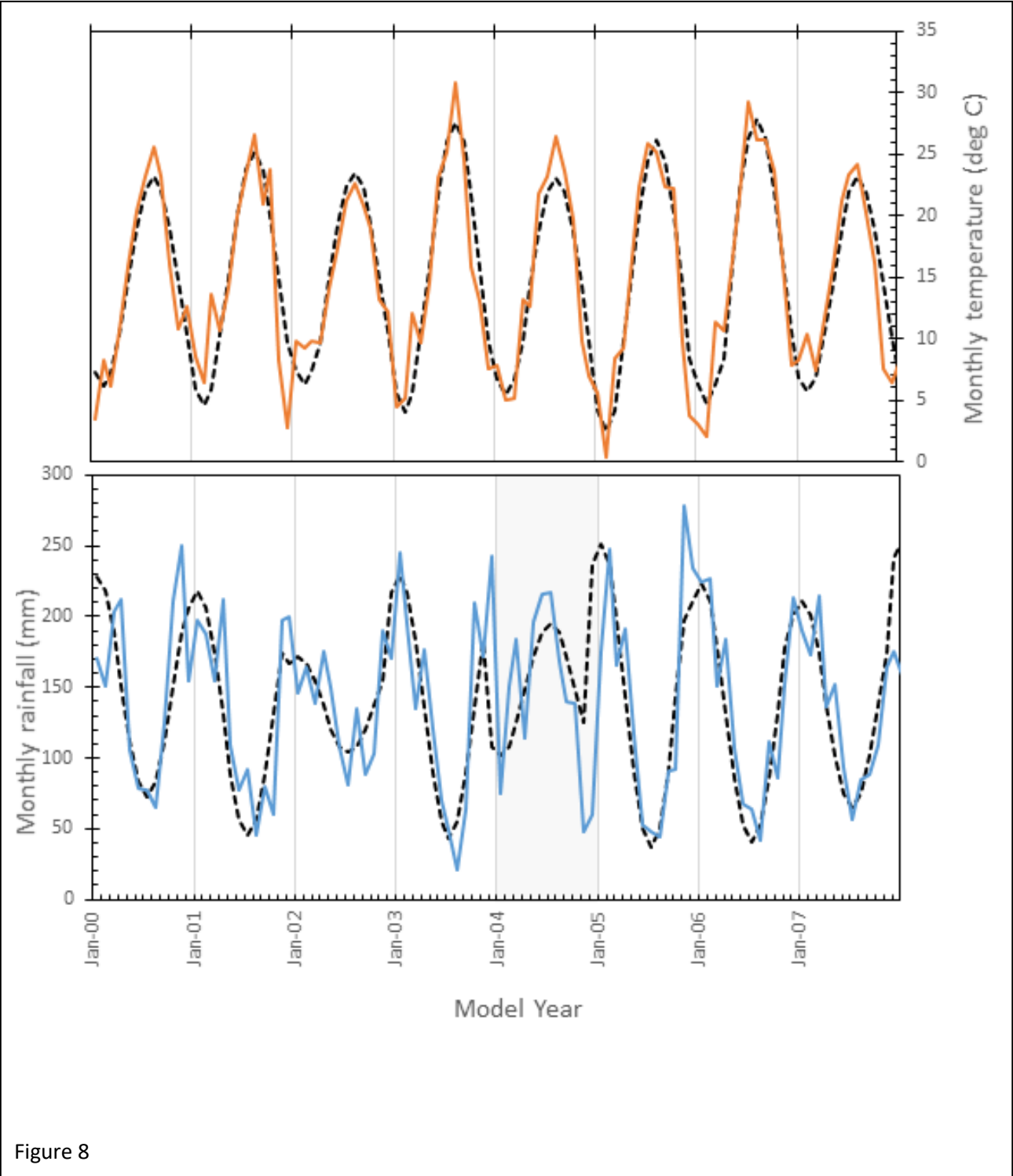


Figure 8

2359

2360

2361

2362

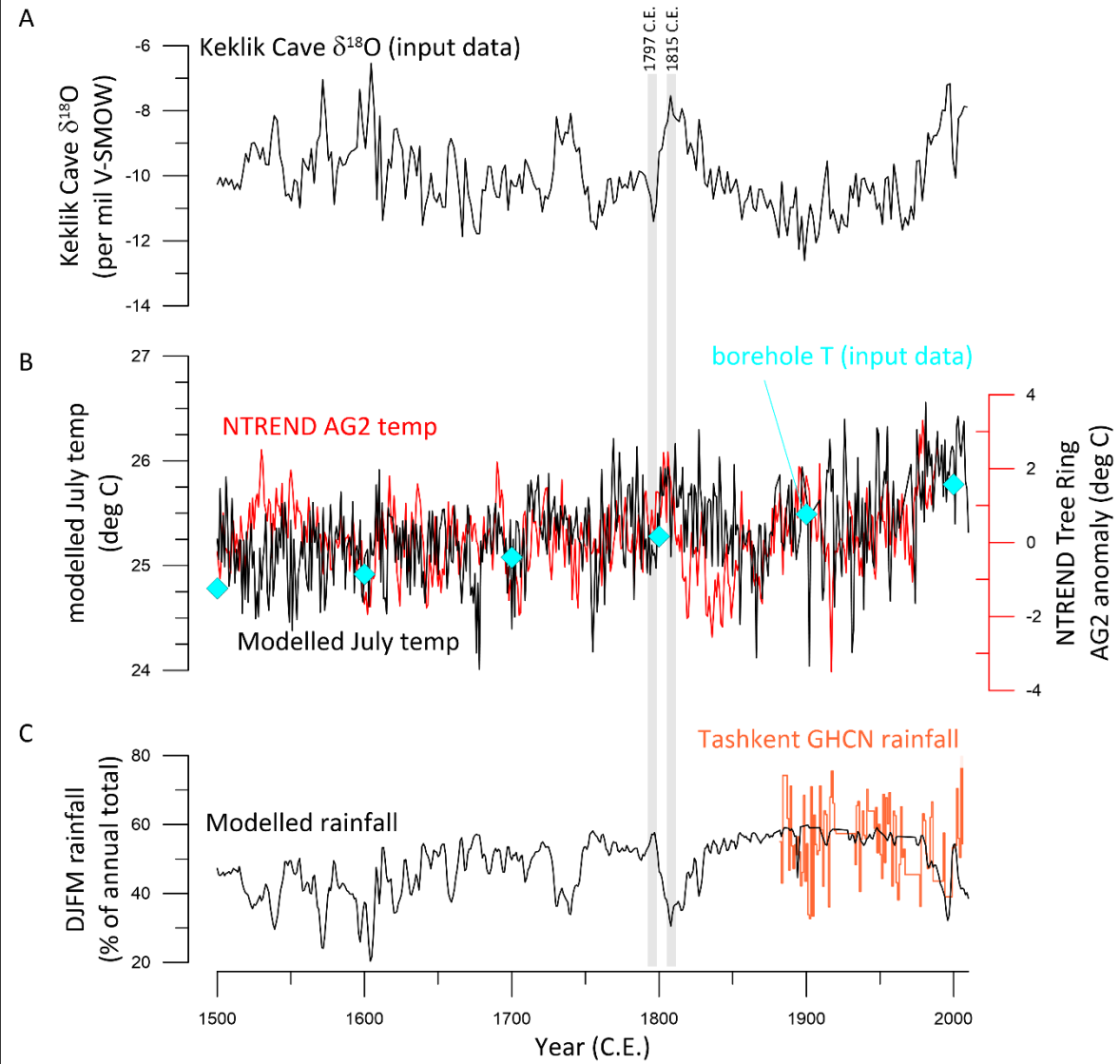


Figure 9

2363

2364

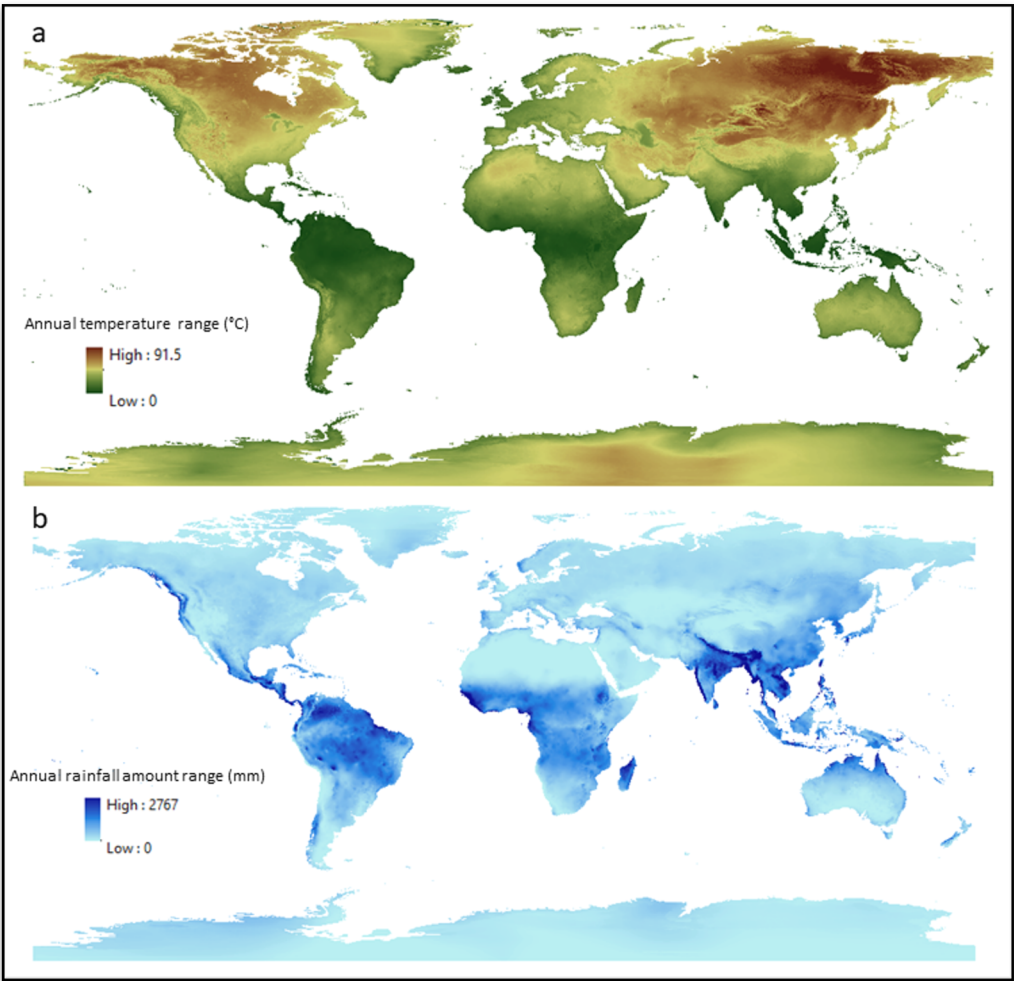


Figure 10

2367

2368

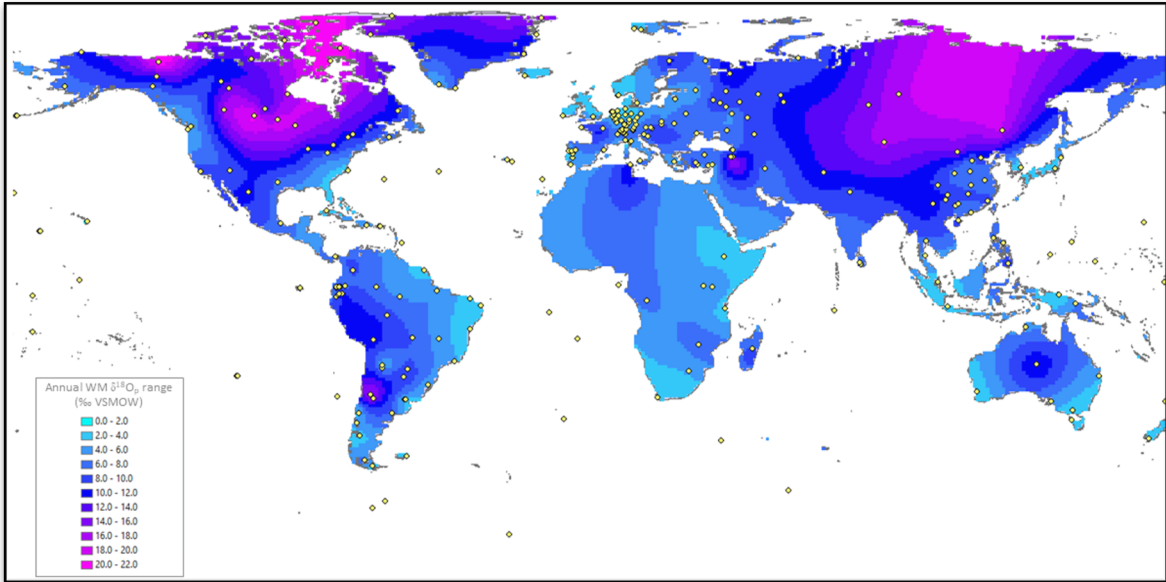
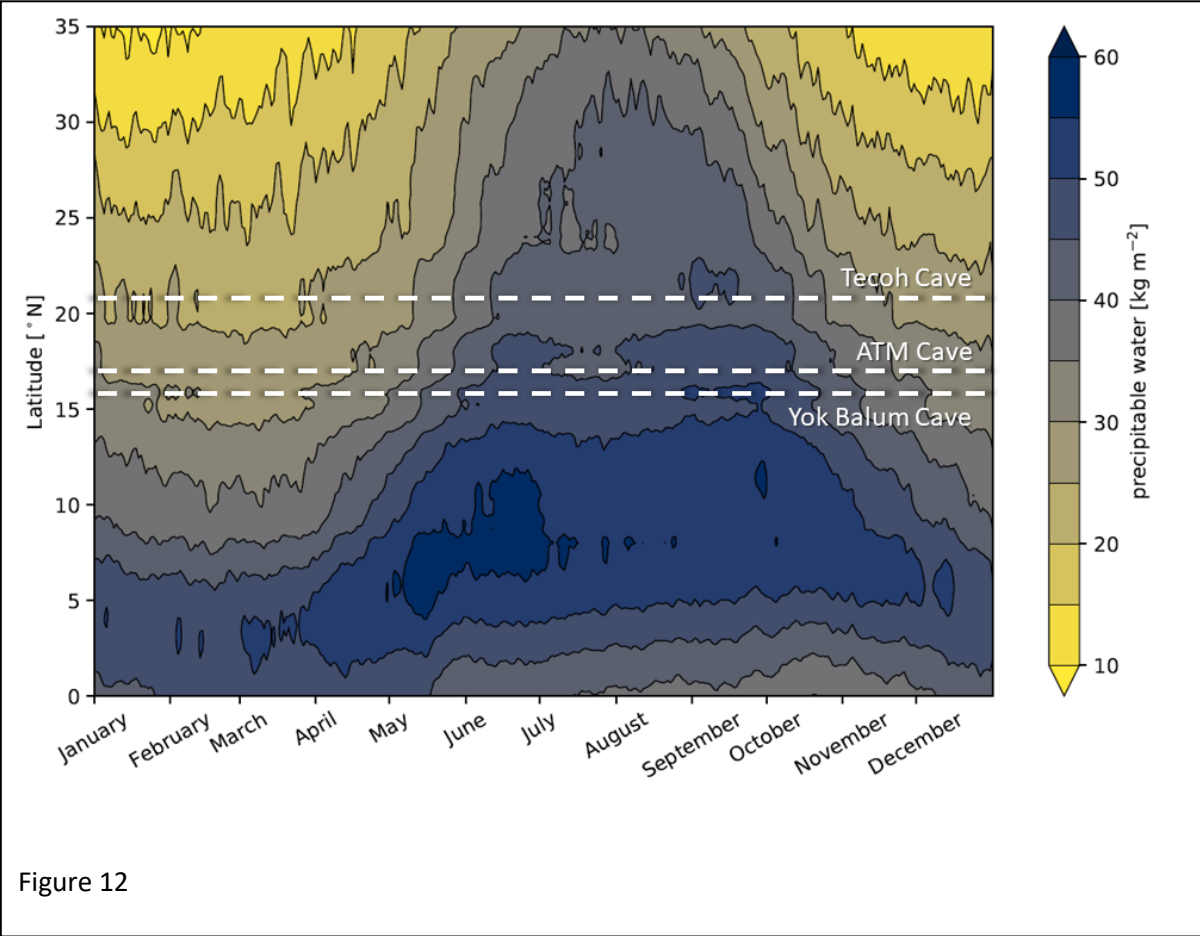


Figure 11

2369



2370

2371

2372